UNIVERSITY OF WARMIA AND MAZURY IN OLSZTYN

Technical Sciences

22(2) 2019

OLSZTYN 2019

The Technical Sciences is indexed and abstracted in BazTech (http://baztech.icm.edu.pl) and in IC Journal Master List (http://journals.indexcopernicus.com)

The Journal is available in electronic form on the web sites
http://www.uwm.edu.pl/techsci (subpage Issues)
http://wydawnictwo.uwm.edu.pl (subpage Czytelnia)

The electronic edition is the primary version of the Journal

PL ISSN 1505-4675
e-ISNN 2083-4527

Address
ul. Jana Heweliusza 14
10-718 Olsztyn-Kortowo, Poland
tel.: +48 89 523 36 61
fax: +48 89 523 34 38
e-mail: wydawca@uwm.edu.pl

Ark. wyd. 7,1, ark. druk. 6,0, nakład 85 egz.
Druk – Zakład Poligraficzny UWM, zam. 286

Contents

Technical Sciences, 2019, 22(2), 109–118

UNIWERSYTET WARMIŃSKO-MAZURSKI W OLSZTYNIE

Quarterly peer-reviewed scientific journal
ISSN 1505-4675
e-ISSN 2083-4527
TECHNICAL SCIENCES
Homepage: www.uwm.edu.pl/techsci/

IDENTIFICATION OF REPRESENTATIVE SEGMENT OF ROOT FOR COLOUR DETERMINATION OF CARROT

Małgorzata Jaros, Mateusz Słowik, Ewa Golisz, Monika Janaszek-Mańkowska

Faculty of Production Engineering
Warsaw University of Life Sciences

Received 24 August 2018, accepted 11 March 2019, available online 8 April 2019.

K e y w o r d s: carrot, colour measurement, representative section, image analysis.

A b s t r a c t

The aim of the work was to verify hypothesis that colour of longitudinal section of carrot root may be represented by a selected segment of root or a cross-section. An image analysis was based on image data obtained for longitudinal sections of carrot roots using flatbed scanner and graphics editing software. Colour images were acquired into sRGB colour space and converted to CIE Lab. Sixteen segments of equal height were separated over whole length of root image. The colour difference metric was determined to present how colour of each segment differs from the mean colour of whole root. The root section was considered to be representative for whole root if colour difference metric was the least. The analysis of results confirmed a research hypothesis and allowed for finding representative section which was located at $^{10}/_{16}$ of total root length measuring from the carrot root head.

Introduction

Colour is one of inseparable and fundamental parameters used for the assessment of food products and materials. It affects the consumer reception of the product and may provide information about its chemical composition as well as suitability for processing, storage and transportation (GIEMZA 2004, ZAPOTOCZNY, ZIELIŃSKA 2005, KOLEK 2008, RÓJ, PRZYBYŁOWSKI 2012).

Correspondence: Małgorzata Jaros, Katedra Podstaw Inżynierii, SGGW w Warszawie, ul. Nowoursynowska 164, 02-787 Warszawa, e-mail: malgorzata_jaros@sggw.pl

Colour may be measured by instrumental or sensory methods. Sensory methods involve human vision but the values obtained in this way are subjective and imprecise. Measurements performed by means of spectrophotometers are precise and repeatable for a very small area. Colour assessment of large area object is usually the average of numerous random samples, which causes it may be not necessarily representative for this object (TRAJER, JAROS 2005, ZAPOTOCZNY, ZIELIŃSKA 2005, AGUILÓ-AGUAYO et al. 2017). More representative average colour may be determined based on the scanner or camera image of whole object or of a powdered sample using computer image analysis-related methodology (GONG et al. 2015).

It was proved that there is a correlation between carrot root colour and the content of carotenoids, sugars and vitamin C. Thus, colour measurement of carrot root may be extremely applicable for carrot quality assessment, since it may replace expensive and time-consuming chemical analyses (TRAJER, JAROS 2005, JANASZEK, TRAJER 2011, SHARMA et al. 2012, KOWALSKI et al. 2013, GONG et al. 2015, LIU et al. 2016).

In food processing the uniform colour of carrot roots is desirable. Thus, carrot roots with core and cortex having similar colour, i.e. without distinct line between them, are considered of the best quality. Nonetheless, different carrot varieties are characterised by different internal colour of root. The average values of colour discriminants of transverse sections (cross sections) or longitudinal sections images may be different than of size-reduced carrot. The lack of standard method for capturing images of plant objects complicates their utilization in production or food processing practice, and it also does not allow for comparing results of different imaging analyses, obtained by different researchers (BILLER et al. 2005, TRAJER, JAROS 2005, ZAPOTOCZNY, ZIELIŃSKA 2005). Therefore, the method of colour-related measurements of carrot roots must be precisely specified every time, due to the heterogeneity of roots' structure.

Generally, the analysis of changes in core and cortex colour, depending on the distance from the end of the root, as well as instrumental comparative assessment of the difference between the colour of the cortex and the core are based on the image of the longitudinal section of the root. Obtaining an appropriate research sample requires longitudinal cutting of root, which is both inconvenient and imprecise, because the root may crumble and even break due to stresses arising during cutting. Thus, transverse cutting of root is much more easier, since cutting out a cylinder segment, followed by obtaining its longitudinal section is fast and precise. This approach was applied to develop a simple and fast methodology to obtain an image of a sample representative for the whole carrot root. Logical analysis, supported by observations, allowed for making an assumption that changes of colour along whole carrot root are smooth. For the purpose of this work the following hypothesis was therefore assumed, that in the continuous material characterised by uniform variability, there must be an area with the

colour representing the average colour of the whole object. This assumption required empirical confirmation.

In preliminary tests, it was verified that the mean values of colour discriminants, determined for a certain transverse section of carrot root, may be the same as for the whole longitudinal section (BERNER 2010). The research was performed using spectrophotometer, and it was determined that transverse section with colour corresponding to the colour of longitudinal section of carrot root was located at ¾ of root length, measuring from root head. The deviation of colour discriminants of transverse section from the average colour of longitudinal section amounted to 10%. In order to confirm the existence of representative section, the research was repeated using more precise computer-based techniques.

Therefore, the aim of this study was to indicate a segment of carrot root longitudinal section, with the colour representative for whole root. The segment corresponded to the fragment of image of carrot root longitudinal section limited by two straight lines perpendicular to root longitudinal axis. Thus, it was necessary to determine length and place of cutting out the cylinder to obtain a research sample for colour reliable assessment of whole carrot root.

Material and methods

The study was carried out in two stages: image acquisition and colour analysis of images. Carrot roots of three varieties: 'Amsterdam 3', 'Flakke 2' and 'Daucus Carota' from own cultivation were used as a research material. Each cultivar was represented by roots of possibly the most uniform shape, mass and size: cultivar 'Amsterdam 3' – length 180±5 mm and head diameter 40±3 mm; cultivar 'Flakke' – length 170±3 mm and head diameter 353 mm; cultivar 'Daucus Carota' – length 200±5 mm and head diameter 45±3 mm. Research sample of each carrot cultivar consisted of six root longitudinal cross-sections for which smooth cutting surfaces were obtained (without cracks and patterns left by the cutting blade). Obtaining such sections required an immobilizing the root in a special matrix, followed by marking a straight line on root surface and cutting it cross with a sharp blade. The root was discarded from the research sample if any crack occurred during cutting or uneven cross-sectional area was obtained. Both halves of each selected, longitudinally cut root were scanned using Cannon 5600F flatbed scanner. Images were acquired using sRGB standard (IEC 61966-2-1) and were saved as bitmaps with resolution of 300 dpi. Each image has undergone pre-processing tasks leading to replacing original image background with a transparent layer. Subsequently, each image was divided in half perpendicular to the longitudinal root axis and the procedure was repeated four times, which allowed for obtaining image of root segments of the same length in each step. Colour components for two, four, eight and

sixteen obtained segments were determined for each segment independently. Segmentation of the carrot root image is presented in Figure 1. A simple algorithm searched for coloured pixels in the image and extracted their RGB values. Then RGB colour components were made linear using inverse sRGB companding. From chromaticity coordinates of sRGB components and its reference white 3×3 RGB to XYZ conversion matrix was calculated and finally CIE Lab colour coordinates were obtained using reference white corresponding to 2° standard observer and standard illuminant D65. No chromatic adaptation was used since sRGB is also relative to D65 reference white (CIE 15 2004, SCHANDA 2007).

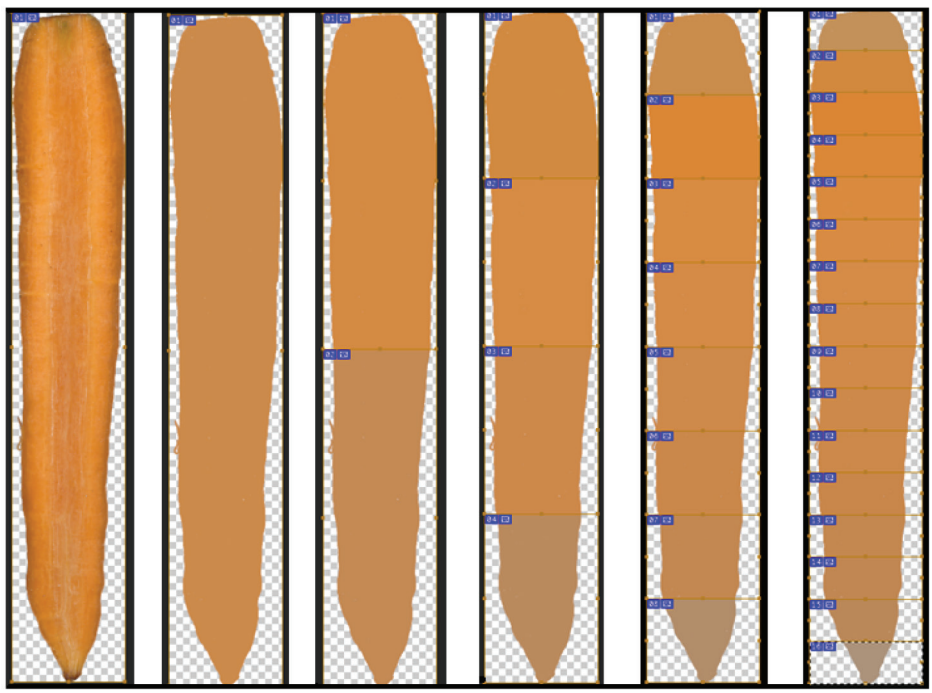

Fig. 1. Segmentation of carrot root image

The CIE Lab colour components allowed to compare mean colour of whole root (consider as a standard), with mean colour of each segment (consider as a sample) using colour difference metric (ΔE) as follows (CIE 15 2004):

$$\Delta E = \sqrt{(\Delta L)^2 + (\Delta a)^2 + (\Delta b)^2} \tag{1}$$

where: Δ symbol stands for the difference between sample and standard in lightness L, redness a (green-to-red colour component) and yellowness b (blue-to-yellow colour component) respectively.

Results and discussion

In the first stage, an initial colour assessment of selected material was conducted based on colour analysis of unsegmented longitudinal sections of examined roots. Standard deviations of colour components reached the highest value for 'Amsterdam 3' which indicates that this cultivar was characterised by the greatest degree of uneven colouring (Tab. 1). The values of ΔE metric were also determined between mean colour components obtained for all roots of the same cultivar (standard) and mean colour components obtained for individual roots of a given cultivar (sample). The ΔE symbol of this metric was marked with the upper horizontal line to distinguish it from other metrics (Tab. 2). Assuming that ΔE metric reflects human ability of colour perception, its values may be classified into five ranges, starting from difference not perceivable by human eye (ΔE<1) and finishing at the impression of perceiving two different colours (ΔE>5) (SHARMA 2003). On this basis it was concluded that roots of 'Amsterdam 3' cultivar were characterised by noticable differences in colour, while for other examined cultivars differences were definitely smaller. High values of variation coefficients determined for each cultivar allowed for making the following conclusion: identification of representative (in terms of colour) segment of carrot root within a sample of much higher cardinality is not cultivar-dependent.

Table 1

Mean values and variations of CIE Lab colour components of root longitudinal sections of examined carrot cultivars

Cultivar	'Amsterdam 3'			'Flakke 2'			'Daucus Carota'		
Colour component	*L* [–]	*a* [–]	*b* [–]	*L* [–]	*a* [–]	*b* [–]	*L* [–]	*a* [–]	*b* [–]
Mean	62	20	39	61	18	35	56	26	44
Standard deviation	3	4	6	1	1	4	1	2	1

Table 2

Means and variation coefficients of ΔE metric determined individually for each carrot cultivar

Specification	Symbol	'Amsterdam 3'	'Flakke 2'	'Daucus Carota'
Mean colour difference	$\overline{\Delta E}$	6.82	3.04	2.12
Coefficient of variation	$CV_{\Delta E}$	33.70%	32.60%	35.52%

Colour analysis of carrot roots' segments

Tables 3, 4, 5 and 6 contain ΔE for subsequent divisions of six samples, i.e. sections of six carrot roots of 'Amsterdam 3' cultivar, indicating a distribution of colour difference in subsequent segments of longitudinal sections of roots in comparison with mean colour of whole root. Further divisions of roots' images into segments of smaller length did not change the location of segment characterised with a minimum ΔE metric. Table 7 presents global mean values of colour differences of successive segments in comparison to the whole root, determined for each cultivar. In order to generalise results for all cultivars, an overall mean values of ΔE were obtained for all samples.

Table 3

'Amsterdam 3' cultivar: ΔE values obtained for 2-segment division

Segment	ΔE					
	Root 1	Root 2	Root 3	Root 4	Root 5	Root 6
1	6.02	8.61	4.71	9.05	6.75	7.85
2	6.18	8.43	14.88	20.55	19.69	7.37

In most samples, the segment which colour differed the least from the colour of the whole root, was identified between 9^{th} and 11^{th} segment of the root total length. Figure 2 presents a trend line of ΔE metric between mean colour of longitudinal root section and mean colour of its individual segments. The graph clearly shows an existence of a global minimum of colour difference at $\Delta E \cong 3.55$, within the 10^{th} segment.

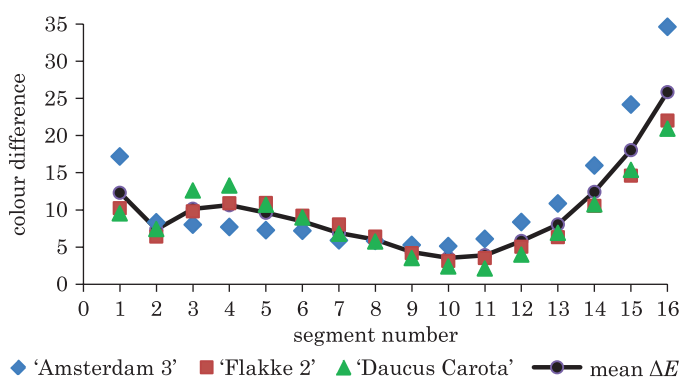

Fig. 2. Values of ΔE metric determined for individual segments of examined carrot cultivars

Table 4

'Amsterdam 3' cultivar: Δ*E* values obtained for 4-segment division

Segment	Δ*E*					
	Root 1	Root 2	Root 3	Root 4	Root 5	Root 6
1	6.16	8.61	8.51	13.66	7.89	4.24
2	6.39	8.61	1.91	4.72	5.32	12.22
3	1.50	2.69	4.74	11.77	11.03	1.44
4	13.41	18.80	24.98	28.91	28.58	14.71

Table 5

'Amsterdam 3' cultivar: Δ*E* values obtained for 8-segment division

Segment	Δ*E*					
	Root 1	Root 2	Root 3	Root 4	Root 5	Root 6
1	1.50	4.96	16.65	22.36	13.38	5.19
2	13.07	11.90	1.31	5.36	3.31	12.13
3	7.87	8.99	2.52	5.73	5.06	13.29
4	5.36	8.24	1.34	4.23	6.02	11.17
5	1.89	4.78	2.54	8.02	10.27	3.69
6	1.39	1.89	7.36	15.56	12.21	4.29
7	5.48	9.43	11.48	22.47	20.74	10.57
8	20.94	28.28	37.68	35.63	36.16	18.86

The most representative section for the examined samples is the section $^{10}/_{16}$ determined for 65% of the examined samples and a neighbouring segment for further 15%. The average error of colour assessment for the above segment was equal 3.7% its minimum was equal 1.36%, and maximum – 11.80%. After the separation of five samples, whose representative sections were not adjacent to the determined section, colour deviation average decreased to 1.84% with the minimum and the maximum values being equal 1.36% and 3.66%. respectively. The results of colour analysis of all representative sections of respective roots indicate that the colour deviation of each of them relative to the average colour of the whole root was between 0.59% and 4.21% with the median equal 1.39% and the average of 1.6%.

In the conducted research. measurement uncertainties might have been caused by the method of material preparation for research. i.e. asymmetrical cutting of carrot roots into two even halves, as well as rough surface of the carrot root section, resulting in inaccurate adherence of the section surface to the scanner glass. Results uncertainty may also be attributed to the material property of carrot roots. i.e. its flexibility, which may also cause inaccurate adherence to the scanner surface. The elimination of these uncertainties in the laboratory conditions is only possible by the use of a more precise cutting tool, or possibly

Table 6

'Amsterdam 3' cultivar: Δ*E* values obtained for 16-segment division and marked with pseudocolours

Segment	Root 1	Root 2	Root 3	Root 4	Root 5	Root 6
1	13.85	22.36	29.74	26.51	1.64	9.07
2	5.41	4.53	14.45	6.56	11.64	7.24
3	12.05	2.28	6.20	1.50	12.27	13.83
4	12.33	3.95	4.52	1.55	11.90	11.96
5	12.33	4.25	5.02	2.85	10.10	8.97
6	13.79	6.07	6.01	2.00	8.15	7.16
7	11.88	4.91	4.21	1.27	8.24	4.94
8	9.75	7.15	4.15	1.34	7.50	4.94
9	5.55	8.34	6.21	2.08	6.54	2.98
10	1.90	11.80	9.83	2.73	2.96	1.47
11	2.82	11.08	13.65	6.25	1.90	0.76
12	6.21	12.95	18.33	8.50	2.22	1.94
13	10.24	18.10	19.81	8.93	3.41	4.73
14	11.23	22.66	25.2	15.00	15.11	6.72
15	11.83	31.65	31.50	32.15	26.02	11.88
16	24.61	40.92	39.61	42.73	30.15	29.89

Table 7

Global mean Δ*E* obtained for root segments of each carrot cultivar and overall mean Δ*E* marked with pseudocolours

Segment	Global mean Δ*E*			Overall mean Δ*E*
	'Amsterdam 3'	'Flakke 2'	'Daucus Carota'	
1	17.20	10.23	9.53	12.32
2	8.31	6.42	7.42	7.38
3	8.02	9.79	12.62	10.14
4	7.70	10.90	13.28	10.63
5	7.25	10.94	10.69	9.63
6	7.20	9.21	8.98	8.46
7	5.91	8.03	6.79	6.91
8	5.81	6.39	5.75	5.98
9	5.28	4.17	3.53	4.33
10	5.12	3.14	2.39	3.55
11	6.08	3.52	2.10	3.90
12	8.36	5.05	4.00	5.80
13	10.87	6.33	6.90	8.03
14	15.99	10.55	10.76	12.43
15	24.17	14.60	15.40	18.06
16	34.65	22.01	20.94	25.87

appropriate adhesives applied temporarily on the section surface adjacent to the scanner surface. In technological conditions, however, where the measurements should be fast simple and accurate, it is necessary to limit the area in order to improve the accuracy of the reading and determine colour discriminants, according to the results of the presented work.

Conclusions

The research assumption that there is a section segment representative for the whole carrot root in terms of colour was confirmed. The obtained results are not absolutely satisfactory due to a limited number of research samples examined. Nevertheless, the results confirmed the existence of a representative section located at ¾ of the carrot root length from the head and limited the area of this section to the area between $^{9}/_{16}$ and $^{11}/_{16}$ – indicating the expected value of colours at $^{10}/_{16}$ of the root length. It was presented in the form of a trend line of a change in the difference between the average colour of the whole carrot root and the average colour of its individual segments. The obtained result applied to 65% of examined sections of roots. This fact can be attributed to the phenotypic growth conditions and error generated by the green colour of carrot root heads, which requires further detailed analysis and explanations.

References

Aguiló-Aguayo I., Gangopadhyay N., Lyng J.G., Brunton N., Rai D.K. 2017. *Impact of pulsed light on colour, carotenoid, polyacetylene and sugar content of carrot slices.* Innovative Food Science & Emerging Technologies, 42: 49-55.

Berner A. 2010. *Wrażliwość metod analizowania barwy na technikę pobierania obrazu*. Praca magisterska. SGGW, Warszawa.

Biller E., Ekielski A., Zaremba R. 2005. *Próba oszacowania niezbędnej liczby pomiarów przy oznaczaniu barwy wybranych produktów spożywczych*. Inżynieria Rolnicza, 11(71): 37-44.

CIE 15. 2004. *Technical Report: Colorimetry*. 3rd edition.

Giemza M. 2004. *Badanie preferencji konsumenckich cech jakościowych miodów naturalnych*. Zeszyty Naukowe Akademii Ekonomicznej w Krakowie, 653: 13-27.

Gong Y., Deng G., Han Ch., Ning X. 2015. *Process optimization based on carrot powder color characteristics.* Engineering in Agriculture, Environment and Food, 8(3): 137-142.

Janaszek M.A., Trajer J. 2011. *Method of evaluating diversity of carrot roots using a self-organizing map and image data.* Computers and Electronics in Agriculture, 79(1): 75-81.

Kolek Z. 2008. *Barwa powierzchni z połyskiem*. Prace Instytutu Elektrotechniki, 237.

Kowalski S.J., Szadzińska J., Łechtańska J. 2013. *Non-stationary drying of carrot: Effect on product quality*. Journal of Food Engineering, 118: 393-399.

Liu C., Liu W., Lu X., Chen W., Yang J., Zheng L. 2016. *Potential of multispectral imaging for real-time determination of colour change and moisture distribution in carrot slices during hot air dehydration.* Food Chemistry, 195: 110-116.

RÓJ A., PRZYBYŁOWSKI P. 2012. *Ocena barwy jogurtów naturalnych*. Bromat. Chem. Toksykol. XLV, 3: 813-816.

SCHANDA J. 2007. *CIE Colorimetry*. In: *Colorimetry*. Ed. J. Schanda. Understanding the CIE System. John Wiley & Sons, Inc. Hoboken, New Jersey.

SHARMA G. 2003. *Digital Imaging handbook*. Taylor & Francis Group, New York.

SHARMA K.D., KARKI S., THAKUR N.S., ATTRI S. 2012. *Chemical composition, functional properties and processing of carrot – a review*. Journal of Food Science and Technology, 49(1): 22-32.

TRAJER J., JAROS M. 2005. *Zastosowanie metod sztucznej inteligencji do oceny zmian jakości wybranych warzyw w procesach ich suszenia i przechowywania*. Wyd. SGGW, Warszawa.

ZAPOTOCZNY P., ZIELIŃSKA M. 2005. *Rozważania nad metodyką instrumentalnego pomiaru barwy marchwi*. Żywność. Nauka. Technologia. Jakość, 1(42): 121-132.

Technical Sciences, 2019, 22(2), 119–133

UNIWERSYTET WARMIŃSKO-MAZURSKI W OLSZTYNIE

Quarterly peer-reviewed scientific journal
ISSN 1505-4675
e-ISSN 2083-4527
TECHNICAL SCIENCES
Homepage: www.uwm.edu.pl/techsci/

INVESTIGATION OF THERMAL CONDUCTIVITY PROPERTY OF PLASMONIC NANOFLUIDS BASED ON GOLD NANORODS PREPARED BY SEED-MEDIATED GROWTH METHOD

***Mahsa Mohammadzadeh*[1], *Mohsen Ashjari*[1,2*], *Davoud Zare*[3,4]**

[1]Nanochemical Engineering Department
Institute of Nanoscience and Nanotechnology
University of Kashan, Iran
[2]Chemical Engineering Department
Faculty of Engineering
University of Kashan, Iran.
[3]MacDiarmid Institute for Advanced Materials and Nanotechnology
School of Chemical and Physical Sciences
Victoria University of Wellington, New Zealand
[4]Riddet Institute
Massey University, New Zealand

Received 20 November 2018, accepted 13 March 2019, available online 8 April 2019.

Key words: Nanofluid, Gold nanorods, Thermal conductivity, Transient hot wire method, Aspect ratio, Volume fraction.

Abstract

In this paper, nanofluids were prepared based on gold nanorods in basic fluid, water, by single-stage chemical reduction and in different volume fractions and the used gold nanorods were synthesized by seed-mediated growth method in different dimensional ratios. The properties of the prepared nanoparticles, including crystalline size, aspect ratio, surface properties, nanoparticle purity, shape and morphology of nanostructures were investigated using x-ray diffraction, UV-vis spectroscopy, FT-IR, and transmitted electron microscopy. The effect of changing parameters of Nano rod dimensions, changes in Nano rod volume fraction in water and also the effect of temperature on the nanofluid thermal conductivity coefficient were investigated using transient hot wire method. The results showed that reducing the aspect ratio, increasing the volume fraction and increasing the temperature increase the thermal conductivity. In fact, results show that an increase

Correspondence: Mohsen Ashjari, MacDiarmid Institute for Advanced Materials and Nanotechnology School of Chemical and Physical Sciences, Victoria University of Wellington, P.O. Box 600, Wellington 6140, New Zealand, e-mail: ashjari.m@kashanu.ac.ir

in the nanorods aspect ratio with a constant volume fraction of 1:50 of gold in water nanorod and at room temperature leads to a decrease in the thermal conductivity of the nanofluid. Also, increasing the two parameters of volume fraction and temperature significantly increases the thermal conductivity coefficient.

Introduction

Heat transfer plays a very important role in several key engineering sectors including microelectronics, power generation, transportation, automotive, aerospace, and nuclear power plants. Due to bugs in the use of traditional fluids and even micro-fluids, including sedimentation and deposition of particles, erosion, fouling of tubes and increasing pressure drop of the flow channel, the researchers turned to nanofluids (EASTMAN et al. 2001). The idea of using a nanofluid was proposed by CHOI and EASTMAN (1995), and a major evolution in fluid heat transfer was generated. In fact, a new look at solid suspensions with particles in nanoscale dimensions presented, in which the small amount of corrosion reduced the impurities and pressure loss problems, and improved fluidity stability over sedimentation.

The nanofluid consists of two main components: base fluid and nanoparticles. The base fluid is the fluid to which nanoparticles are added, and the common fluids contain water, ethylene glycol and engine oil. Nanoparticles are also divided into three groups which are metallic, metallic oxides and non-metallic oxides that are dispersed in the base fluid. In general, two methods are considered for the preparation of nanoparticles: a two-stage method and a single-stage method. In a two-step procedure, the nanoparticles are first synthesized and then dispersed in a base fluid. In a one-stage process the synthesis of nanoparticles (by methods such as chemical/physical deposition or chemical reduction) is occurred with the combination of it with the base fluid simultaneously (YU, XIE 2012). One-stage method for nanofluid production showed better stability than the two-stage method (LI et al. 2009). For more than a decade, researchers have used a single-step method to study nanofluids (YU, XIE 2012, LI et al. 2009). Nanoparticles of several precious metals such as gold, silver, palladium and platinum have been investigated for the manufacture of nanofluids and their use in a variety of engineering applications due to their unique catalytic, electrical, magnetic, optical and mechanical properties (TSENG et al. 2013).

The thermal conductivity coefficient is one of the most important factors in the study of heat transfer. An overview of existing research shows that adding a small amount of nanoparticles would significantly increase the thermal conductivity of the nanofluid relative to the base fluid (WANG, FU 2011, LI et al. 2005). Also, the thermal conductivity of the nanofluid depends on the parameters such as the composition of the chemical percent of the nanoparticles

and nanofluids, the volumetric percent of nanoparticles, the shape and size of the particles, the activated surface materials, and the temperature (PAUL et al. 2011, SURESH et al. 2011). Two mechanisms are considered to increase the thermal conductivity of nanoparticles. The first mechanism is Brownian motion of the nanoparticles inside the fluid, which results in increased mixing and, in fact, heat transfer is facilitated and the thermal conductivity is increased. The second mechanism is the coupling between particles, which increases the thermal conductivity coefficient. In this mechanism, nanoparticles stick together, and create chains through which heat transfer becomes faster (YU, XIE 2012, LI et al. 2009). Various theories, including Maxwell's theory, the Hamilton-Crosser model and Bragman model have been proposed to calculate the thermal conductivity of Nano fluid, which Bragman model has better predictions than other models (SURESH et al. 2011):

$$\frac{k_{nf}}{k} = \frac{1}{4}[(3\varphi - 1)k_s + (2 - 3\varphi)K] + \frac{k}{4}\sqrt{\Delta} \tag{1}$$

$$\Delta = \left[(3\varphi - 1)^2 \left(\frac{k_s}{k}\right)^2 + (2 - 3\varphi)^2 + 2(2 + 9\varphi - 9\varphi^2)\left(\frac{k_s}{k}\right)\right] \tag{2}$$

In the above equations, K_{nf}, k, k_s, and φ are the thermal conductivity of the nanofluid, the thermal conductivity of the base fluid, the thermal conductivity of the solid and the volume fraction of the nanoparticles (According to reference papers, the thermal conductivity of water and solids of gold were considered to be k=0.6 W/(m·k) and k_s=318 W/(m·k), respectively). It should be noted that these theories are not complete. SURESH et al. (2011) concluded that these predictions show less value than the measurements, and the reason for these observations is that the effects of particle size and intermolecular forces are not applied in these models. The researchers have proposed several laboratory methods for measuring thermal conductivity, the most common of which are: THW Transient hot- wire technique, Steady-state parallel-plate method, cylindrical cell method, and omega-3 method. Surface plasmon oscillations caused by free electron oscillations in the surface of metal nanoparticles are activated by appropriate wavelength and its rate depends on the permeation coefficient and particle geometry (RAETHER et al. 1988, ZAYATS et al. 2005). When surface plasmon oscillations are induced, the input photon energy is transmitted oscillatingly, and results in a significant amount of heat in the particles (RAETHER et al. 1988, GOVOROV et al. 2006). If the nanoparticle is placed in an environment such as water, it absorbs heat generated in the environment and increases its temperature (RICHARDSON et al. 2006). In other words, the absorption of light increases by the environment with using of nanoparticles which have surface plasmon oscillations (BOHREN et al. 2007). Therefore, the main goal is to improve the performance of nanofluids, and many researchers have studied various nanofluids to achieve this goal.

SANI et al. (2010, 2011) showed that single-wall carbon nanohorns could improve the nanoparticle optical properties. In another study, TYAGI et al. (2009) reported an increase of 10% in the efficiency of flat plate solar collectors when water fluid was used with aluminum nanoparticles instead of pure water. Also, KHULLAR et al. (2012) showed that aluminum nanofluid can be used to concentrate solar collectors. LEE et al. (2012) showed that it is possible to achieve a broadband absorption plasmonic nanofluid with the dispersion of gold nanocages in water fluid. Due to the solar radiation is includes all spectrum sizes, range from ultraviolet to infrared, broadband absorption is very desirable for solar energy applications. TAYLOR et al. (2013) reported that the shell thickness of gold should be less than 10 nm in order to stimulate surface plasmon oscillations of nanocages in the visible and near-infrared region, and making this shell is very difficult. A promising option to solve this problem is the use of gold nanorods. Gold nanorods can be easily prepared compared to gold nanocages, and their optical properties can be controlled simply by adjusting their aspect ratios. Nanoparticles of several noble metals like gold, silver, palladium and platinum have extensively been studied because of their unique catalytic, electrical, magnetic, optical, and mechanical properties that are different from the coarse grained counterparts of the same materials (LO et al. 2007). Therefore, nanofluid optical properties optimization when used with gold nanorods can be very convenient, cost effective and functional. Therefore, it is very important to study the thermal conductivity of nanofluids on the basis of gold nanorods for use in industrial and medical fields in the future.

According to studies, no experimental article has ever investigated the thermal conductivity of nanofluids based on gold nanorods. The objectives of this study is to prepare nanofluids based on gold nanorods, to detect gold nanostructures by UV-vis, FT-IR spectroscopy, X-ray diffraction and transmitted electron microscopy, as well as measuring the thermal conductivity coefficient and evaluating its variation as a function of the nanorods' dimension and their volume fraction in water and temperature. It is likely that the level of thermal conductivity improvement will be significantly higher than all reported studies.

Materials and methods

Materials

Tetrachloroauric acid ($HAuCl_4.3H_2O$, 99.95%), Ascorbic acid (99%), Cetyltrimethylammonium bromide (CTAB, 99%), Sodium borohydride ($NaBH_4$, 99%) and Silver nitrate ($AgNO_3$) has been purchased from Merck company. Deionized water was used in the preparation of all aqueous solutions, as well as the washing of test dishes.

Preparation

In order to perform the experiment, gold nanorods was first prepared from seed-mediated growth method in three different proportions by changing the growth volume of silver nitrate growth controller (JANA et al. 2001a, b). The seed solution was prepared by adding $HAuCl_4$ (0.5 ml, 0.005 M) and $NaBH_4$ (0.6 ml, 0.01 M) to a continuously stirred CTAB (5 ml, 0.2 M) solution. Then stirring was continued for 2 minutes and the solution was kept at room temperature for 2 hours. In the preparation of the growth solution, a solution of CTAB (5 ml, 0.2 M) was separately mixed with 0.05 ml, 0.2 ml and 0.4 ml of $AgNO_3$ (0.004 M) and $HAuCl_4$ (1 ml, 0.005 M) solution. After gentle stirring, 70 µl of ascorbic acid solution (0.08 M) was added to the reaction containers. Ascorbic acid, as a weak reducing agent, changes the color of the growth solution from dark yellow to pale color. In the final step, 12 µl of the seed solution prepared in the previous step was added to the growth solution at 27-30°C. The color of the solvent in the stirring mode has gradually changed in 10 to 15 minutes. The order of the volumes of silver nitrate in the growth solution, respectively, produce gold nanorods with a short, medium and long dimension, with the color of blue, violet and red solutions. Nanofluids of gold-water nanorods with the different volume fractions were prepared with the same method. In this case, three volume fractions of nanofluids of gold-water nanorods, 1:50, 2:50 and 3:50 were prepared, while the aspect ratio of short gold nanorods were kept constant. The color of the solution turned out from violet to light pink. To investigate the effect of temperature on the thermal conductivity coefficient, the Nano fuids prepared with gold nanorods with a short aspect ratio and diluted in water with a volume fraction of 1:50, was incubated in baths with different temperatures of 25, 35, 45 and 55°C for 30 minutes and was sampled to measure thermal conductivity.

Properties Determination

The gold nanoscale absorption spectra were recorded using, the UV-1800 model of the UV-vis spectrophotometer manufactured by Japan's Shimadzu Corporation, and the aspect ratio of the prepared nanorods were obtained according to the linear relationship between peak position and the aspect ratio of the prepared nanorods (LINK, EL-SAYED 1999, HUTTER, FENDLER 2004, MOHAMMADI et al. 2009, TAKAHASHI et al. 2008, PALIK 1998, WANG et al. 2009, JAIN et al. 2006). Then, the properties of the surface of the gold nanorods were measured by FT-IR spectroscopy using the MagnaIR -550 model of FT-IR, manufactured by Nicolet Corporation, USA. The structure of synthesized gold nanorods was recorded using a XRD diffraction pattern, which was recorded using the X-ray

diffraction device model X' Pert Pro MPD manufactured by Philips Corporation. Also, to investigate the morphology of the synthesized gold nanostructures, Hitachi 2010's TEM has been used. The samples were deposited on copper networks for analysis of TEM.

Measuring the Thermal Conductivity Coefficient

In this study, the thermal conductivity of nanofluids was measured using the KD2 thermal analysis device based on the principles of the transient hot wire method (Decagon, online). In this device, a platinum wire with a diameter of 25 micrometers operates both as a heat sink and a thermometer. For induction of heat input (q), the thermal conductivity coefficient (k) is calculated from Equation 3 (this equation is derived from a solution of the appropriate solution of a Fourier-Kirchoff transient heat conduction problem solution in cylidrical coordinates. The erroneous interpretation is copied from PAUL 2011):

$$k = \left[\frac{q}{4\pi(T_2 - T_1)}\right] \ln\left(\frac{t_2}{t_1}\right) \tag{3}$$

In this equation T_1 and T_2 are, respectively, the temperatures at t_1 and t_2 times. To normalize the possible variation due to human and instrumental errors, the data is expressed as the ratio between the thermal conductivity of the nanofluid with respect to that of the base fluid.

Discussion and Results

Identification of properties of nanofluids based on gold nanorods

Figure 1 shows the XRD pattern of gold particles prepared by the growth method using seeds. The X-ray source used was Cu-Kα radiation at 40 kV and 20 mA, and diffraction was analyzed using the X-ray diffraction device model X' Pert Pro MPD. All the conventional Bragg reflections of this face centered cubic (FCC) metal exist. The amount of the fairly wide peaks is evidence of the crystalline nature of gold nanorods in a nanometer range (ZHANG et al. 2009, JIA et al. 2014). The results of the FT-IR spectroscopy (Fig. 2) show that the surface of the prepared nanorods is completely coated with CTAB (GENTILI et al. 2009).

Figure 3 shows the spectrum of UV-vis nanofluids of gold nanorods diluted in water at a volume ratio of 1 to 50. CTAB absorption peaks and deionized water are indistinguishable and can be ignored. Thus, we can see have two absorption peaks in each nanofluid of gold nanorods: One is in the range of 520 nm and

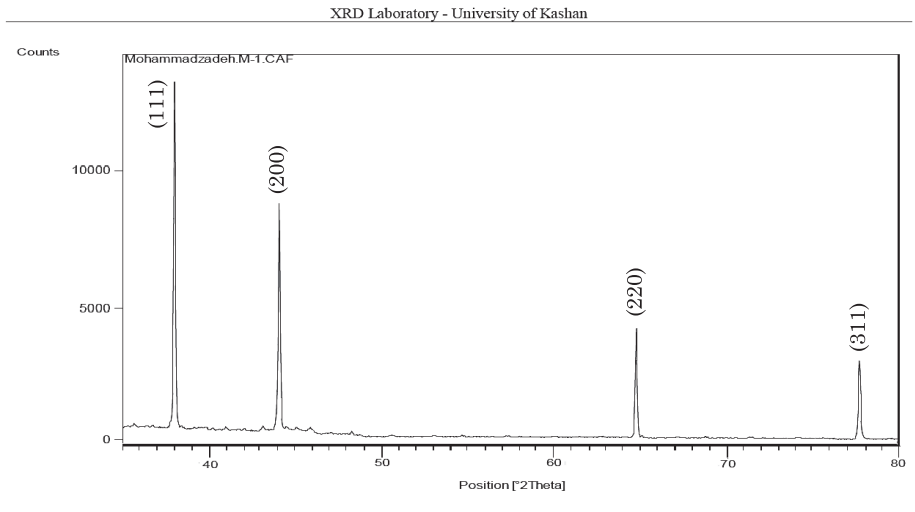

Fig. 1. Gold Nanorods XRD Pattern

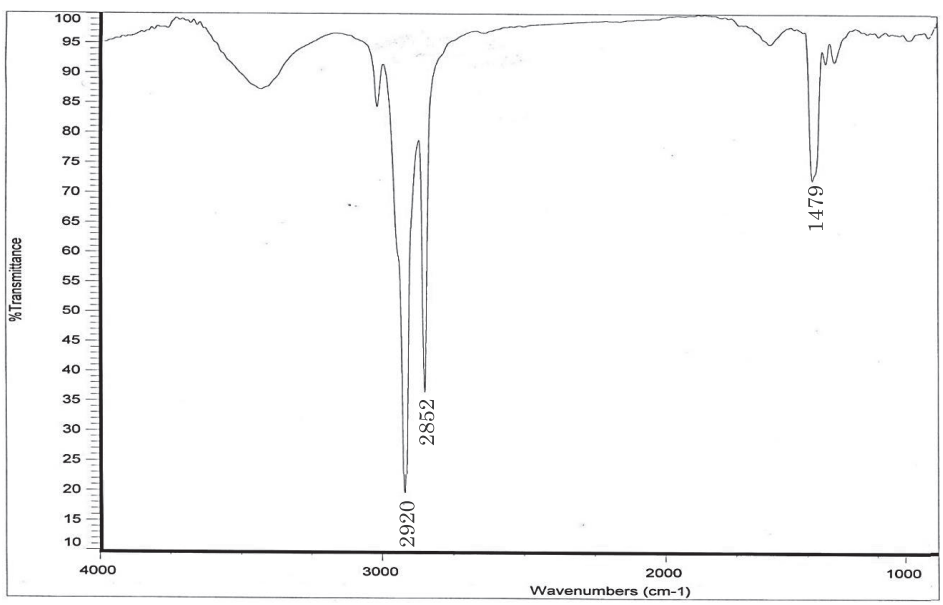

Fig. 2. FT-IR Spectrum of Synthesized Gold Nanorods Using Growth Method of Seeds

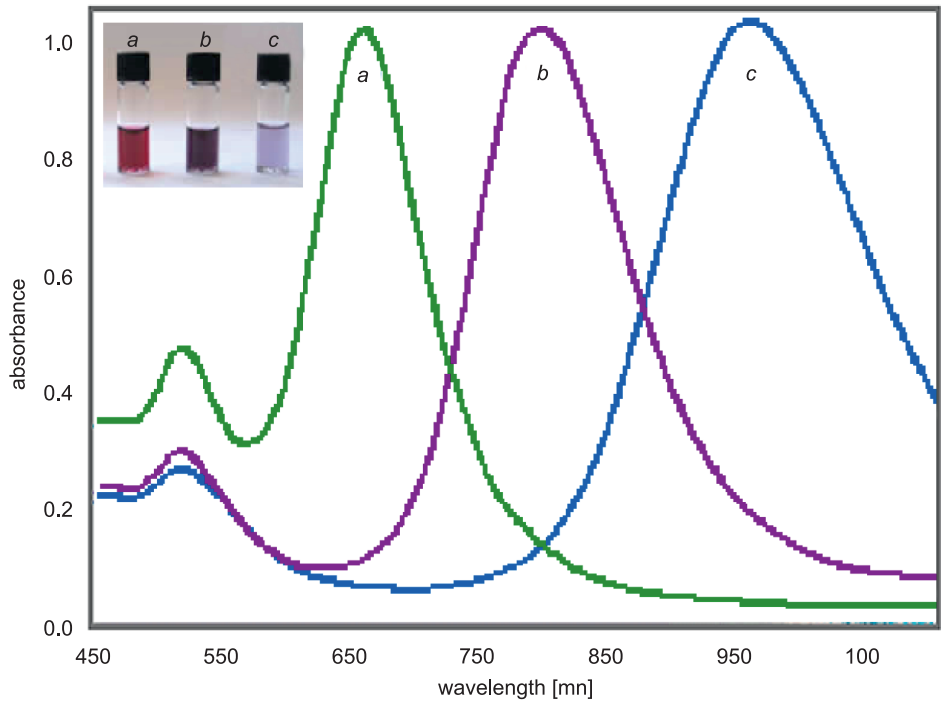

Fig. 3. The UV-vis spectrum of gold nanorods diluted in water with a ratio of 1 to 50 (1/50)

the other occurred at a higher wavelength depending on the aspect ratio of nanorods (BURDA et al. 2005). The longitudinal resonance wavelength in each sample of gold nanorods is 660 nm, 780 nm and 950 nm, respectively, for short, medium and high nanorods. Also, Figure 4 shows the transmitted electron microscopy (TEM) images of the prepared samples, confirming the results obtained from the absorption spectra of the samples and samples are called "short", "medium", and "high" based on their aspect ratios. From the LSPR absorption peak (Fig. 3),

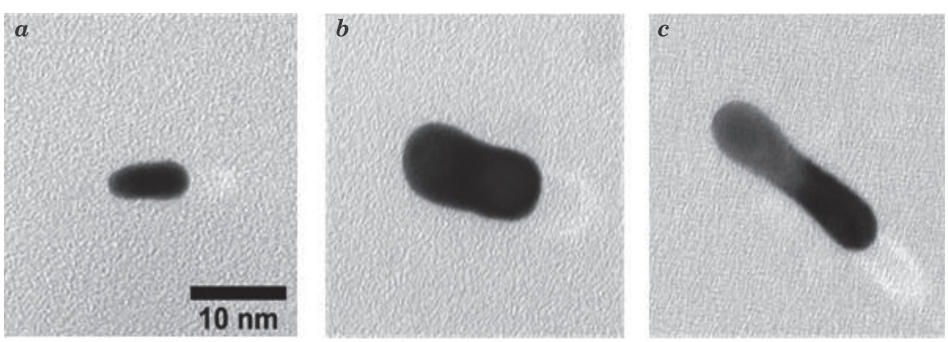

Fig. 4. TEM images of gold nanorods samples: *a* – "short", *b* – "medium", and *c* – "high"

we can obtain comprehensive information of the prepared gold nanorods. Because of the calculations done DRAINE and FLATAU (1994), using a discrete dipole approximation (DDA), an exact relationship is established between the longitudinal LSPR peak wavelength and the aspect ratio of the gold nanorods (equation 4). Therefore, we can calculate even the nanorods aspect ratio with the UV-vis spectrum.

$$\mathrm{AR} = \frac{\text{peak position [nm]}}{99.3} - 4.6 \tag{4}$$

In this regard, by determining the longitudinal LSPR peak wavelength, the nanorods aspect ratio (AR) is calculated. It should be noted that there is a linear relationship between the peak position and the nanorods aspect ratio in other works (NIKOOBAKHT, El-Saye 2003, JAIN et al. 2012). In this equation the least squares method for the data set was used to declare the aspect ratio and position of the corresponding peak, so that the shown linear equation was gained. The aspect ratio of the synthesized gold nanorods with regards to the longitudinal LSPR peak wavelength is given in Table 1.

Table 1

The average aspect ratio of prepared gold nanorods

Resonance [nm]	Aspect Ratio
660	2.1
780	3.2
950	4.9

Thermal conductivity of nanofluids

In this research, the nanofluids' thermal conductivity coefficient of gold/water nanorods was investigated in different aspect ratios, volume fractions and temperatures. Figure 5 shows variations in the thermal conductivity of the nanofluid in different aspect ratios of the gold nanorods. As shown in the figure, the thermal conductivity of the nanofluid decreases with the increase in the nanorods' aspect ratio in a 1:50 constant volume fraction of gold nanorods in water at room temperature. Many studies have shown that rod-shaped nanoparticles impact on the nanofluid effective thermal conductivity is greater than spherical nanoparticles, due to the larger aspect ratio and the larger ratio of surface area of the particle to its volume (LEI et al. 2015). But according to the results, the smaller the aspect ratio of the gold nanorods, the higher the thermal conductivity, which is due to their Brownian motion (CHOPKAR et al. 2008). On the contrary, another model (PATEL et al. 2008), taking into account

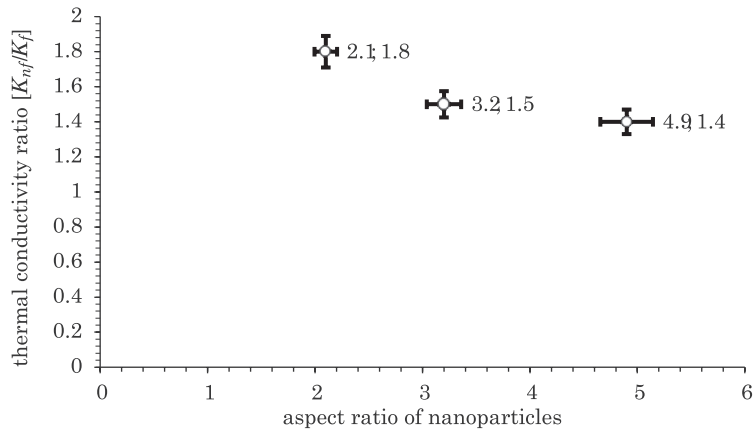

Fig. 5. Nanofluid thermal conductivity coefficient of gold/water Nano rod in various aspect ratios (volume fraction: 1:50, temperature: 25°C)

the combined effects of high specific surface area of the particles, liquid layering at the solid–liquid interface and convective heat transfer enhancement associated with the Brownian motion of the particles quite accurately predicts the thermal conductivity enhancement of the present experimental data as a function of both concentration and particle size. Thus a cumulative effect of several mechanisms such as liquid layering, high nanoparticle specific surface area, and Brownian motion of the particles can be considered to be the possible contributing factors for the phenomenal enhancement of thermal conductivity in nanofluids. Also, smaller nanoparticles have high resistance to sedimentation and precipitation, which is one of the greatest technical challenges in nanofluids (PRASHER et al. 2006). It may be pointed out that the maximum uncertainty limit of thermal conductivity data recorded by the hot-wire device is ±5%, which is consistent with the error bar for the experimental data on thermal conductivity enhancement observed for nano-gold dispersed water based nanofluids (Figs. 5, 6, 7).

Figure 6 shows an increase in the thermal conductivity of the nanofluid with the increase of the volume fraction of the gold nanorods in the base water, with a ratio of 2.1 and in room temperature. Probably, the fundamental factor in increasing thermal conductivity is the degree of dispersion of nanoparticles in the base fluid. In spite of the dramatic increase in thermal conductivity due to the increase of the volume fraction, it should be noted that the volumetric fraction of nanorods in the base fluid is high and it is not appropriate to call the Nano fluid the Nano suspension. Also, this will result in a pressure drop in the flow of fluid. For this reason, it is more common to use the nanofluid in lower volume fractions (KARTHIKEYAN et al. 2008).

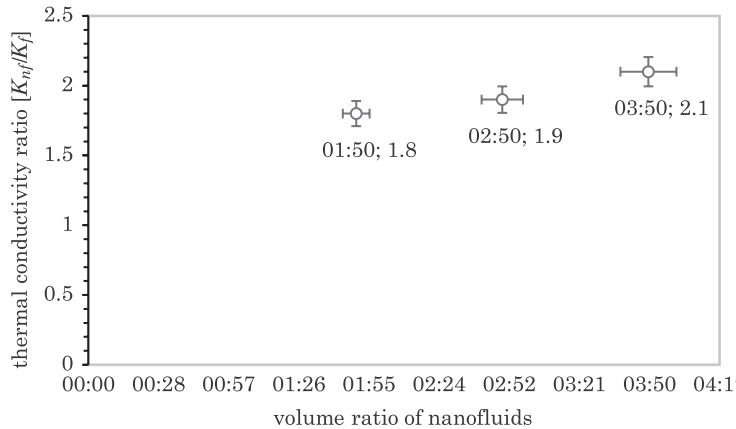

Fig. 6. Nanofluid thermal conductivity coefficient of gold/water nanorods in different volume fractions (aspect ratio: 2.1, temperature: 25°C)

Also, the increase in the thermal conductivity coefficient of nanofluid at various temperatures is shown in Figure 7. The thermal conductivity of the nanofluid is increased by increasing their Brownian motion with increasing temperature, while the thermal conductivity of the fluid without nanoparticles does not change with temperature change (TAHA-TIJERINA et al. 2012). On the contrary, it changes for about 10% with the temperature increase of about 50 C degree from the room temperature (cf. ROHSENOW et al. 1998, table 2.16). An increase of 66% was observed in thermal conductivity at 55°C with a 1:50 volume fraction of nanorods with an aspect ratio of 2.1, relative to the base fluid.

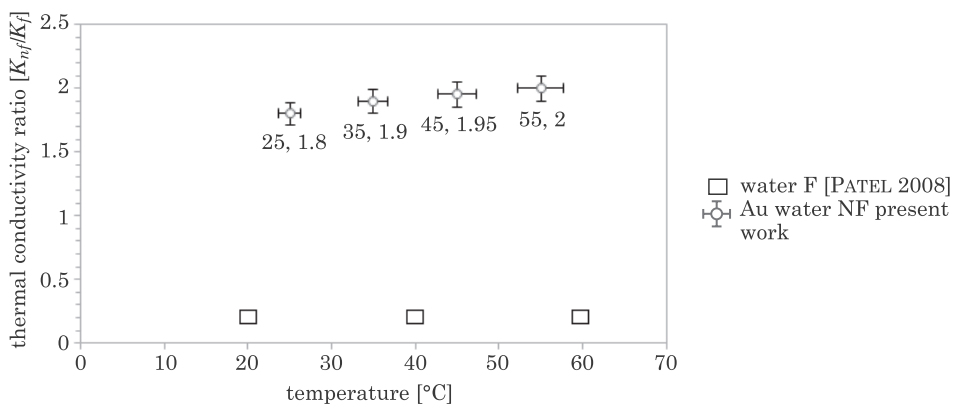

Fig. 7. The effect of temperature on the thermal conductivity of nanofluids in gold/water nanorods (aspect ratio: 2.1, volume fraction: 1:50)

Among the limited number of studies reported in the literature on thermal conductivity of pure gold dispersed water based nanofluids, JHA and RAMPRABHU (2009) have recently reported about 28% enhancement in thermal conductivity for gold and carbon-nanotube (multi wall) composite nanoparticle dispersed water based nanofluids as compared to only 15% enhancement for similar water based nanofluid with only carbon nanotube dispersion. Since thermal diffusivity is directly proportional to thermal conductivity for the same component or system, it is logical to anticipate thermal conductivity may also follow a similar trend in case of gold nanoparticle dispersed nanofluids. Among the proposed mechanisms for increasing the thermal conductivity of nanofluids, the presence of a nanolayer of fluid molecules in a solid-liquid joint-phase is one of the strong ideas put forth by researchers all over the world (YU, CHOI 2003, 2004, YAN et al. 2007, XIE et al. 2005, TILLMAN, HILL 2006, MURSHED et al. 2008). According to the studies and theories proposed by YU and CHUI (2003), XIE et al. (2005) and TILLMAN and HILL (2006), it can be concluded that the presence of a liquid layer in the solid-liquid interface cannot singly increase the thermal conductivity of nanofluids. As a result, in addition to increasing the surface-to-volume ratio of nanofluids based on gold nanorods and increasing the nanolayer formed on the solid-liquid interface along with the increase of Brownian motion of particles, increases the thermal conductivity, which can be considered as a function of the aspect ratio, volume fraction and temperature. Therefore, a theory consisting of several mechanisms, such as liquid layering in the solid-liquid interface, the high surface-to-volume ratio of nanoparticles, and the Brownian motion of particles, can be considered as effective factors in increasing the thermal conductivity of nanofluids.

Conclusion

In this study, nanofluids based on gold nanorods were prepared by a one-stage seed-mediated growth method. Then, the nanofluid thermal conductivity coefficient of gold/water nanorods was investigated experimentally in different aspect ratios, volume fractions and temperatures. In order to determine the thermal conductivity coefficient, the KD2 transient hot wire method was used. The results show that an increase in the nanorods aspect ratio with a constant volume fraction of 1:50 of gold in water nanorod and at room temperature leads to a decrease in the thermal conductivity of the nanofluid, while in general, the increase in this coefficient in the Nano fluid based on Nano rod is more than nanofluid based on measured spherical gold nanoparticles. Also, increasing the two parameters of volume fraction and temperature significantly increases the thermal conductivity coefficient. On the other hand, based on the laboratory findings, new and useful models for estimating the thermal conductivity

of the nanofluid were presented. And a theory consisting of several mechanisms, such as liquid layering in the solid-liquid interface, the high surface-to-volume ratio of nanoparticles, and the Brownian motion of particles, can be considered as effective factors for increasing thermal conductivity in nanofluids.

Acknowledgements

The authors would like to acknowledge the Institute of Nanoscience and Nanotechnology, and Faculty of Engineering, University of Kashan, for their support contribution to this study. We also thank MacDiarmid Institute for Advanced Materials and Nanotechnology, New Zealand, for providing us technical supports.

References

BOHREN C.F., HUFFMAN D.R. 2007. *Absorption and Scattering of Light by Small Particle*. WILEY-VCH, Hoboken, New Jersey, USA.

BURDA C., CHEN X., NARAYANAN R., EL-SAYED M.A. 2005. *Chemistry and properties of nanocrystals of different shapes*. Chemical Reviews, 105(4): 1025-1102.

CHOI S.U.S., EASTMAN J.A. 1995. *Enhancing thermal conductivity of fluids with nanoparticles*. American Society of Mechanical Engineers (ASME), 66: 99-105.

CHOPKAR M., SUDARSHAN S., DAS P.K., MANNA I. 2008. *Effect of Particle Size on Thermal Conductivity of Nanofluid*. Metallurgical and Materials Transactions A, 39(7): 1535-1542.

Decagon, USA; http://issuu.com//decaweb/docs/kd2man.

DRAINE B.T., FLATAU P.J. 1994. *Discrete-dipole approximation for scattering calculations*. Journal of the Optical Society of America, 11(4): 1491–1499.

EASTMAN J.A., CHOI S.U.S., LI S., YU W., THOMPSON L.J. 2001. *Anomalously increased effective thermal conductivities of ethylene glycol-based nanofluids containing copper nanoparticles*. Applied Physics Letters, 78(6): 718-720.

GENTILI D., ORI G., FRANCHINI M.C. 2009. *Double phase transfer of gold nanorods for surface functionalization and entrapment into PEG-based nanocarriers*. Chemical Communications, 39: 5874-5876.

GOVOROV A.O., ZHANG W., SKEINI T., RICHARDSON H., LEE J., KOTOV N.A. 2006. *Gold nanoparticle ensembles asheaters and actuators: melting and collective plasmon resonances*. Nanoscale Research Letters, 1(1): 84–90.

HUTTER E., FENDLER J.H. 2004. *Exploitation of localized surface plasmon resonance*. Advanced Materials, 16(19): 1685–1706.

JAIN P.K., LEE K.S., EL-SAYED I.H., EL-SAYED M.A. 2006. *Calculated absorption and scattering properties of gold nanoparticles of different size, shape and composition: applications in biological imaging and biomedicine*. The Journal of Physical Chemistry, 110(14): 7238–7248.

JAIN S., HIRST D.G., O'SULLIVAN J.M. 2012. *Gold nanoparticles as novel agents for cancer therapy*. The British Journal of Radiology, 85(1010): 101-113.

JANA N.R., GEARHEART L., MURPHY C.J. 2001. *Seed-Mediated Growth Approach for Shape-Controlled Synthesis of Spheroidal and Rod-Like Gold Nanoparticles Using a Surfactant Template*. Advanced Materials, 13(18): 1389−1393.

JANA N.R., GEARHEART L., MURPHY C.J. 2001. *Wet Chemical Synthesis of High Aspect Ratio Cylindrical Gold Nanorods*. The Journal of Physical Chemistry, 105(19): 4065−4067.

JHA N., RAMPRABHU S. 2009. *Thermal conductivity studies of metal dispersed multiwalled carbon nanotubes in water and ethylene glycol based nanofluids*. Journal of Applied Physics, 106(8): 084317.

Jia Y., Sun T.Y., Wang J.H., Huang H., Li P.H., Yu X.F., Chu P.K. 2014. *Synthesis of hollow rare-earth compound nanoparticles by a universal sacrificial template method*. CrystEngComm, 16(27) 6141–6148.

Karthikeyan N.R., Philip J., Raj B. 2008. *Effect of clustering on the thermal conductivity of nanofluids*. Materials Chemistry and Physics, 109(1): 50-55.

Khullar V., Tyagi H., Phelan P.E., Otanicar T.P., Singh H., Taylor R.A. 2012. *Solar Energy Harvesting Using Nanofluids-Based Concentrating Solar Collector*. Journal of Nanotechnology in Engineering and Medicine, 3(3): 259-267.

Lee B.J., Park K., Walsh T., Xu L. 2012. *Radiative Heat Transfer Analysis in Plasmonic Nanofluids for Direct Solar Thermal Absorption*. Journal of Solar Energy Engineering, 134(2): 021009.

Lei W., Mochalin V., Liu D., Qin S., Gogotsi Y., Chen Y. 2015. *Boron nitride colloidal solutions, ultralight aerogels and freestanding membranes through one-step exfoliation and functionalization*. Nature Communications, 6(1): 8849.

Li Q., Xuan Y., Wang J. 2005. *Experimental investigations on transport properties of magnetic fluids*. Experimental Thermal and Fluid Science, 30(2): 109-116.

Li Y., Zhou J., Tung S., Schneider E., Xi S. 2009. *A review on development of nanofluid preparation and characterization*. Powder Technology, 196(2): 89-101.

Link S., El-Sayed M.A. 1999. *Spectral properties and relaxation dynamics of surface plasmon electronic oscillations in gold and silver nanodots and nanorods*. The Journal of Physical Chemistry, 103(40): 8410–8426.

Lo C.H., Tsung T.T., Lin H.M. 2007. *Preparation of silver nanofluid by the submerged arc nanoparticle synthesis system (SANSS)*. Journal of Alloys and Compounds, 434-435: 659-662.

Mohammadi A., Kaminski F., Sandoghdar V., Agio M. 2009. *Spheroidal nanoparticles as nanoantennas for fluorescence enhancement*. International Journal of Nanotechnology, 6(10-11): 902–914.

Murshed S.M.S., Leong K.C., Yang C. 2008. *Thermophysical and electrokinetic properties of nanofluids – a critical review*. Applied Thermal Engineering, 28(17-18): 2109-2125.

Nikoobakht B., El-Sayed M.A. 2003. *Preparation and Growth Mechanism of Gold Nanorods (NRs) Using Seed-Mediated Growth Method*. Chemistry of Materials, 15(10): 1957−1962.

Palik E. 1998. *Handbook of optical constants of solids*. 1st Edition. Academic Press, London.

Patel H.E., Sundararajan T., Das S.K. 2008. *A cell model approach for thermal conductivity of nanofluids*. Journal of Nanoparticle Research, 10(1): 87–97.

Paul G., Philip J., Raj B., Kumar-Das P., Manna I. 2011. *Synthesis, characterization, and thermal property measurement of nano-$Al_{95}Zn_{05}$ dispersed nanofluid prepared by a two-step process*. International Journal of Heat and Mass Transfer, 54(15-16): 3783-3788.

Prasher R., Bhattacharya P., Phelan P.E. 2006. *Brownian-motion-based convective-conductive model for the effective thermal conductivity of nanofluids*. Journal of Heat Transfer, 128(6): 588-595.

Raether H. 1988. *Surface Plasmons on Smooth and Rough Surfaces and on Gratings*. Springer-Verlag.

Richardson H.H., Hickman Z.N., Govorov A.O., Thomas A.C., Zhang W., Kordesch M.E. 2006. *Thermooptical Properties of Gold Nanoparticles Embedded in Ice: Characterization of Heat Generation and Melting*. Nano Letters, 6(4): 783–788.

Sani E., Barison S., Pagura C., Mercatelli L., Sansoni P., Fontani D., Jafrancesco D., Francini F. 2010. *Carbon nanohorns-based nanofluids as direct sunlight absorbers*. Optics Express, 18(5): 5179–5787.

Sani E., Mercatelli L., Barison S., Pagura C., Agresti F., Colla L., Sansoni P. 2011. *Potential of carbon nanohorn-based suspensions for solar thermal collectors*. Solar Energy Materials and Solar Cells, 95(11): 2994–3000.

Suresh S., Venkitaraj K.P., Selvakumar P., Chandrasekar M. 2011. *Synthesis of Al_2O_3–Cu/water hybrid nanofluids using two step method and its thermo physical properties*. Colloids and Surfaces A: Physicochemical and Engineering Aspects, 388(1-3): 41-48.

Taha-Tijerina J., Narayanan T.N., Gao G., Rohde M., Tsentalovich D.A., Pasquali M., Ajayan P.M. 2012. *Electrically Insulating Thermal Nano-Oils Using 2D Fillers*. ACS Nano, 6(2): 1214-1220.

Takahashi H., Niidome T., Kawano T., Yamada S., Niidome Y. 2008. *Surface modification of gold nanorods using layer-by-layer technique for cellular uptake.* Journal of Nanoparticle Research, 10(1): 221-228.

Taylor R.A., Otanicar T.P., Herukerrupu Y., Bremond F., Rosengarten G., Hawkes E.R., Jian X., Coulombe S. 2013. *Feasibility of nanofluid-based optical filters*. Applied Optics, 52(7): 1413–1422.

Tillman P., Hill J.M. 2006. *A new model for thermal conductivity in nanofluids.* Proceeding of 2006 International Conference on Nanoscience and Nanotechnology. Eds. C. Jagadish, G. Lu. Canberra, Australia, p. 673-676.

Tseng K.H., Lee H.L., Liao C.Y., Chen K.C., Lin H.S. 2013. *Rapid and Efficient Synthesis of Silver Nanofluid Using Electrical Discharge Machining*. Journal of Nanomaterials, 2013: 6-12.

Tyagi H., Phelan P., Prasher R. 2009. *Predicted Efficiency of a Low-Temperature Nanofluid-Based Direct Absorption Solar Collector*. Journal of Solar Energy Engineering, 131(4): 041004.

Wang L.P., Lee B.J., Wang X.J., Zhang Z.M. 2009. *Spatial and temporal coherence of thermal radiation in asymmetric Fabry-Perot resonance cavities*. International Journal of Heat and Mass Transfer, 52(13-14): 3024–3031.

Wang Q., Fu F. 2011. *Removal of heavy metal ions from wastewaters: A review*. Journal of Environmental Management, 92(3): 407-418.

Xie H., Fujii M., Zhang X. 2005. *Effect of interfacial nanolayer on the effective thermal conductivity of nanoparticle-fluid mixture*. International Journal of Heat and Mass Transfer, 48(14): 2926-2932.

Yan K.Y., Xue Q.Z., Zheng Q.B., Hao L.Z. 2007. *The interface effect of the effective electrical conductivity of carbon nanotube composites*. Nanotechnology, 18(25): 255705.

Yu W., Choi S.U.S. 2003. *The Role of Interfacial Layers in the Enhanced Thermal Conductivity of Nanofluids: A Renovated Maxwell Model*. Journal of Nanoparticle Research, 5(1-2): 167-171.

Yu W., Choi S.U.S. 2004. *The role of interfacial layers in the enhanced thermal conductivity of nanofluids: A renovated Hamilton – Crosser model*. Journal of Nanoparticle Research, 6(4): 355-361.

Yu W., Xie H. 2012. *A Review on Nanofluids: Preparation, Stability Mechanisms, and Applications.* Journal of Nanomaterials, 2012: 17-34.

Zayats A.V., Smolyaninov I.I., Maradudin A.A. 2005. *Nano-optics of surface plasmon polaritons.* Physics Reports, 408(3-4): 131–314.

Zhang F., Shi Y.F., Sun X.H., Zhao D.Y., Stucky G.D. 2009. *Formation of hollow upconversion rare-earth fluoride nanospheres: Nanoscale Kirkendall effect during ion exchange*. Chemistry of Materials, 21(21): 5237–5243.

Technical Sciences, 2019, 22(2), 135–149

UNIWERSYTET WARMIŃSKO-MAZURSKI W OLSZTYNIE

Quarterly peer-reviewed scientific journal
ISSN 1505-4675
e-ISSN 2083-4527
TECHNICAL SCIENCES
Homepage: www.uwm.edu.pl/techsci/

DEVELOPMENT OF A METHOD FOR FINDING THE OPTIMAL SOLUTION WHEN UPGRADING A MOTORCYCLE ENGINE

Oleksandr Vrublevskyi*, *Radomir Wojnowski

Department of Vehicle and Machine Construction and Operation
University of Warmia and Mazury

Received 11 January 2019, accepted 13 February 2019, available online 8 April 2019.

Keywords: spark ignition engine, thermodynamic cycle simulations, optimization, design of experiments (DoE), Monte Carlo method, Nonlinear Programming Quadratic Line search (NLPQL).

Abstract

This paper describes a method for finding the optimal parameters of a spark-ignition engine gas exchange system for a motorcycle. The vectors of the initial data for filling the parameter space, in which the search for the optimal solution has been made, have been formed through methods of experiment planning and technique nonlinear programming quadratic line search. As the quality criteria, the engine power has been used at selected points of the external speed characteristic. The results of the work have shown how using the proposed optimization method allows modernization of a gas exchange systems in order to increase the engine power.

Introduction

All stages of the life cycle of an engine, from design to the recycling process, require optimization methods that improve the processes included in its production and exploitation. Bearing in mind the subject of studies – a four-stroke spark-ignition engine of a sport motorcycle, the following specific character must be taken into consideration. Almost every motorcycle of that class

Correspondence: Oleksandr Vrublevskyi, Katedra Budowy, Eksploatacji Pojazdów i Maszyn, Uniwersytet Warmińsko-Mazurski, ul. Oczapowskiego 11, 10-710 Olsztyn, e-mail: aleksander.wroblewski@uwm.edu.pl

is exclusive. In that case, the quality indicators differ from the indicators assumed for consumer products (BRANNEN et al. 2012). Primarily, what is taken into account includes power, torque, visual and acoustic effects of the machine. On rare occasions, we pay attention to fuel consumption, oil consumption, or a set of environmental standards.

For the first time, such engines were presented before a larger audience in the last century and, from that time, they have been constantly improved and optimized. The traditional approach towards optimization of engines employs a sequential change of individual parameters (factors). The univariate approach appeared to be expensive and inefficient, especially when the requirements concerning modernization become more numerous and contradictory to each other.

Many of the exploited motorcycles are equipped with an engine with natural suction. An increase of the power of such engines during modernization is possible thanks to application of inertia supercharging of engine cylinders (HARRISON, DUNKLEY 2004). It is possible to implement all the advantages of such boost, which involves all wave phenomena during the flow of air and exhaust in the discharge and inlet ducts of the engine, provided that the geometrical dimensions and regulation of systems responsible for the gas exchange have been selected in an optimum manner. The application of the boost, thanks to an improved method of filling the cylinder with a fresh feed and of cleaning the combustion by-products also leads to a certain decrease in fuel consumption.

Thus, it is important to elaborate optimization methods for processes of gas exchange in high-speed motorcycle engines. In order to achieve this goal, it is necessary to develop an algorithm that will cover the verified optimization techniques as well as methods for planning and processing the experimental results.

Apart from the traditional univariate approach, in the recent years, new optimization methods have been proposed which have been successfully applied in the industry (SHIH et. al. 2012, DESHMUKH et. al. 2004, MACKEY et. al. 2002, YONGFAN et. al. 2017, SYAHRULLAH, SINAGA 2016, STELIOS et. al. 2014, WANG et. al. 2016). The possibility of quick data processing becomes complicated due to the statistical methods applied in the case of optimization, as well as due to modeling and computing methods used to model cycles of an engine (HEYWOOD 1988). When it comes to the analysis of engine performance, engine processes can be described in detail by using laws of mechanics, hydrostatic and gas dynamics, and laws of thermodynamics. Advanced process models of an engine can be integrated in a simulation of a complete cycle of a particular subject, in order to predict its capacities, provided that relevant data are provided, as well as more general aspects of the cycle operation. Opportunities to create integrated models of vehicles and power sources are being established.

The problems that arise during the optimization of an internal combustion engine are explained by the need to consider a large number of factors affecting

the process being optimized. These factors usually have a weakly pronounced correlation. The engine of the vehicle operates in a wide range of changes in load, equipment, and, as a consequence, changes in fuel consumption, environmental indicators. This leads to problems when choosing the quality criteria of the investigated thermodynamic, hydro-gas-dynamic, mechanical processes.

Currently, researchers and engine developers have at their disposal software systems that simulate these processes with high accuracy. Simulation techniques can take into account almost all the factors affecting the processes. When forming the engine design model, hundreds of input design and adjustment parameters are used, as well as fitting coefficients. The use of such a "virtual engine" shortens the product design period. And also allows you to upgrade existing engines in operation.

Computer models of engines can be used to analyze a high number of construction and operational variables. The analysis of results of the simulation will show the possibility of improving the required quality of the subject, for instance its power in particular load points, which will help in choosing an optimum combination of construction factors and adjusting elements. Consequently, of course, the demand for experimental devices, the time to develop a product, and costs of testing equipment become significantly lower.

The task of optimization can be now performed by applying one or a combination of the following strategies:

1. Design of Experiments (DoE) Methods (ROSS 1998). Usually, the application of those methods allows choosing an optimum solution. However, the outcome of application of those methods can be unsatisfactory, especially in the case of choosing a complete or partial factor. If robust screening methods are selected such as the use of orthogonal arrays, then result testing is more efficient, and the method becomes viable.

2. Methods of optimization. There are many such methods available on the market. However, the choice of the optimization algorithm that must be used is a very important element, since some optimization methods are permitted in the case of some application, depending on the spatial parameter (spatial modality, continuity, linearity, etc.).

The efficiency of those methods increases, when they are used together. At the initial stage, for instance, one method can be used for experiment planning in order to test the space determined by limit values of factors being the subject of interest and to find the intended best option. After construction of the surface, it is possible to use a relevant optimization method in order to find the ultimately optimum construction point. The search for an optimum solution, in this case, does not start from scratch nor at random in any area of design. Results of DoE used to have a deliberate choice of the initial searching conditions. In practice, the optimization method will work when DoE had been stopped. It leads to a significant decrease in number of optimization iterations for convergence.

The optimum solution is an ultimately optimum solution since the approximation of the answer surface is mathematically set before the commencement of optimization (the optimizer already knows the surface topology of the answer – peaks, gradients, bottoms from DoE coefficients). It should ensure that the local optimum will not be selected as the global optimum.

Objective and scope of the optimization

The optimization work covered in this paper is pertinent to the performance of a S+S 113 CID (Fig. 1) spark-ignition engine used mainly in automotive applications such as motorcycles. The said engine, as any power plant, has to meet some requirements, such as power output, fuel consumption, emissions levels, and noise limits. The optimization work at hand covers exclusively the optimization of power output, using the finite volume modeling scheme to solve the thermodynamic equations for all the control volumes in the engine simulation (valves, manifolds, exhaust components, etc. (Fig. 2). Detailed geometry and engine operating conditions are defined as input data.

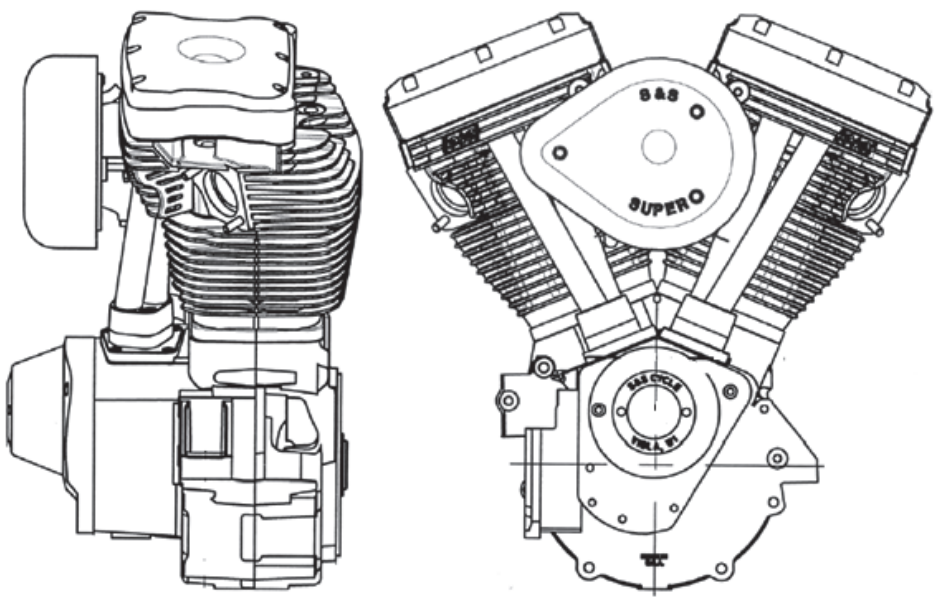

Fig. 1. Motorcycle engine HD S+S 113 CID (HD Manual 2015)

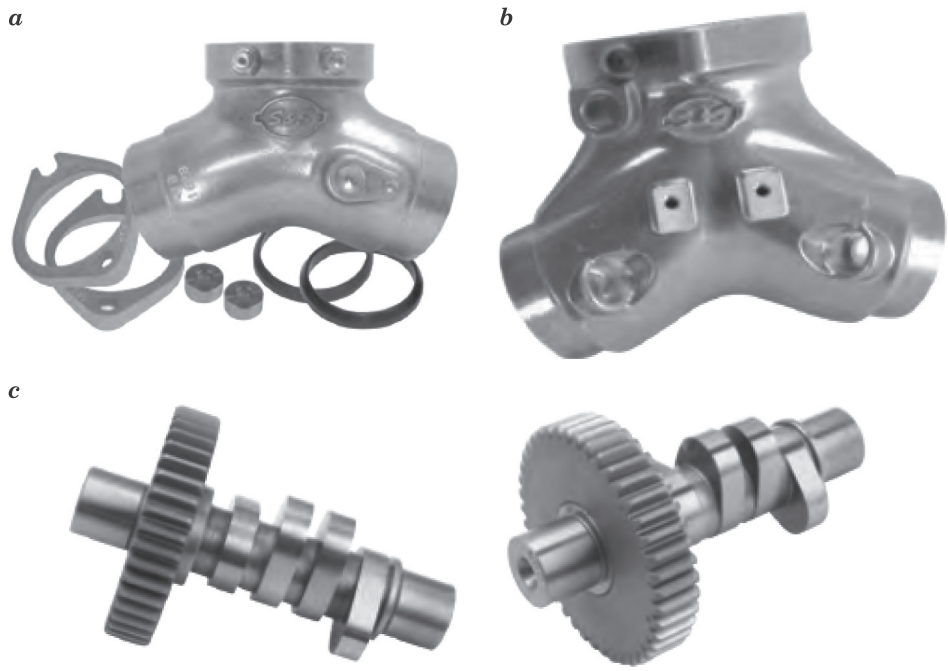

Fig. 2. Optimized elements of an engine: *a* – intake manifold of an engine with a carburettor, *b* – intake manifold of an engine with a dispersed injection system, *c* – camshaft

Selection of controllable factors

Selection of factors based on operational and modernization experiments of such a motorcycle class has been presented in Table 1 as well as in the set of tests presented in works (JAWAD et. al. 2001, BLAIR et. al. 2003, ZHAO 2011, ALESSANDRO, MARCO 2014). However, authors also applied methods of modeling of the physical and mathematical model. Such parameters influence the engine power. Thus, their optimum combination allows increasing the engine power in characteristic points. So far, little attention has been devoted to the interaction between selected factors (Tab. 1), starting from such interaction, including a high number of factors that are not too obvious, prior to the commencement of testing of the planned experiment.

In this investigation, the applied answer function is the criterion of «myObjective» synthesis quality, which allows searching for an optimum criterion through a value the goal of which is "0". As it has been mentioned, the quality criterion constitutes a condition to achieve the maximum power in the tested charging mode. As an example of application of the proposed

Table 1

List factors and Output parameter

Factor	Name	Units	Default value	Lower bound	Upper bound
Intake valve diameter	IVD	mm	50	45	55
Intake Valve Opening timing (cad BTDC)	IVO	degree	5	0	10
Intake plenum pipe length	len	mm	125	110	140
Exhaust valve diameter	EVD	mm	42	38	46
Exhaust Valve Closure timing (cad ATDC)	EVC	degree	10	0	20
Pipe exhaust diameter	diameter	mm	50	45	55
Exhaust plenum pipe length	Lex	mm	500	250	750
Exhaust orifice area	pole	mm^2	1,500	1,000	2,000
Output parameter					
myObjective					

optimization record, this article considers the possibility of achieving 75 kW at 4,000 rpm. In that case, the criterion «myObjective» = 75-Pi, where Pi is the engine power in that calculation.

Based on the selected eight controlling factors, the minimum number of projects implemented with the method of a full-scope experiment is 256. Usually, there is a need for an additional flow in order to verify the proposed optimum for the project. Of course, after DoE, there will be more launches necessary to complete the third part of the optimization of the study. However, the number of flows required to optimize to convergence is significantly lower, since optimization starts near the intended optimum solution. Again, the NLPQL surface approximation ensures that the optimum solution is a global (ultimate) one.

Selection of the optimization technique

Different design problems require different optimization techniques. As such, the selection of an optimization technique is a big challenge, and oftentimes, a combination of two or more techniques should be used to get a specific optimization task done. Generally, optimization techniques can be divided into three broad categories:

1. Numerical optimization techniques assume the parameter space is unimodal, convex, and continuous. Popular techniques in this category are sequential linear or quadratic programming, methods of feasible directions, etc.

2. Exploratory techniques evaluate designs throughout the parameter space in search of the global optimum. Like most search problems, the techniques in

this category typically, but not necessarily, require a larger number of iterations than the numerical techniques.

3. Expert system techniques follow user defined directions on what to change, how to change it, and when to change it.

Due to the large number of control factors considered in the study at hand and the lack of in-advance information about the response surface, the optimization techniques in the third category above are not considered. Also, since a DoE method is used prior to the optimization part of the study, the second category may not be the best choice in terms of optimization convergence time. Therefore, the designer is left with choosing a numerical technique.

The most appropriate numerical technique for the study in this paper is the NLPQLP method, a newer version of NLPQL, solves smooth nonlinear programming problems by a Sequential Quadratic Programming (SQP) algorithm. The new version is specifically tuned to run under distributed systems. In case of computational errors, caused for example by inaccurate function or gradient evaluations, a non-monotone line search is activated. The code is easily transformed to C by f2c and is widely used in academia and industry.

NLPQL is a sequential quadratic programming (SQP) method which solves problems with smooth continuously differentiable objective function and constraints. The algorithm uses a quadratic approximation of the Lagrangian function and a linearization of the constraints. To generate a search direction a quadratic subproblem is formulated and solved. The line search can be performed with respect to two alternative merit functions, and the Hessian approximation is updated by a modified BFGS formula (SCHITTKOWSKI 2011, 1986).

The aim of an optimization process is to find the best design (parameter settings) that matches a given objective (minimize a value), and does not violate the constraints.

$$x \in \Re^n \qquad \begin{aligned} &\min f(x) \\ &g_j(x) \geq 0 \quad j = 1,\ldots,m \\ &x_l \leq x \leq x_u \end{aligned}$$

f is the objective function, and the g_j ($j = 1,\ldots, m$) functions represent the constraints. Constraints are different from bounds. Indeed, bounds are known a priori and are never violated, whereas constraints are known a posteriori and are something the algorithm tries not to violate (then they may be violated).

Set up of the doe study and software integration

Figure 3 presents the basic engine model used in the study that has been described in this article. Constructive solutions for that scheme involve installing an inlet distributor (submodel "Intake") to the point fuel injector (Fig. 2*b*), separated from every piston of the exhaust system (submodel "Exhaust").

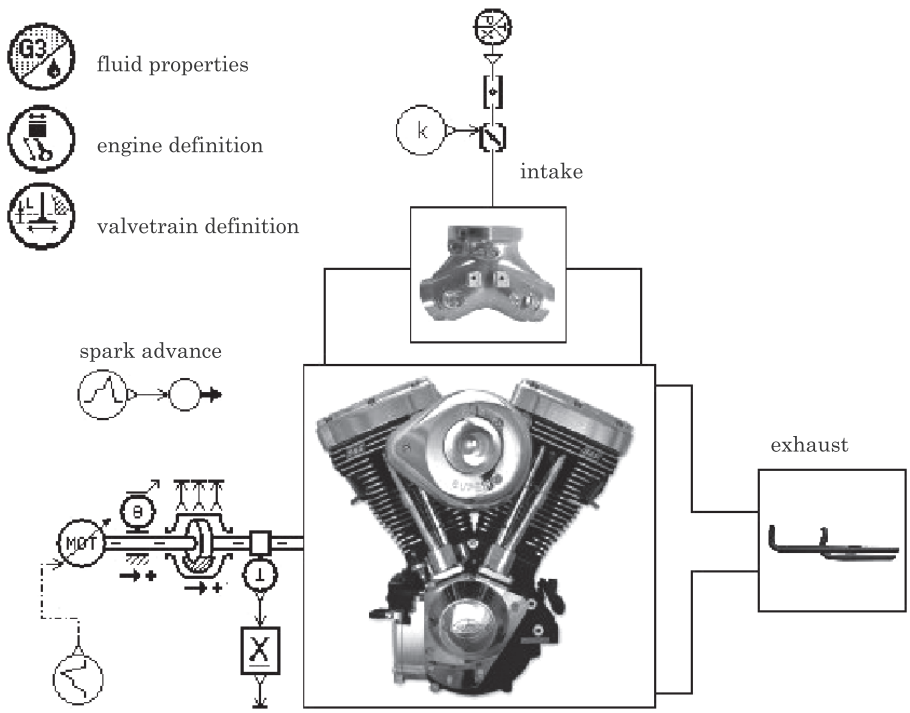

Fig. 3. Baseline Engine Model

They also involve choosing one of two methods for fuel supply (to the carburetor or the injectors) without changing the design scheme. The study of opportunities for application and optimization of such a system is the subject of further research. Calculations concerning one variant are made in a way that allows giving access for the program to the input file containing eight factors, while the output file contains quality criteria, in this case: «myObjective». Our goal is to reach a power value of 75 kW, we have to set the parameter «myObjective» as the objective function. Thus, the NLPQL process will try to decrease this quantity down to zero. The NLPQL algorithm is based on the use of gradients and is an iterative

process. It tries to decrease the objective function to zero. For this, it computes the gradients of the objective function and constraints in all directions available in the design space (each input parameter involved in the optimization process is a direction).

In our physical example, the problem is to find an appropriate set of parameters to reach a specified injected quantity, and to keep the constraints not violated.

Program automatically parses input and output files, as specified by the designer. Parsing input file for the input parameters, and substituting values from the DoE matrix (Tab. 2) for eight factors for those parameters in input files for each run case, saves the designer a considerable amount of time.

Table 2

DoE matrix of full factorial

Point	Diameter	len	IVD	EVD	Lex	Pole	IVO	EVC
1	-1	-1	-1	-1	-1	-1	-1	-1
2	1	-1	-1	-1	-1	-1	-1	-1
3	-1	1	-1	-1	-1	-1	-1	-1
4	1	1	-1	-1	-1	-1	-1	-1
5	-1	-1	1	-1	-1	-1	-1	-1
...	...	...	...	...	...	...	...	...
255	-1	1	1	1	1	1	1	1
256	1	1	1	1	1	1	1	1

Accordingly, such automation of tasks would help the designers spend less time on routine tasks, and focus their attention on more creative engineering work. The time difference between using a traditional routine engineering approach and an automation engineering approach is called the cycle time reduction.

Selecting a DoE and/or an Optimization technique is straightforward and is done using the graphical menus to select the method or technique of interest. Optimization solution constraints are also provided at this time. In the current study, the intake and exhaust valve diameters were constrained using a special relation with the cylinder bore. This was done to ensure that the area of all valves did not exceed a specified fraction of the cylinder bore area, based on packaging, stress analysis results, and other practical considerations.

Simulation Runs The average time for running one experiment is 30 seconds. The combined number of runs to convergence for both the DoE and Optimization was found to be 279. Knowing that the DoE is comprised of 256 runs would indicate that the optimization convergence, from the DoE estimated optimal, occurred over 23 runs (or 12.5 minutes of CPU run-time.) Using the same simple calculation, the DoE run-time was 128.5 minutes.

Post-processing and Analysis of Results keeps track of the input parameters and output response for each run case in a database. The program also has the capability of displaying dynamically the output results on a graphical scope. Figure 4 shows a sample graph of the «myObjective» response, as the DoE and then the optimization progressed, against the run (trial) counter. Please note that following the DoE part of the study (after run counter = 23), the optimization technique is automatically started and one can easily see how the optimization drives the response to convergence.

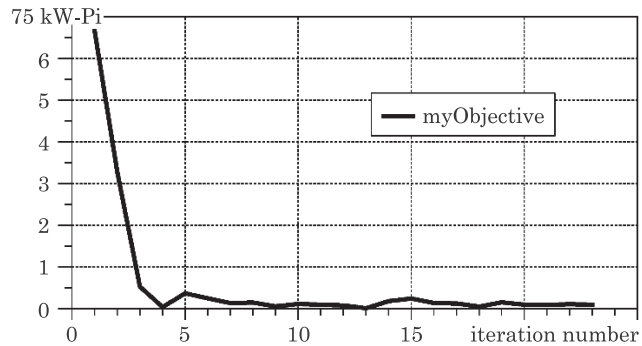

Fig. 4. Optimization Graphical Scope

One of the useful post-processing tools that provides the designer with is the Pareto graphs. These are ordered bar charts showing the average effects of the input factors on the selected response. Using such graphs helps the designer identify the top factors that significantly contributed to the response under study. Figure 5 shows an example Pareto graph from the study covered in this paper. Red bars are used to indicate positive values since the absolute values of the effects are plotted. Green bars indicate a negative relationship between a factor and its average effect on the response. For example, let's consider the two factors at the top in Figure 5*a*. These are labeled "diameter" and EVD, which represent, for the engine covered in this paper, the exhaust valve and pipe diameters respectively. These were the two top contributing factors to the change in the response of the study. The Pareto graph (CZYZAK, JASZKIEWICZ 1998) shows a direct relationship between the aforementioned factors and the response (red bar color). What is more, the reliance of quality on "diameter" in the accepted conditions of the 3rd factor experiment is 43%, while EVD has influence on quality of 36%. On the other hand, the fourth factor diameter/IVD (grey bars) in Figure 5*a* show an inverse relationship with the response. The designer can benefit from the Pareto graph by identifying fewer factors than had resulted from the brainstorming session. Now instead of considering all 8 factors (parameters),

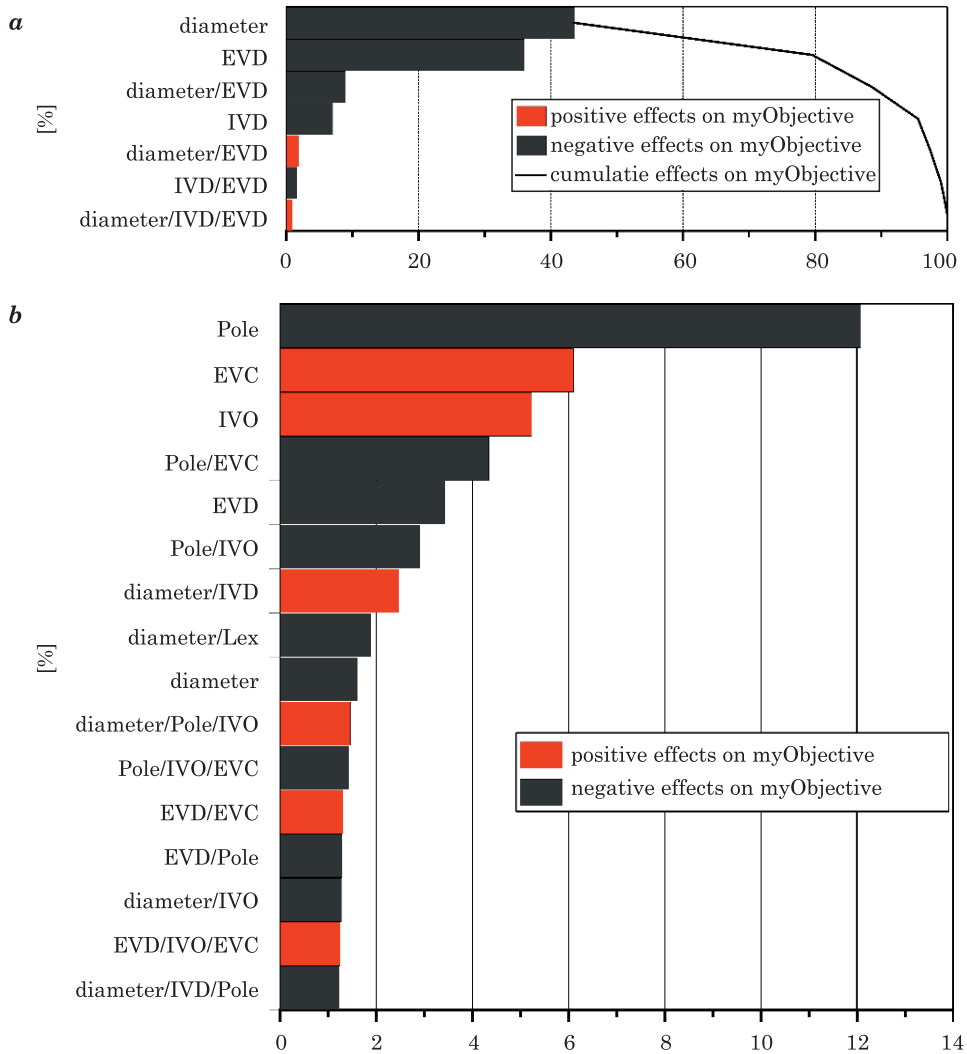

Fig. 5. Pareto diagram for results: *a* – 3 factors DoE (Fig. 4), *b* – 8 factors DoE (Tab. 1)

the designer may choose to focus only on the top 3 or more (Fig. 5*b*) factors that affected the response most significantly.

Under the conditions of the 8^{th} factor experiment, the impact of "pole" the highest it amounts 12.1%. The reliance of "myObjective" on "diameter" is reduced to 1.65%, while the EVD level of 3.5%. The results reveal the difficulties encountered during the analysis of the results obtained with the use of DoE. Thus, the next reasonable step in formalization of the task to find optimum parameters of the engine intake system and the exhaust system is to apply one of the optimization methods.

The results of using the method NLPQL

In the second stage of the solution process regarding optimization, with the use of the NLPQL method, the value of global optimum was achieved in accordance with the set criterion of «myObjective». The limits for changes in

Table 3

The dependence of the quality criterion «myObjective» on changes in selected factors

Factor	Distribution of calculated points
Intake valve diameter (IVD)	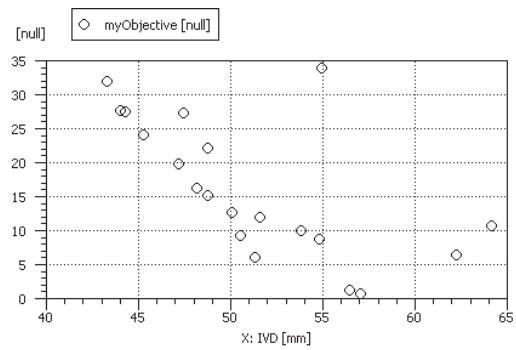
Exhaust valve diameter (EVD)	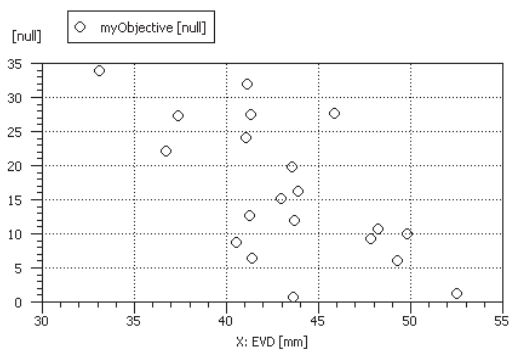
Pipe exhaust diameter (diameter)	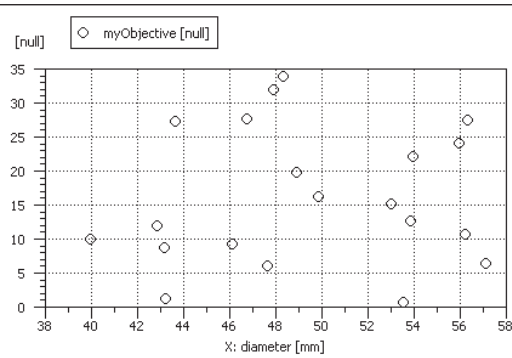

factors, presented in Table 1, as well as the parameter vector for the initial point of the optimum search were selected on the basis of an analysis of DoE results and a test of parameter space by using the Monte Carlo method (RUBINSTEIN, KROESE 2008, SHLOMO, SHAUL 2011). Partial results for scans of the parameter space with the Monte Carlo method have been presented in Table 3.

The results in Table 3 imply that it is possible to have an unambiguous determination of the reliance of correlation for the diameter of the inlet pipe; the change effect for the diameter of the outlet pipe is harder to predict. In the case of the diameter of the exhaust pipe, the reliance is also obvious, but it has a vivid stochastic character.

The application process of the NLPQL method that covered the search for an optimum value of 8 factors in accordance with the «myObjective» criterion consisted of 23 iterations (Fig. 6). What is more, the last 4 iterations were conducted with the accuracy of search for optimum set to 0.01. Consequently, the search for an optimum process was complete when the obtained value of «myObjective» = 9.7214789533E-02.

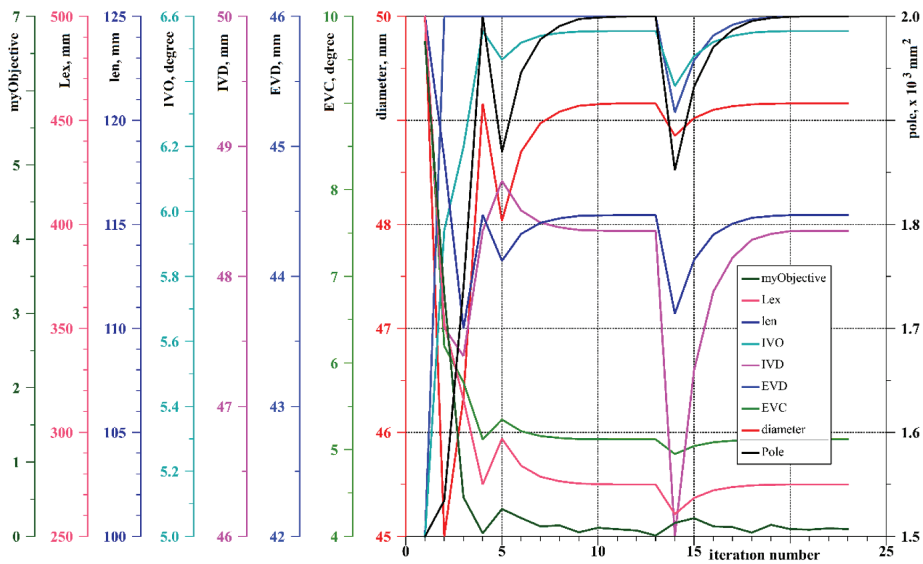

Fig. 6. Optimization Graphical Scope 8 factors

The last entry in the database file is the most feasible, and also the global optimal, design. The final results of the optimization study showed a brake power improvement of about 5.4% at rated power compared with the baseline value. Improvement on the power response was also observed at low and high RPMs of the engine operation range.

Conclusions

The application of the known methods of studying spatial parameters allows optimizing the design and tunable parameters of the engine and thereby improving its operating parameters at selected points of the external velocity characteristic. As an example, the elements of the engine intake and exhaust system are considered, which determine the quality of gas exchange. The chosen optimization strategy makes it possible to use the concept of inertia supercharging of engine cylinders, in the conditions of modernization. The consideration involved 8 design parameters of systems and one quality criterion – engine power. The proposed optimization method can be used to upgrade motorcycle engines in operation.

To find the optimal solution, the initial parameter vectors are formed using the full-factor experiment planning methods.

Literature

ALESSANDRO R., MARCO T. 2014. *Dynamic analysis of a motorbike engine timing system: Experimental and numerical investigation of the geartrain*. Mechanical Systems and Signal Processing, 48(1-2): 325-338.

BLAIR G.P., MACKEY D.O., ASHE M.C., CHATFIELD, G.F. 2003. *Exhaust Tuning on A Four-Stroke Engine: Experimentation and Simulation*. SAE Trasaction, American Technical Publishers LTD, 112: 22-34.

BRANNEN D.E., MILLER J.R., IBRAHIM N.A. 2012. *Harley-Davidson*. Inc. Journal of Applied Case Research. 10(1).

CZYZAK P., JASZKIEWICZ A. 1998. *Pareto simulated annealing – A metaheuristic technique for multipleobjective combinatorial optimization*. Journal of Multi-Criteria Decision Analysis, 7(1): 34-47.

DESHMUKH D., KUMAR R., GARG M., NAYEEM M.J., LAKSHMINARASIMHAN V. 2004. *Optimisation of Gas Exchange Process on a Single Cylinder Small 4-Stroke Engine by Intake and Exhaust Tuning: Experimentation and Simulatio*. SAE Trasaction, American Technical Publishers LTD, 113: 1741-1749.

HARRISON M.F., DUNKLEY A. 2004. *The acoustics of racing engine intake systems*. Journal of Sound and Vibration, 271: 959–984.

HD Manual. 2015.

HEYWOOD J.B. 1988. *Internal Combustion Engines Fundamentals*. McGraw-Hill Book Co., Singapore.

JAWAD B.A., LOUNSBERY A.L., HOSTE J.P. 2001. *Evolution of Intake Design for a Small Engine Formula Vehicle*. SAE Trasaction, American Technical Publishers LTD, 110: 1318-1325.

MACKEY D.O., CRANDALL J.G., CHATFIELD G.F., ASHE M.C. 2002. *Optimization of Exhaust-Pipe Tuning on a 4-Stroke Engine Using Simulation*. SAE Trasaction, American Technical Publishers LTD, 111: 242-255.

ROSS P.J. 1998. *Taguchi Techniques for Quality Engineering*. McGraw-Hill, New York.

RUBINSTEIN R.Y., KROESE D.P. 2008. *Simulation and the Monte Carlo Method*. Second Edition. J. Wiley & Sons Inc., New York.

SCHITTKOWSKI K. 1986. *NLPQL: A Fortran subroutine for solving constrained nonlinear programming problems*. Annals of Operations Research, 5(2): 485–500.

SCHITTKOWSKI K. 2011. *A robust implementation of a sequential quadratic programming algorithm with successive error restoration*. Optimization Letters, 5(2): 283-296. http://dx.doi.org/10.1007/s11590-010-0207-9.

SHIH C.-J., YEH C.-N., CHANG T.-H. 2012. *Experimental Optimization and Analysis of Intake and Exhaust Pipeline for Small Engine Motorcycle*. Journal of Applied Science and Engineering, 15(1): 21-30.

SHLOMO M., SHAUL M. 2011. *Applications of Monte Carlo Method in Science and Engineering*. Published by InTech, Rijeka, Croatia.

STELIOS D.G, STELLA S., MANOHAR A. 2014. *A class of composite designs for response surface methodology*. Computational Statistics & Data Analysis, 71: 1124-1133.

SYAHRULLAH L.O.I., SINAGA N. 2016. *Optimization and Prediction of Motorcycle Injection System Performance with Feed-Forward Back-Propagation Method Artificial Neural Network (ANN)*. American Journal of Engineering and Applied Sciences, 9(2): 222-235. doi: 10.3844/ajeassp.2016.222.235.

WANG J., MA Y., OUYANG L., TU Y. 2016. *A new Bayesian approach to multi-response surface optimization integrating loss function with posterior probability*. European Journal of Operational Research, 249(1): 231-237.

YONGFAN L., SHUAI Z., JING W. 2017. *Research on the Optimization Design of Motorcycle Engine Based on DOE Methodology*. Procedia Engineering, 174: 740-747. https://doi.org/10.1016/j.proeng.2017.01.216.

ZHAO F. 2011. *A review of research about variable intake manifold*. Machinery, Materials Science and Engineering Applications, 228: 299-302.

Technical Sciences, 2019, 22(2), 151–167

UNIWERSYTET WARMIŃSKO-MAZURSKI W OLSZTYNIE

Quarterly peer-reviewed scientific journal
ISSN 1505-4675
e-ISSN 2083-4527
TECHNICAL SCIENCES
Homepage: www.uwm.edu.pl/techsci/

APPLICATION OF SONICATION AND FREEZING AS INITIAL TREATMENTS BEFORE MICROWAVE-VACUUM DRYING OF CRANBERRIES

Izabela Staniszewska, Szymon Staszyński, Magdalena Zielińska

Department of Systems Engineering
University of Warmia and Mazury in Olsztyn

Received 13 February 2019, accepted 27 February 2019,available online 7 March 2019

Keywords: Cranberry, vacuum drying, microwave drying, drying pretreatment, texture, density, color.

Abstract

The aim of study was to determine the influence of sonication and freezing on the kinetic of the microwave-vacuum drying, energy consumption and physical properties of whole cranberries as well as evaluate the applicability of sonication instead of freezing in order to change their physical properties and the drying kinetic of whole cranberries. Microwave-vacuum drying of whole cranberries with/without initial treatments took from 12±1 to 14.5±0.5 minutes. All of treatments did not significantly shorten the drying time of cranberries. However, they increased SMER values even by 31%. Despite of cryogenic freezing, all of treatments significantly increased the values of D_{ew}. Sonication combined with drying allowed to obtain dried berries characterized by the lowest cohesiveness (0.19±0.02), springiness (0.62±0.02) and chewiness (3.4±0.8 N), while cryogenic freezing combined with drying allowed to obtain dried fruits characterized by highest springiness (0.75±0.03) and low chewiness (3.3±0.5 N). The highest lightness (32.2±0.7), redness (32.6±0.8), and yellowness (11.1±0.7) were found for fruits subjected to initial convective freezing before drying. The efficiency of sonication in color change was comparable to cryogenic freezing and much lower than convective freezing. All of initial treatments increased such thermal properties of dried cranberries as thermal conductivity and thermal diffusivity.

Correspondence: Izabela Staniszewska, Katedra Inżynierii Systemów, Wydział Nauk Technicznych, Uniwersytet Warmińko-Mazurski, ul. Heweliusza 14, 10-718 Olsztyn, phone: +48 89 523 49 72, e-mail: izabela.staniszewska@uwm.edu.pl

Introduction

Cranberries (*Vaccinium macrocarpon* L.) contain high amount of biologically active substances, including phenolic acids (benzoic, hydroxycinnamic and ellagic acids) and flavonoids (anthocyanins, flavonols and flavan-3-ols) (McKay, Blumberg 2007). They provide minerals, organic acids, pectins, vitamins such as A, B_1, B_2 and C to the body. Raw and dried cranberry fruits can be used as ingredients of breakfast cereals, salads and other dishes (Skrovankova et al. 2015). Cranberries consist mainly of water, which constitutes about 86% of the composition of fresh fruits. Due to their high moisture content, cranberries are usually processed in order to reduce microbial activity, minimize product deterioration and extend their shelf-life (Zielinska et al. 2018a). Dried fruits with sufficiently low A_W may ensure the both low enzymatic activity and microbial spoilage.

Hot air drying makes cranberries available to consumers throughout the whole year. Removal of moisture from the whole cranberries is difficult due to its waxy skin, which inhibits the moisture movement. For example, hot air drying takes from 310 to 11,700 minutes (Zielinska, Zielinska 2019). The exposure of berry fruits to high air temperature and significant moisture loss during drying lead to significant changes in sample texture (Zielinska et al. 2018a). Hot air drying produces brittle fruits that are difficult to store and transport and are not suitable for direct consumption. Hot air can be replaced by the alternative heat source, such as microwaves. Drying with microwaves shortens the drying time, limits oxidation and positively influences physicochemical properties of dried products (Soysal et al. 2009). However, the application of microwaves under atmospheric pressure may significantly deteriorate the quality of the final product. Microwaves cause volumetric heating, while reduced pressure eliminates the risk of excessive material temperature and degradation of bioactive compounds (Zhang et al. 2006). The application of microwaves under reduced pressure allows to produce dried snacks characterized by hard and crispy texture and considerable resistance to stress associated with manufacturing, packaging, storage, and delivery. Microwave-vacuum drying results in high retention of polyphenols and high antioxidant activity of dried cranberries (Zielinska, Zielinska 2019). Microwave-vacuum drying of cranberries at microwave power of 150 to 500 W leads to rapid evaporation of moisture from capillaries (Zielinska et al. 2019). Whole cranberries lost moisture several dozen times faster during microwave-vacuum than hot air drying. The time of microwave-vacuum drying of whole cranberries is significantly shorter than the time of hot air drying and it ranges from 8 to 91 minutes (Zielinska et al. 2019). The five-fold increase in microwave power from 100 to 500 W decreases drying time by up to 90%. Among the various variants of microwave-vacuum drying used for drying of whole cranberries, drying at low microwave powers, i.e. from 100 to 300 W

is recommended as a good alternative to the hot air drying of cranberries, in terms of their phytochemicals and color (ZIELINSKA, ZIELINSKA 2019). Effective moisture diffusivities and drying rates are higher, whereas drying times are shorter for the samples dried by microwave-vacuum drying compared with the samples processed by hot air drying.

The negative effect of microwave-vacuum drying on the material properties can be minimized by the application of low microwave power and pressure in the drying chamber. Additionally, various initial treatments can be applied before drying to change material properties and speed up the drying process. Up to date, initial treatments of berries before drying processes have relied on mechanical, chemical and thermal treatments or their combinations, such as sonication, convective freezing, cryogenic freezing, osmotic dehydration, ultrasound-assisted osmotic dehydration, osmotic dehydration combined with microwave-vacuum pretreatment, etc. (GRABOWSKI et al. 2007, NOWAK et al. 2018, RENNIE, MERCER 2013, SUNJKA et al. 2004, ZIELINSKA et al. 2015, 2018a, b, 2019, ZIELINSKA, MARKOWSKI 2018, ZIELINSKA, ZIELINSKA 2019). Among mechanical pretreatments, sonication performed at frequency between 18 and 100 kHz and intensity higher than 1 $W \cdot cm^{-2}$ (typically in the range from 10 to 1000 $W \cdot cm^{-2}$) can be used as an initial treatment of different food products (MCCLEMENTS 1995). It can be used to increase e.g. the permeability of the skin of berry fruits and increase the drying rate (ZIELINSKA et al. 2015). The effect of acoustic microstreaming accelerates heat and mass transfer processes during drying (NASCIMENTO et al. 2016). Additionally, sonication prevents high losses of polyphenols and flavonoids during drying and increases the availability of vitamins B_1, B_2, B_3, and B_6 in the dried product (FERNANDES et al. 2015, RODRIGUEZ et al. 2014). Sonication represents an interesting technique for processing of raw blueberries and can be a good alternative for time and energy-consuming convective freezing of whole fruits (NOWAK et al. 2018). Also, convective and cryogenic freezing can be applied to biological materials before drying in order to change material properties and influence the drying kinetic. Nevertheless, the combination of freezing and drying adversely affects the quality of the final product, generating harder, more chewy and gummy fruits compared with those dried without initial pretreatment. Convective freezing significantly reduces time and specific energy consumption of hot air drying (ZIELINSKA et al. 2015). However, it does not significantly shorten the time of microwave-vacuum drying (ZIELINSKA, ZIELINSKA 2019). Sonication and freezing may significantly decrease particle density and increase porosity of whole blueberries. Additionally, sonication as well as freezing may produce significantly softer, less chewy and gummy blueberries compared to raw samples (NOWAK et al. 2018). Among thermal treatments, initial microwave-vacuum treatment has gained relevance in food processing (ZIELINSKA, MARKOWSKI 2018). Microwave-vacuum pretreatment at low microwave power (100 W) before osmo-microwave-vacuum drying of berries

results in high retention of phenolic compounds, high antioxidant activity and attractive color, which indicates the high content of total anthocyanins and flavonoids (ZIELINSKA et al. 2018b).

Literature studies on drying of berry fruits show the need for development of innovative drying processes and pretreatments, which help to change the structure of the material, shorten the drying time, and thus obtain a high quality of dried products determined by their physical properties. There is a general scarcity of research into the possibility of using sonication (short mechanical treatment) instead of convective freezing (time and energy-consuming thermal treatment) or cryogenic freezing (a process that generates high costs due to continuous refilling of the refrigerant) of whole berries (NOWAK et al. 2018). A better understanding of changes in the physical properties of whole cranberries subjected to different initial treatments and microwave-vacuum drying could contribute to preserving the desirable characteristics of the dried products. Therefore, the aim of this study was to:

a) determine the influence of sonication (non-thermal) and freezing (thermal) treatments on the kinetic of the microwave-vacuum drying, energy consumption and physical properties of whole cranberries (*Vaccinium macrocarpon* L.);

b) evaluate the applicability of sonication instead of convective or cryogenic freezing in order to change their physical properties and thus change the drying kinetic of whole cranberries.

Among thermal and non-thermal treatments, sonication, convective freezing, ultrasound-assisted convective freezing, and cryogenic freezing were used. Additionally, samples were dried without any initial treatments. Among the material properties, such properties as moisture content, water activity, moisture diffusion, lightness, redness, yellowness, total differences in color, saturation and hue, thermal conductivity, thermal diffusivity, specific heat, density, porosity, hardness, cohesiveness, springiness, and chewiness were analyzed.

The results of this study can be used in practice by producers of berries, processed cranberry fruits suppliers, and manufacturers of equipment used in cranberry processing.

Research methodology

The test material consisted of whole cranberry fruits (*Vaccinium Macrocarpon* L.) delivered by GP Klasa Sp. z o.o (Klementowice, Poland). Fruits were manually harvested several weeks before the study, sorted and packed in sealed plastic containers. Cranberries were similar in color, shape and size. Raw cranberries (R) were refrigerated (2±2°C) at 90% relative humidity for up to 2 weeks. Whole cranberries were subjected to initial treatments (sonication, convective freezing, convective freezing preceded by sonication as well as cryogenic freezing) and

microwave-vacuum drying (Fig. 1). The initial moisture content of fresh fruits was about 7.49±0.02 kg $H_2O \cdot kg\ DM^{-1}$. The control sample composed of raw berries was not subjected to the drying processes. Sonication was conducted using ultrasonic disruptor Scientz-650E (Ningbo Scientz Biotechnology Co. Ltd., China) equipped with 6 mm titanium ultrasound probe. Sonication was conducted for 10 min (1 s impulse and 1 s gap between impulses) in a water bath containing 1 dm^3 of distilled water. The ultrasound frequency was 25±5 kHz, while ultrasonic power input was 600 W. Cranberries were convectively and cryogenically frozen. They were placed in a freezer operating at -18°C and left for 48 hours. Additionally, they were immersed in a liquid nitrogen (a boiling temperature of -196°C).

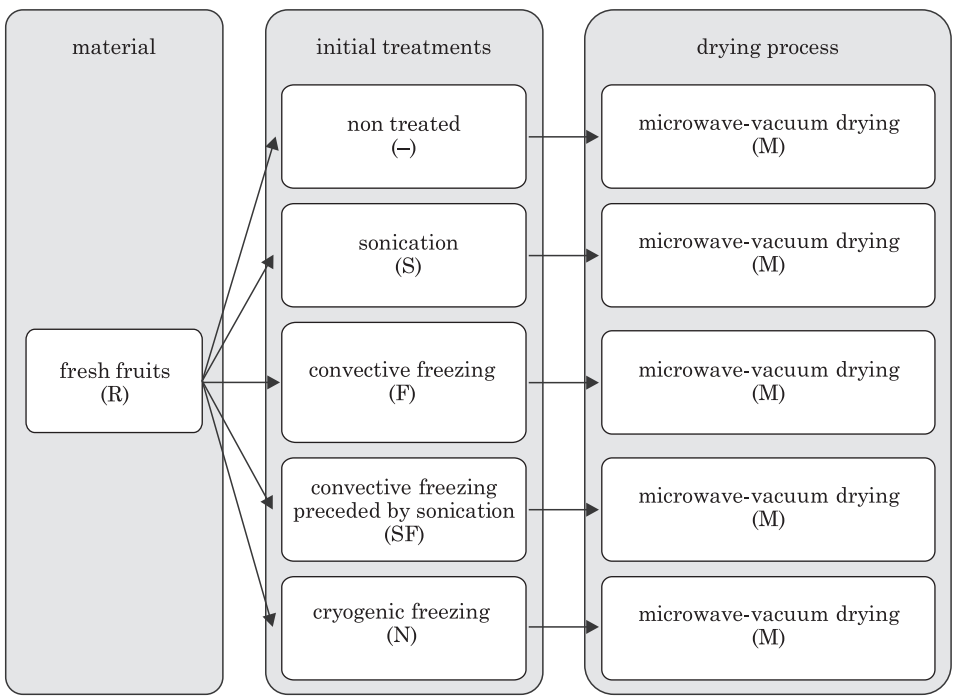

Fig. 1. Processing scheme of cranberry fruits

A microwave-vacuum dryer (PROMIS TECH, Wroclaw, Poland) was used for drying experiments (Fig. 2). System comprised a motor, a drying chamber, a regulating valve, a condensation unit, a microwave generator, a microwave circulator, a temperature measuring unit, a pressure measuring unit, a control unit. Dryer operated at a microwave power of 300 W and absolute pressure of 5± kPa. During drying, changes in sample mass, sample temperature, pressure in the drying chamber and energy consumption were recorded. To evaluate

changes in sample mass, the drying time of every portion of fruits was prolonged. The mass of the sample used in each drying experiment was 0.200±0.003 kg. Microwave-vacuum drying was stopped when the surface temperature of fruits increased sharply. The experiments were conducted in duplicate.

Fig. 2. Microwave-vacuum drying set up

The energy consumption during drying was measured using the energy meter (MPR-53/EPM-07, model MPR-53S, ENTES Elektronik Cihazlar Imalatve Ticaret A.S., Istanbul, Turkey). The specific moisture extraction rate (SMER) was expressed as follows (SCHMIDT et al. 1998):

$$\text{SMER} = \frac{M_{\text{mr}}}{E_{\text{input}}} \tag{1}$$

where:

M_{mr} – the mass of moisture removed from the dried material [kg H_2O],

E_{input} – energy input [kWh].

The moisture content of fruits was determined gravimetrically using vacuum drying oven DZ ZBC II (Chemland, Stargard Szczeciński, Poland). Cranberries were dried at 70°C for 24 h (AOAC 2002). The water activity (A_W) was measured using the Aquaspector AQS-31-TC (NAGY, Germany). The final result was the arithmetic mean of the two repetitions carried out for a given sample.

Color measurements were carried out using spectrophotometer (Hunterlab MiniScan XE Plus, Reston, VA, USA) under standard illuminant D65, 10° observer and 8° diaphragm. The spectrophotometer cooperated with the MultiScan v.11.06 software. The color of fruits was expressed in CIEL*a*b* space, where achromatic component L*, as well as two chromatic components a*, and b* denoted

lightness, redness, and yellowness, respectively. The color of cranberries was measured directly on the fruit surface. The total changes in color (ΔE^*), saturation (ΔC^*) and hue (ΔH^*) during processing were calculated according the formulas presented in the literature (ZIELINSKA, MARKOWSKI 2012). The results were averaged over 32 measurements.

Thermal conductivity (λ) and thermal diffusivity (a) of cranberries were determined using thermal analyzer (KD2 Pro meter, Decagon Devices, Pullman, USA) with the dual-needle SH-1 probe. The specific heat (C_p) of cranberries was calculated based on the measured values of Thermal conductivity (λ), thermal diffusivity (a) and apparent density (ρ_p). The measurements were performed in five replicates.

Texture profile analysis was performed using a TA-HD plus texture analyzer (Stable Micro Systems, Godalming, UK). The time between compressions was equal to 1 s, relative deformation was equal 50%, the speed of piston was equal to 2 mm $\cdot$ s^{-1}. Each sample was analyzed in 15 replications. Mechanical properties of fruits were automatically computed using texture analyzer software, Texture Exponent Stable Micro Systems v.6.1.11.0. Hardness was defined as the maximum force measured during the first compression. Cohesiveness was defined as the ratio of the area during the second compression of the sample to the area of the first sample compression. Springiness was defined as the ratio of time from the start of the second area up to the second probe reversal over time between the start of the first area and the first probe reversal. Chewiness was defined as the product of hardness, cohesiveness, and springiness (CHONG et al. 2014).

Particle density (ρ_p) was measured using hydrostatic method. The measurements were done in triplicate. It was calculated from the following formula (RAHMAN 1995):

$$\rho_p = \frac{m_p}{m_p - m_w} \cdot \rho_w \tag{2}$$

where:

ρ_p – particle density [g $\cdot$ cm^{-3}],
ρ_w – water density [g $\cdot$ cm^{-3}],
m_w – mass of sample immersed in water [g],
m_p – mass of sample [g].

Apparent porosity (ε_{ap}) was calculated from the following formula (NOWAK et al. 2018):

$$\varepsilon_{ap} = (1 - \frac{\rho_p}{\rho_{DM}}) \cdot 100\% \tag{3}$$

where:

ρ_p – particle density [g $\cdot$ cm^{-3}],
ρ_{DM} – density of dry mass [g $\cdot$ cm^{-3}].
The measurements were done in triplicate.

Density of dry mass of cranberries powder was determined by the liquid pycnometer method. Cranberries were dried at 105°C for 24 h in an air-oven (FED53 127 Binder, US) according to the standard requirements (AOAC 1975) and were ground in a laboratory mill. Samples of approximately 2 g were used in each experiment. The mass of the sample was measured to the nearest 0.001 g using an electronic balance (RADWAG, WPS 4000/C/2, Radom, Poland). Non-water miscible liquid (xylene) and a calibrated glass pycnometer with estimated volume of 50 ml (LG-3838-3658, Chemland Ltd., Poland) were used. Xylene density was determined at 864±1 kg · m^{-3}. The measurements were done in triplicate. Density of dry mass was calculated from the following equation (ZIELINSKA et al. 2015):

$$\rho_{DM} = \frac{0.864 \cdot (m_3 - m_1)}{m_2 + (m_3 - m_1) - m_4} \tag{4}$$

where:

ρ_{DM} – density of dry mass [kg · m^{-3}],
m_1 – mass of an empty pycnometer [g],
m_2 – mass of the pycnometer with the non-solvent [g],
m_3 – the total mass of the pycnometer and the powder [g],
m_4 – total mass of the pycnometer, the non-solvent liquid and the powder [g].

Volumetric shrinkage (S_v) of particle was calculated from the following formula (ZIELINSKA et al. 2015):

$$S_v = (1 - \frac{V_s}{V_0}) \cdot 100\% \tag{5}$$

where:

V_s – volume of sample after drying [cm^3],
V_0 – volume of sample before drying [cm^3].
The measurements were done in triplicate.

The coefficient of moisture diffusion was determined on the basis of the least-squares nonlinear estimation, Levenberg-Marquardt test, from equation (6) assuming constant values of the effective moisture diffusion coefficient and fruit shape as well as considering initial (7) and boundary conditions (8) (ZIELINSKA, MARKOWSKI 2018).

$$u(t = 0, x, y, z) = u_0 \tag{6}$$

$$t > 0 \rightarrow u(t, x, y, z) = u_r \tag{7}$$

$$\frac{u(\tau) - u_r}{u_0 - u_r} = \frac{6}{n^2} \cdot \sum_{n=1}^{\infty} \frac{1}{n^2} \exp(-n^2 \cdot n^2 \cdot \frac{D_{ew} \cdot \tau}{R^2}) \tag{8}$$

where:

$u(\tau)$ – moisture content at the moment τ [kg H_2O·kg DM^{-1}],
u_r – equilibrium moisture content [kg H_2O · kg DM^{-1}],

u_0 – initial moisture content [kg $H_2O \cdot$ kg DM^{-1}],
n – number of measurements [-],
D_{ew} – effective moisture diffusivity [$m^2 \cdot s^{-1}$],
τ – time of drying [s],
R – radius of a sphere [m].

The calculations were done using STATISTICA 12.0 software (StatSoft Inc., Tulsa, OK, USA). The analysis of variance for independent samples (Kruskal–Wallis's test) was carried out for samples without a normal distribution ($p \leq 0.05$). One-way ANOVA analysis (Duncan's test) was performed for samples with normal distribution ($p \leq 0.05$).

Results and discussion

To evaluate the effect of initial treatment on the kinetic of microwave-vacuum drying of whole cranberries, the changes in moisture contents (MC) vs. drying time (*t*) were monitored (Fig. 3). All of initial treatments significantly influenced the initial moisture contents of cranberries (Tab. 1). Even if it happened, they did not significantly shorten the drying time of cranberries. Microwave-vacuum drying of whole cranberries at 300 W, with or without initial treatments, took from 12±1 to 14.5±0.5 minutes. Also, they did not significantly change the shape of drying curve (Fig. 3). Microwave-vacuum drying allowed to obtain fruits of the final moisture contents and water activities of dried fruits in the range from 0.21±0.03 to 0.22±0.02 kg $H_2O \cdot$ kg DM^{-1} and from 0.267±0.005 to 0.314±0.002, respectively (Tab. 1). There were no significant differences between the final moisture contents of differently treated fruits. However, initial treatments significantly influenced the values of water activity of dried berries (Tab. 1). The results show that all of initial treatments allowed for the preservation of fruits and protection of biological material against the development of undesirable microorganisms. Among different treatments, sonication and ultrasound-assisted freezing before drying allowed to obtain final products of the lowest water activity.

To evaluate the effect of initial treatment on the kinetic of microwave-vacuum drying of whole cranberries, also the changes in material temperatures (*T*) and specific moisture evaporation rates (SMER) vs. moisture content (MC) were monitored (Fig. 3). The sudden jumps and drops in surface temperature of dried berries can be observed during microwave-vacuum drying of whole (treated or non-treated) cranberries (Fig. 3). It can be explained by the fact that an increase in capillary pressure inside the dried objects increased the tensile stress and promoted microcracks in the berry skin followed by steam emission and increase in surface temperature of material. Subsequently, the sudden outflow of water

Table 1

Drying time, moisture content, water activity, specific moisture evaporation rate and moisture diffusion coefficient of cranberries subjected to different pretreatments and microwave-vacuum drying at microwave power of 300 W

Sample	t [min]	MC_i [kg $H_2O \cdot$ kg DM^{-1}]	MC_f [kg $H_2O \cdot$ kg DM^{-1}]	A_W [-]	SMER [kg $H_2O \cdot kWh^{-1}$]	$D_{ew} \cdot 10^8$ [$m^{-2} \cdot s$]
RM3	12.0 ± 1.0^b	7.50 ± 0.02^a	0.22 ± 0.02^a	0.314 ± 0.002^a	3.5 ± 0.2^b	0.76 ± 0.03^c
SM3	14.5 ± 0.5^a	7.00 ± 0.02^a	0.21 ± 0.01^a	0.267 ± 0.005^d	3.9 ± 0.2^b	0.97 ± 0.02^b
FM3	14.0 ± 0.5^a	7.00 ± 0.02^a	0.22 ± 0.01^a	0.304 ± 0.001^b	4.6 ± 0.2^a	1.60 ± 0.04^a
SFM3	14.5 ± 0.5^a	7.27 ± 0.02^a	0.21 ± 0.03^a	0.270 ± 0.001^d	3.8 ± 0.2^b	1.52 ± 0.04^a
NM3	14.5 ± 0.5^a	7.32 ± 0.02^a	0.22 ± 0.01^a	0.287 ± 0.002^c	3.6 ± 0.2^b	0.58 ± 0.03^d

Table contains mean values ± standard errors.
$^{a, b, c, d, e}$ – the same letters in columns mean no statistical differences between samples ($p \leq 0.05$).
Symbols: RM3, SM3, FM3, SFM3, NM3 – raw (non-treated), sonicated, convectively frozen, sonicated and convectively frozen as well as cryogenically frozen fruits subjected to microwave-vacuum drying at microwave power of 300 W, t – drying time [min], MC_i – initial moisture content [kg $H_2O \cdot$ kg DM^{-1}], MC_f – final moisture content [kg $H_2O \cdot$ kg DM^{-1}], A_W – water activity [–], SMER – specific moisture evaporation rate during microwave-vacuum drying at microwave power of 300 W [kg $H_2O \cdot kWh^{-1}$], D_{ew} – coefficient of effective moisture diffusion [$m^{-2} \cdot s$].

vapor from the surface of berries reduced pressure inside the dried particles. It allowed to close the microcracks that occurred on the surface of dried fruits and thus reduced surface temperature of dried fruits (ZIELINSKA et al. 2019).

Initial treatments increased SMER values during microwave-vacuum drying of whole cranberries and lowered (even ≈ 10%) the surface temperature of dried material (Tab. 1). The changes in local temperatures of material can explain the changes in the values of local SMER (Fig. 3). The highest values of local material temperature and the lowest SMER values were noted during drying of non-treated berries (Fig. 3*a*). In this case, average SMER value reached 3.5±0.2 kg $H_2O \cdot kWh^{-1}$. On the other hand, the lowest values of local material temperature and the highest SMER values were noted during drying of convectively frozen berries (Fig. 3*c*). In this case, average SMER value reached 4.6±0.2 kg $H_2O \cdot kWh^{-1}$. Compared to non-treated samples, much lower energy input registered during microwave-vacuum drying of treated berries was enough to reach quite high material temperature that allowed to evaporate comparable amount of moisture as in case of non-treated berries (Fig. 2). It should be mentioned that the average surface temperature of initially treated berries was higher than 50°C. Regarding energy consumption, the effectiveness of initial treatments was presented as follows: convective freezing (Fig. 3*c*), sonication (Fig. 3*b*), ultrasound-assisted convective freezing (Fig. 3*d*) and cryogenic freezing (Fig. 3*e*).

Compared to non-treated samples, sonication slightly increased the values of $D_{ew.}$ The study demonstrates that initial freezing had a significant effect on the moisture diffusion coefficient. The highest values of D_{ew} ($1.60 \pm 0.04 \cdot 10^{-8}$ and 1.52±0.04 $m^{-2} \cdot s$) were noted for convectively frozen cranberries and those

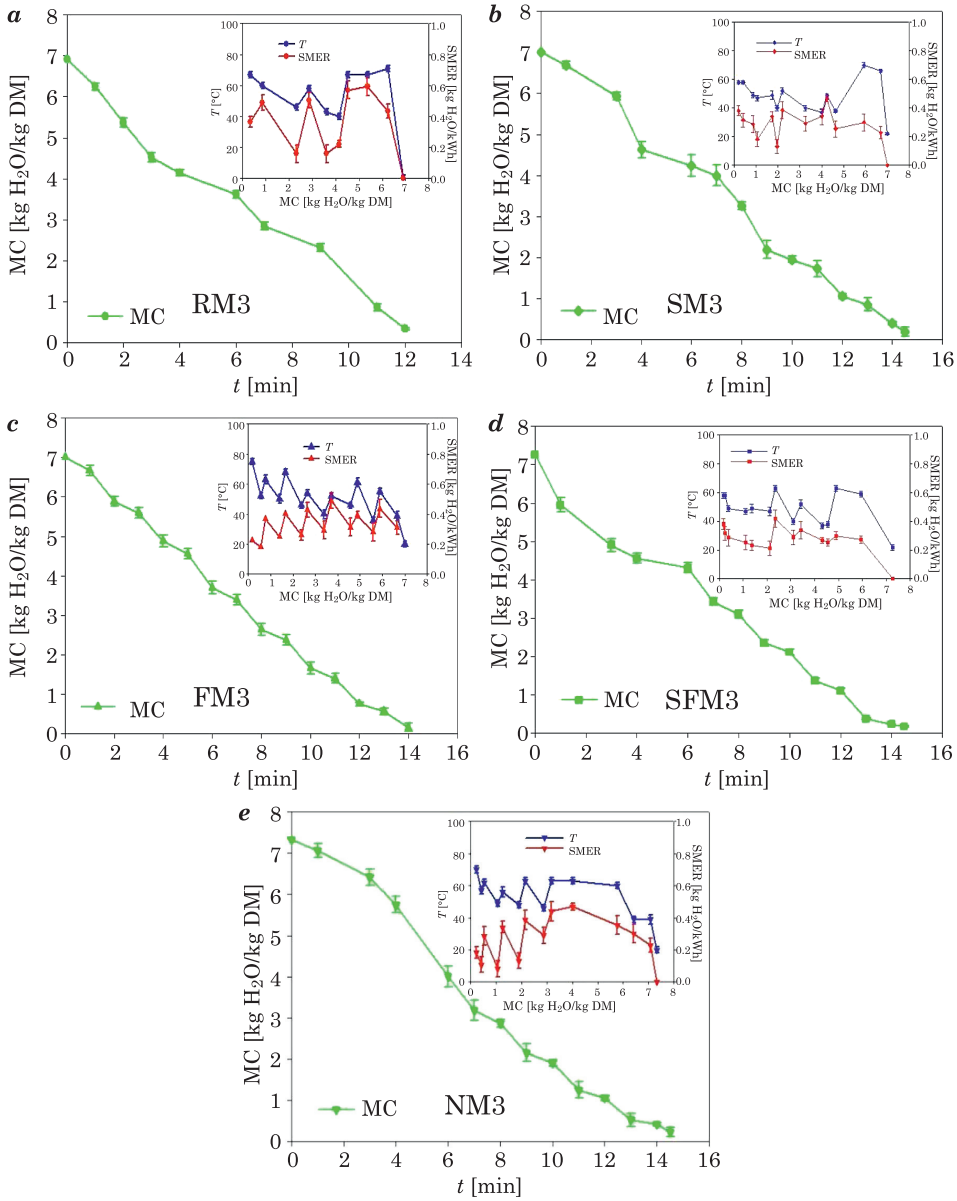

Fig. 3. Changes in moisture contents (MC) vs. drying time (t) as well as changes in material temperatures (T) and specific moisture evaporation rates (SMER) vs. moisture contents (MC) of whole cranberries subjected to different initial treatments and microwave – vacuum drying at microwave power of 300 W: *a* – RM3 – non-treated fruits subjected to drying, *b* – SM3 – fruits subjected to sonication and drying, *c* – FM3 – fruits subjected to convective freezing and drying, *d* – SFM3 – fruits subjected to convective freezing preceded by sonication and then subjected to drying, *e* – NM3 – fruits subjected to cryogenic freezing and drying

subjected to ultrasound-assisted convective freezing, whereas the lowest values of D_{ew} (0.58±0.03·10^{-8} m^{-2}·s) were observed for cryogenically frozen fruits (Tab. 1). The freeze-cracking that occurred during cryogenic freezing caused significant structure damage and thus difficulties in moisture diffusion and low values of D_{ew} during drying of cryogenically frozen fruits. The freeze-cracking was not observed during convective freezing, and thus much higher values of D_{ew} could be obtained (ZIELINSKA et al. 2019). In terms of D_{ew}, ultrasound-assisted convective freezing was even less effective than sonication alone. Regarding the values of D_{ew}, the effectiveness of initial treatments was presented as follows: convective freezing, ultrasound-assisted convective freezing, and sonication (Tab. 1).

Table 2 shows the values of color parameters as well as indices of total difference in color, saturation and hue of cranberries subjected to different pretreatments and microwave-vacuum drying at microwave power of 300 W. Fruits subjected to microwave-vacuum drying without any initial treatments were characterized by the lowest values of lightness (29.1±0.3), redness (21.4±1.0) and yellowness (4.6±0.5). Sonication did not significantly influence the lightness of dried fruits. However, it significantly increased redness (25.1±1.0) and yellowness (7.0±0.5) of dried berries. Its efficiency in color change was comparable to cryogenic freezing and much lower than convective freezing. Among different treatments, the highest values of lightness (32.2±0.7), redness (32.6±0.8), and yellowness (11.1±0.7) of dried fruits as well as the greatest changes in color (13.7±1.1), saturation (1.5±0.1) and hue (13.0±1.0) were found for fruits subjected to initial convective freezing before drying. Also ultrasound-assisted convective freezing can be recommended for cranberries processing, when the color of dried fruits is considered. However, this method was found to be less effective than sonication alone.

Table 2

The values of color parameters as well as indices of total difference in color, saturation and hue of cranberries subjected to different pretreatments and microwave-vacuum drying at microwave power of 300 W

Sample	L^* [-]	a^* [-]	b^* [-]	ΔE^* [-]	ΔC^* [-]	ΔH^* [-]
RM3	29.1±0.3^c	21.4±1.0^c	4.6±0.5^d	–	–	–
SM3	29.2±0.5^c	25.1±1.0^b	7.0±0.5^c	6.9±0.7^c	0.5±0.1^c	6.4±0.7^c
FM3	32.2±0.7^a	32.6±0.8^a	11.1±0.7^a	13.7±1.1^a	1.5±0.1^a	13.0±1.0^a
SFM3	31.0±0.5^{ab}	31.0±0.8^a	9.1±0.4^b	11.3±0.8^b	1.2±0.1^b	10.9±0.7^b
NM3	30.3±0.4^b	26.5±0.8^b	6.7±0.4^c	6.7±0.7^c	0.6±0.1^c	6.2±0.7^c

Table contains mean values ± standard errors.
$^{a, b, c, d}$ – the same letters in columns mean no statistical differences between samples ($p \leq 0.05$).
Symbols: RM3, SM3, FM3, SFM3, NM3 – raw (non-treated), sonicated, convectively frozen, sonicated and convectively frozen as well as cryogenically frozen fruits subjected to microwave-vacuum drying at microwave power of 300 W, L^* – lightness [-], a^* – redness [-], b^* – yellowness [-], ΔE^* – total color difference [-], ΔC^* -–total saturation difference [-], ΔH^* – total hue difference [-].

The overall appearance of cranberries subjected to different initial treatments and microwave-vacuum drying at microwave power of 300 W is shown in Figure 4. Figure 4 proves that fruits subjected to initial convective freezing as well as ultrasound-assisted freezing and then drying were apparently brighter and more red then other fruits. It can be explained by the fact that the texture of berries was considerably altered by the ice crystals formed during freezing. It promoted greater leakage of natural juice from frozen fruits during drying than from other treated or untreated fruits and the presence of juice on the surface of berries increased the redness, yellowness and glossiness of dried berries (ZIELINSKA, ZIELINSKA 2019).

Fig. 4. The overall appearance of cranberries subjected to different initial treatments and microwave-vacuum drying at microwave power of 300 W: *a* – RM3 – non-treated fruits subjected to microwave-vacuum drying, *b* – SM3 – fruits subjected to sonication and microwave-vacuum drying, *c* – FM3 – fruits subjected to convective freezing and microwave-vacuum drying, *d* – SFM3 – fruits subjected to convective freezing preceded by sonication and then dried by microwave-vacuum drying, *e* – NM3 – fruits subjected to cryogenic freezing and microwave-vacuum drying

The effect of initial treatments on the values of hardness, cohesiveness, springiness and chewiness of microwave-vacuum dried cranberries was evaluated and the values are shown in Table 3. Sonication and microwave-vacuum drying at 300 W allowed to obtain dried berries characterized by the lowest values of cohesiveness, springiness and chewiness and can be recommended for the production of dried crispy snacks. It did not significantly influence the hardness of dried fruits. Hardness, cohesiveness, springiness and chewiness of fruits subjected to microwave-vacuum drying without any initial treatments were 20±4 N, 0.42±0.02, 0.73±0.02, and 6.2±0.5 N, while the hardness, cohesiveness, springiness and chewiness of fruits subjected to sonication and microwave-vacuum drying were 25±4 N, 0.19±0.02, 0.62±0.02, 3.4±0.8 N, respectively.

Table 3

Hardness, cohesiveness, springiness and chewiness of cranberries subjected to different pretreatment methods and microwave-vacuum drying at microwave power of 300 W

Sample	H [N]	C [-]	S [-]	Ch [N]
RM3	20 ± 4^{b}	0.42 ± 0.02^{a}	0.73 ± 0.02^{a}	6.2 ± 0.5^{b}
SM3	25 ± 4^{b}	0.19 ± 0.02^{d}	0.62 ± 0.02^{b}	3.4 ± 0.8^{c}
FM3	20 ± 1^{b}	0.43 ± 0.01^{a}	0.73 ± 0.02^{a}	6.2 ± 0.5^{b}
SFM3	32 ± 2^{a}	0.37 ± 0.01^{b}	0.70 ± 0.02^{a}	8.0 ± 0.4^{a}
NM3	15 ± 2^{c}	0.29 ± 0.01^{c}	0.75 ± 0.03^{a}	3.3 ± 0.5^{c}

Table contains mean values ± standard errors.
$^{a, b, c}$ – the same letters in columns mean no statistical differences between samples ($p \leq 0.05$).
Symbols: RM3, SM3, FM3, SFM3, NM3 – raw (non-treated), sonicated, convectively frozen, sonicated and convectively frozen as well as cryogenically frozen fruits subjected to microwave-vacuum drying at microwave power of 300 W, H – hardness [N], C – cohesiveness [-], S – springiness [-], Ch – chewiness [N].

Cryogenic freezing and microwave-vacuum drying at 300 W allowed to obtain dried fruits characterized by the highest values of springiness and low values of chewiness and can be recommended for the production of soft dried fruits used in breakfast mixes. Hardness, cohesiveness, springiness and chewiness of fruits subjected to microwave-vacuum drying preceded by cryogenic freezing were 15±2 N, 0.29±0.01, 0.75±0.03, and 3.3±0.5 N, respectively. Convective freezing did not significantly influence the hardness, cohesiveness, springiness and chewiness of dried fruits. In terms of texture changes, ultrasound-assisted sonication was more effective than sonication alone.

The effect of initial treatments on the values of particle density, porosity and volumetric shrinkage of microwave-vacuum dried cranberries was evaluated and the values are shown in Table 4. Initial treatments did not significantly influence the particle density, apparent porosity and the shrinkage of whole cranberries subjected to microwave-vacuum drying at 300 W. The values of particle density, porosity and volumetric shrinkage for microwave-vacuum dried fruits with or without initial treatment were in the range from 157±15 $kg \cdot m^{-3}$ to 198±52 $kg \cdot m^{-3}$, from 86±4 to 89±1% and from 46±3 to 52±5%, respectively.

The effect of initial treatments on the values of thermal conductivity, thermal diffusivity and specific heat of microwave-vacuum dried cranberries was evaluated and the values are shown in Table 5. Cranberries subjected to microwave-vacuum drying without any initial treatment were characterized by the lowest values of thermal conductivity λ (0.056 ± 0.004 $W \cdot m^{-1} \cdot K^{-1}$) and thermal diffusivity a (1.19 ± 0.10 $m^2 \cdot s^{-1}$). All of initial treatments increased thermal conductivity and thermal diffusivity of dried cranberries. However, some differences were not statistically different ($p \leq 0.05$). Most of initial treatments did not significantly influence specific heat of dried berries.

Table 4

Particle density, porosity and volumetric shrinkage of cranberries subjected to different pretreatments and microwave-vacuum drying at microwave power of 300 W

Sample	ρ_p [kg·m^{-3}]	ε_p [%]	S_v [%]
RM3	177±24^a	87±2^a	46±3^a
SM3	198±52^a	86±4^a	52±5^a
FM3	162±15^a	89±1^a	47±7^a
SFM3	157±15^a	89±1^a	48±3^a
NM3	177±33^a	87±2^a	52±5^a

Table contains mean values ± standard errors.
$^{a, b, c, d, e}$ – the same letters in columns mean no statistical differences between samples ($p \leq 0.05$).
Symbols: RM3, SM3, FM3, SFM3, NM3 – raw (non-treated), sonicated, convectively frozen, sonicated and convectively frozen as well as cryogenically frozen fruits subjected to microwave-vacuum drying at microwave power of 300 W, ρ_p – density of the particle [kg·m^{-3}], ε_p – porosity of the particle [%], S_v – volumetric shrinkage [%].

Table 5

Thermal conductivity, thermal diffusivity and specific heat of cranberries subjected to different pretreatments and microwave-vacuum drying at microwave power of 300W

Sample	λ [W·m^{-1}·K^{-1}]	$a \cdot 10^9$ [m^2·s^{-1}]	C_p [J·kg^{-1}·K^{-1}]
RM3	0.056±0.004^a	1.19±0.10^b	2878±201^a
SM3	0.063±0.003^a	1.40±0.07^a	2122±37^b
FM3	0.064±0.004^a	1.26±0.02^b	2946±122^a
SFM3	0.064±0.006^a	1.48±0.08^a	2876±261^a
NM3	0.076±0.004^b	1.40±0.14^a	3257±209^a

Table contains mean values ± standard errors.
$^{a, b, c, d, e}$ – the same letters in columns mean no statistical differences between samples ($p \leq 0.05$).
Symbols: RM3, SM3, FM3, SFM3, NM3 – raw (non-treated), sonicated, convectively frozen, sonicated and convectively frozen as well as cryogenically frozen fruits subjected to microwave-vacuum drying at microwave power of 300 W, λ – thermal conductivity [W·m^{-1}·K^{-1}], a – thermal diffusivity [m^2·s^{-1}], C_p – specific heat [J·kg^{-1}·K^{-1}].

Summary and Conclusions

Microwave-vacuum drying of whole cranberries with or without initial treatments took from 12±1 to 14.5±0.5 minutes. All of treatments did not significantly shorten the drying time of cranberries. However, they reduced the average material temperature during drying and significantly increased SMER values. Regarding energy consumption, the effectiveness of initial treatments was presented as follows: convective freezing, sonication, convective freezing

preceded by sonication and cryogenic freezing. Despite of cryogenic freezing, all of treatments significantly increased the values of D_{ew}. Regarding the values of D_{ew}, the effectiveness of initial treatments was presented as follows: convective freezing, ultrasound-assisted convective freezing, and sonication. Initial treatments significantly influenced the color as well as the mechanical and thermal properties of dried fruits. Sonication significantly increased the redness and yellowness of dried fruits. Its efficiency in color change was comparable to cryogenic freezing and much lower than convective freezing. All of treatments increased such thermal properties of dried cranberries as thermal conductivity and thermal diffusivity. Sonication combined with microwave-vacuum drying at 300 W allowed to obtain dried berries characterized by the lowest values of cohesiveness, springiness and chewiness and can be recommended for the production of dried crispy snacks. Cryogenic freezing combined with microwave-vacuum drying at 300 W allowed to obtain dried fruits characterized by highest values of springiness and low values of chewiness and can be recommended for the production of soft dried fruits used in breakfast mixes. Initial treatments did not significantly influence such physical properties of dried cranberries, as density, porosity and volumetric shrinkage.

As it is expected that the effect of sonication on the microwave-vacuum drying kinetic and material properties could be more visible in case of mechanically treated samples, i.e. sliced or cutted in half cranberries, further studies should be conducted in this specific area. Also, most consumers would characterize cranberries as sour. Therefore, it would be interesting to combine the initial treatments with osmotic dehydration and evaluate their effect on the drying kinetic and material properties.

Acknowledgements

This study was supported by the Polish National Science Center (grant No. 2015/17/B/NZ9/03601, title: *The effect of unconventional pretreatment methods on the kinetic of hybrid dehydration and physical and chemical properties of cranberries (Vaccinum macrocarpon*) and the University of Warmia and Mazury in Olsztyn (grant No. 16.610.001-300).

References

CHONG CH.H., FIGIEL A., CHUNG L.L., WOJDYLO A. 2014. *Combined Drying of Apple Cubes by Using of Heat Pump, Vacuum-Microwave, and Intermittent Techniques.* Food Bioprocess Technology, 7: 975–989.

FERNANDES F.A.N., RODRIGUES S., CÁRCEL J.A., GARCÍA-PÉREZ J.V. 2015. *Ultrasound-assisted air-drying of apple (malus domestica L.) and its effects on the vitamin of the dried product.* Food Bioprocess Technology, 8(7): 1503–1511.

GRABOWSKI S., MARCOTTE M., QUAN D., TAHERIAN A.R., ZAREIFARD M.R., POIRIER M., KUDRA T. 2007. *Kinetics and quality aspects of Canadian blueberries and cranberries dried by osmo-convective method*. Drying Technology, 25(2): 367–374.

MCCLEMENTS D.J. 1995. *Advances in the application of ultrasound in food analysis and processing*. Trends in Food Science and Technology, 6: 293-299.

MCKAY D.L., BLUMBERG J.B. 2007. *Cranberries (Vaccinium macrocarpon) and cardiovascular disease risk factors*. Nutrition Reviews, 65(11): 490–502.

NASCIMENTO E.M.G.C., MULET A., RAMÍREZ ASCHERI J.L., PILER DE CARVALHO C.W., CARCEL J.A. 2016. *Effects of high-intensity ultrasound on drying kinetics and antioxidant properties of passion fruit peel*. Journal of Food Engineering, 170: 108-118.

NOWAK K.W., ZIELINSKA M., WASZKIELIS K.M. 2018. *The effect of ultrasound and freezing/thawing treatment on the physical properties of blueberries*. Food Science and Biotechnology, 28(3): 741–749. doi: 10.1007/s10068-018-0528-5.

RAHMAN S. 1995. *Food Properties Handbook*. CRC Press Inc, Boca Raton.

RENNIE T.J., MERCER D.G. 2013. *Effect of blanching on convective drying and osmotic dehydration of cranberries*. Transactions of ASABE, 56(5): 1863–1870.

RODRIGUEZ Ó., SANTACATALINA J.V., SIMAL S., GARCÍA-PÉREZ J.V., FEMENIA A., ROSSELLO C. 2014. *Influence of power ultrasound application on drying kinetics of apple and its antioxidant and microstructural properties*. Journal of Food Engineering, 129: 21–29.

SCHMIDT E.L., KLOCKER K., FLACKE N., STEIMLE F. 1998. *Applying the transcritical CO_2 process to a drying heat pump*. International Journal of Refrigeration, 21(3): 202–211.

SKROVANKOVA S., SUMCZYNSKI D., MLCEK J., JURIKOVA T., SOCHOR J. 2015. *Bioactive compounds and antioxidant activity indifferent types of berries*. International Journal of Molecular Sciences, 16(10): 24673–24706.

SOYSAL Y., AYHAN Z., ESTURK O., ARIKAN M.F. 2009. *Intermittent microwave–convective drying of red pepper: drying kinetics, physical (color and texture) and sensory quality*. Biosystem Engineering, 103: 455–463.

SUNJKA P.S., RENNIE T.J., BEAUDRY C., RAGHAVAN V.G.S. 2004. *Microwave-Convective and Microwave-Vacuum Drying of Cranberries: A Comparative Study*. Drying Technology, 22(5): 1217-1231.

ZHANG M., TANG J.M., MUJUMDAR A.S., WANG S. 2006. *Trends in microwave related drying of fruits and vegetables*. Trends in Food Science and Technology, 17: 524–534.

ZIELINSKA M., MARKOWSKI M. 2018. *Effect of microwave-vacuum, ultrasonication, and freezing on mass transfer kinetics and diffusivity during osmotic dehydration of cranberries*. Drying Technology, 36(10): 1158–1169.

ZIELINSKA M., MARKOWSKI M. 2012. *Color Characteristics of Carrots: Effect of Drying and Rehydration*. International Journal of Food Properties, 15: 450-466.

ZIELINSKA M., MARKOWSKI M. ZIELINSKA D. *2019. The effect of freezing on the hot air and microwave vacuum drying kinetics and texture of whole cranberries*. Drying Technology, doi: 10.1080/07373937.2018.1543317.

ZIELINSKA M., ROPOLEWSKA E., MARKOWSKI M. 2017. *Thermophysical properties of raw, hot-air and microwave-vacuum dried cranberry fruits (Vaccinium macrocarpon)*. LWT – Food Science and Technology, 85: 204–211.

ZIELINSKA M., ROPOLEWSKA E., ZAPOTOCZNY P. 2018a. *Efffects of freezing and hot air drying on thephysical, morphological and thermal properties ofcranberries (Vaccinium macrocarpon)*. Food and Bioproducts Processing, 110: 40–49.

ZIELINSKA M., SADOWSKI P., BŁASZCZAK W. 2015. *Freezing/thawing and microwave assisted drying of blueberries (Vaccinium corymbosum L.)*. LWT-Food Science and Technology, 62(1, 2): 555–563.

ZIELINSKA M., ZIELINSKA D. 2019. *Effects of freezing, convective and microwave-vacuum drying on the content of bioactive compounds and color of cranberries*. LWT – Food Science and Technology, 104: 202-209. doi: 10.1016/j.lwt.2019.01.041.

ZIELINSKA M., ZIELINSKA D., MARKOWSKI M. 2018b. *The effect of microwave-vacuum pretreatment on the drying kinetics, color and the content of bioactive compounds in osmo-microwave-vacuum dried cranberries (Vaccinium macrocarpon)*. Food and Bioprocess Technology, 11: 585–602.

Technical Sciences, 2019, 22(2), 169–182

UNIWERSYTET WARMIŃSKO-MAZURSKI W OLSZTYNIE

Quarterly peer-reviewed scientific journal
ISSN 1505-4675
e-ISSN 2083-4527
TECHNICAL SCIENCES
Homepage: www.uwm.edu.pl/techsci/

FLEXURAL CHARACTERIZATION OF POLYMER CONCRETE COMPRISING WASTE MARBLE AND DATE PALM FIBERS

Mansour Rokbi[1], *Zine El Abidine Rahmouni*[2], *Brahim Baali*[3]

[1]Department of Mechanical Engineering
Faculty of Technology
University of M'sila, Algeria
[2]Department of Civil Engineering
Faculty of Technology
University of M'sila, Algeria
[3]Sarl Maghreb Pipe
Industriel Zone, M'sila, Algeria
URMPE/MESOnexTeam
Faculty of Engineering
University of Boumerdes, Algeria

Received 7 April 2019, accepted 29 May 2019, available online 3 June 2019.

Keywords: Polymer concrete, Date palm fibers, Quartz, Marble, Fibers sizing, Three-point bending.

Abstract

This work is an experimental approach for the development and characterization of a polymer concrete reinforced with natural fibers. The polymer concrete consists of sand (Quartz) and orthophthalic polyester used as a binder. Marble powder was used to ensure the continuity of the particle size of the granular mixture. As reinforcement, 2% of chopped date palm fibers (short, very short or mixed) were added. For comparison, identical polymer concrete flexure specimens reinforced with the same content of short E-glass fibers were also prepared and tested. All specimens were initially cured at room temperature and then post-cured for 6 h at 70°C. The results of three-point bending on smooth specimens with different rates of charges (marble), showed that the flexural and compressive strength were improved by adding 20% of marble, and were 31.80 MPa and 67.42 MPa respectively. The flexural strength of specimens showed that the improvement or the degradation of polymer concrete properties seemed to be attributed to the nature of fibers (treated or untreated), and/or to the fibers sizing (short, very short or mixed).

Correspondence: Mansour Rokbi, Department of Mechanical Engineering, Faculty of Technology, University of M'sila, 28000, Algeria, phone: +6 99 03 88 05, e-mail: mansour.rokbi@univ-msila.dz

Introduction

Polymer concrete (PC) is a material composed of different types of aggregates bound together by polymeric resins sometimes thermoplastic but generally thermosetting. The lightness of this material and its water absorption percentage practically nil guarantee a total waterproofness of the material, moreover its inalterability to the cycles of freeze-thaw, its high resistance to most chemicals and impact, as well as its minimal wear by abrasion are other features that make polymer concrete a high quality material, and therefore, long life of concrete structures can be considered (MOHAMMADHOSSEINI et al. 2017). Compared with Portland cement concrete, polymer concrete has greater mechanical strength, Knowledge of the behavior of these materials and its development is necessary. In the context of sustainable development, intense efforts are made by researchers to develop new alternative materials including recycled materials or integrating industrial waste. This initiative focuses on producing health-friendly materials by reducing the environmental impact (MAGNIONT et al. 2012, ROKBI et al. 2017). In other words, many waste materials from various industrial sources can be seen as potentially valuable materials (AWAL, MOHAMMADHOSSEINI 2016). Naturally available materials such as waste marble which is an environmental problem, can be used effectively as mineral aggregate (ROKBI et al. 2017).

Recently, several works deal with the reinforcement of polymer concrete. The most used reinforcements are glass fibers, steel, polypropylene (PP), waste fiber and natural fibers (AWAL, MOHAMMADHOSSEINI 2016, MOHAMMADHOSSEINI et al. 2018). Nowadays, the reinforcement of concrete structures by natural fibers has attracted substantial interest, and there are various research regarding this particular topic in related literature (ROKBI et al. 2017, BOUGUESSIR et al. 2018, REIS 2012). The advantage of incorporation of natural fiber in polymer concrete structures is because these fibers are abundantly available from renewable resources, biodegradable, renewable and have low density and high specific properties. In addition, the availability of natural fibers in many underdeveloped countries such as Brazil, India and Bangladesh allows them to develop low-cost construction materials with little technology support and a small amount of energy. Lignocellulosic fibers have been used as a reinforcing agent in conventional concrete as well as in innovative concrete. The main purpose of these investigations is to replace metallic or synthetic fibers .

To analyze the possibility of substitution of synthetic fibers by natural fibers, REIS (2006) investigated the mechanical characterization (flexural strength, fracture toughness and fracture energy) of epoxy polymer concrete reinforced with different chopped natural fibers (coconut, sugarcane bagasse and banana fibers). Careful analysis of these results shows that some of these fibers (Coconut and sugar cane bagasse) proved to be an alternative when fracture properties are analyzed. In return, the low interfacial properties between lignocellulosic

fibers and an organic resin system (or inorganic matrix) often reduce their potential as reinforcing agents due to the hydrophilic nature of natural fibers, chemical modifications are considered to optimize this disadvantage. To improve the interfacial characteristics between lignocellulosic fibers and the matrix, several surface modifications including alkali, coupling agents and acetylation have been investigated. The treatment with sodium hydroxide (NaOH) is relatively simple and widely being used to modify the cellulosic structure like Alfa, jute, sisal, kenaf, palm or banana (ROKBI et al. 2018). The experiment work of ACHOUR et al. (2017) show that the treatment of lignocellulosic fibers such as Diss and Doum with NaOH solution (3% and 1% respectively) are very effective to improve adhesion between natural fibers and inorganic matrix. Once treated, the lignocellulosic fibers can contribute to a good interaction between fiber and the cementitious matrix by limiting the propagation of microcracks, by a sewing effect; which improve the performance of cementitious mortars. In recent work (REIS 2012), fiber surface treatments were carried out to enhance bond interface between sisal fiber and polymer matrices to improve the fracture properties. In this study, the effects of the incorporation of the untreated and treated sisal fibers with NaOH and acetic acid into two polymeric mortars, based on epoxy and polyester resins respectively were investigated. Untreated and surface treated sisal fibers when used as reinforcement contributes significantly to improve the fracture properties both energy and toughness of epoxy and unsaturated polyester polymer mortars. It has also been observed that polymer mortars reinforced with untreated sisal fibers have the highest ultimate strength and those reinforced with sisal fibers treatment with 10% of NaOH have the lowest properties. ROKBI et al. (2017) have study the feasibility of using naturally available materials: Alfa fibers and waste marble powder (WMP) in PC material. In their study, two weight percentages of Alfa fibers (1% and 2%) were used. The results show that the reinforcement with 1% of Alfa fiber can improve the fracture toughness better than 2% fiber reinforcement. In addition, the quality of the adhesion between the natural fiber and polymeric resin appeared good when Alfa fiber was treated with 5% NaOH.

It is known that during the process of cross linking of unsaturated polyesters shrin-kage and cracking phenomena are quite present and represent major problems. In addition, this type of resin is not hard enough and has a lower impact strength compared to other thermoset resins such as epoxy. To overcome these problems, several researchers have proposed the use of many types of fillers such as calcium carbonate, silica, alumina trihydrate, clay, mica, fly ash, etc. Thus, the properties of the resin and the filler, the dispersion of the particles, and the state of the interface resin play a primordial role on the mechanical properties of the PC (HRISTOVA, MINSTER 2003, ANISKEVICH, HRISTOVA 2000, VYTLACILOVA 2011, CHOUDHARY et al. 2019). HRISTOVA and MINSTER (2003) described the effect of a particle marble filler on the creep response of a cross-linked

polyester matrix before and after physical aging. It was observed that the values of the creep compliance decrease and the values of the modulus of elasticity increase with increasing filler volume fraction.

The purpose of the present work was to discuss the usability of the naturally available materials: waste marble powder (WMP) and date palm fruit bunches fibers (DPF) in PC material. Firstly, the optimum of the amount of WMP addition by weight was identified and reported. Secondly, the effects of fruit bunches fibers sizing (short, very short or mixed) as well their treatment (5% NaOH during 24 h) as reinforcement on the mechanical performance of PC have been studied.

Materials and Methods

Materials

Fiber and resin

In this study, the date palm fruit bunches fibers were used as reinforcement in PC. These fibers were collected from the region of Biskra. It is a semi-arid region in Algeria. Once the fruit bunches were harvested, they were washed with water (2% detergent solution) to remove the contaminants and adhering dirt. Thereafter, fruit bunches were cut into 6cm and 2cm lengths (Fig. 1*a*).

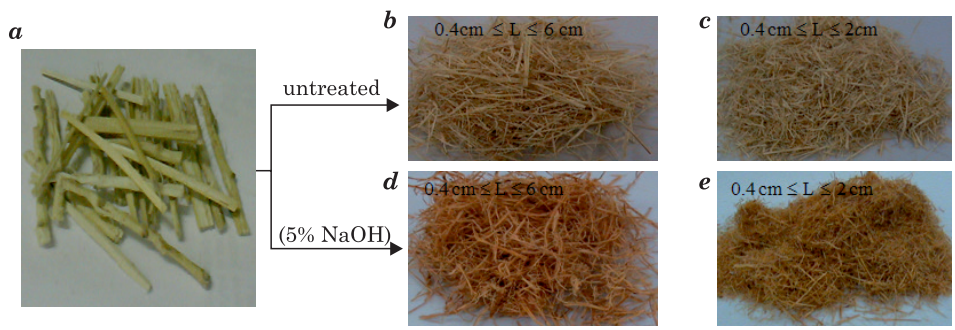

Fig. 1. Different form of used fibers: *a* – DPF before extraction, *b* – Untreated (short), *c* – Untreated (very short), *d* – Treated (short), *e* – Treated (very short)

Pretreatment techniques and fibers processing are similar to those described in (ROKBI et al. 2011). The chopped fruit bunches were soaked in a 5% NaOH solution at 28°C. The fibers were kept immersed in the alkali solution for 24 h. The treated fruit bunches were then washed several times with distilled water. Any traces of NaOH, remaining on the fiber surface, were neutralized with

2% sulfuric acid during 10 min. The fibers were washed again with distilled water until obtaining a pH = 7. Subsequently, the fibers were dried at 60°C for 6 hours. Untreated and treated fibers are represented in Figure 1*b*, *c*, *d*, and *e*. Like other plant fibers, date palm fruit bunches fibers are characterized by good mechanical performances (stength = 397,2 MPa, Young Module = 6.9 GPa) (TAHRI et al. 2016).

The used resin is orthophthalic polyester. It is a pre-accelerated resin with good mechanical properties. It is specially designed for laminating and hand lay-up technique.

Mineral fine aggregate

The aggregate used in PC was Quartz fine sand with a homogeneous grain size with an average diameter of 200 to 500 μm. The chemical compositions of the used Quartz fine sand are listed in Table 1.

Table 1

Chemical compositions of Quartz sand

Fine sand [%]	MgO	CaO	Fe_2O_3	Al_2O_3	SiO_2	TiO_2	H_2O
	0.006	0.010	0.215	0.769	99.02	0.078	0.02

Mineral addition

In this work very fine WMP has been used in the PC as a mineral addition. Marble powder is a compact metamorphic rock marketed through the manufacture of ceramic tiles from an industry in Fil-Fila quarry (Skikda region in the north-east of Algeria). WMP is a useful material obtained as a by-product of marble during sawing, shaping, and polishing process such that about 25% of the processed marble turns into dust or powder form (GÜNEYISI et al. 2009). The recovered waste marble is sieved into marble powder using a fine sieve. The characteristics of marble powder are presented in Table 1 and 2.

Table 2

Physical characteristics of waste marble powder

Couleur	White
Structure	Micro-crystalline
Specific gravity	2.68 g/cm^3
Blaine fineness	7.50 cm^2/g

Table 3

Chemical composition of marble powder

Oxides	SiO_2	CaO	MgO	Fe_2O_3	Al_2O_3	Na_2O	K_2O	SO_3	LOI*
%	1.47	55.30	0.01	0.14	0.35	0.12	0.04	0.01	42.56

*LOI: Loss on ignition at 1000°C

In order to identify the optimum of the amount of WMP addition, flexural specimens were prepared by mixing Quartz fine sand with different WMP contents of 0%, 3%, 5%, 10%, 20% and 30% in weight (Tab. 4). For the formulation, the amount of orthophthalic polyester was taken as 20%, in mass, of concrete aggregate weight (Quartz sand and WMP) (REIS 2006). At least, five flexural specimens, for each amount of WMP, were compacted in a steel mold of dimensions of 40 × 40 × 160 mm (Fig. 3*a*). PC specimens were initially cured at room temperature and then post-cured for 6 h at 70°C.

The gradation of both Quartz and WMP are shown in Figure 2. The particle size distribution of WMP was measured by laser particle analyzer.

Table 4

Different manufacturing unreinforced PC

	Unreinforced PC					
Quartz sand content	100%	97%	95%	90%	80%	70%
WMP content	00%	03%	05%	10%	20%	30%
Designation	PC100-00	PC97-03	PC95-05	PC90-10	PC80-20	PC70-30

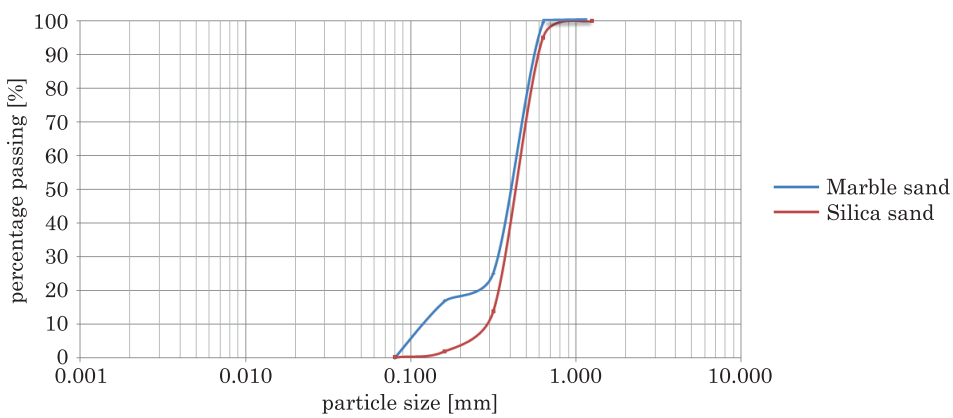

Fig. 2. Particle size distribution of Quartz and WMP

In each series, chopped date palm fruit bunches fibers at 2% of the total weight of specimen was used according to (REIS 2006). Based on the optimum of WMP content, eight mixtures of flexural specimens were prepared using different reinforcement (Tab. 5). As indicated by this table, and in addition to the two series of unreinforced PC specimens and those reinforced by glass fibers, two groups of specimens are elaborated in this investigation: the first group consists of three series of PC specimens reinforced by untreated fibers which are respectively PC/very short fibers (PC-A), PC/short fibers (PC-B) and PC/mixture of fibers (PC-AB). In a similar way, the second group consists of the same formulation, but in this case the three series of PC specimens are reinforced respectively by treated fibers which are PC-C, PC-C and PC-CD.

Table 5

Different manufactured PC

PC	Fibers sizing	Max Fiber length [mm]	Designation
PC /Unteated DPF Group 1	very short	2	PC-A
	short	6	PC-B
	mixed (50% V. Short+50% Short)	6	PC-AB
PC /Teated DPF Group 2	very short	2	PC-C
	short	6	PC-D
	mixed (50% V. Short+50% Short)	6	PC-CD
Unreinforced PC	no fibers	/	PC-E
PC /Glass fibers	short	6	PC-F

Testing procedures

As known, both flexural and compressive properties of construction materials are very useful especially if their intended applications are country road or pavement (PEREIRA et al. 2015). In this work, the flexural and compressive tests were performed on the different PC samples. For flexure testing, the three-point bending tests were performed in a mechanical testing machine YL universal testing machines/25kN (Figure 3(b)), at a crosshead movement rate of 1 mm/min, according to the Technical committee TC-113 test methods for concrete–polymer composites (RILEM 1995). Despite the very short span length compared with specimen thickness, support span of 100 mm, shear effect is disregarded and it is not considered (REIS 2006). Flexural strength, considered as the strength under normal stresses, was determined by applying the following equation known from the strength of materials:

$$\sigma_f = \frac{3\,Pl}{2\,b\,h^2} \tag{1}$$

where:

σ_f – the flexural strength,
P – the maximum load recorded,
l – the span length,
b and h are, respectively, the width and the height of the prismatic specimens.

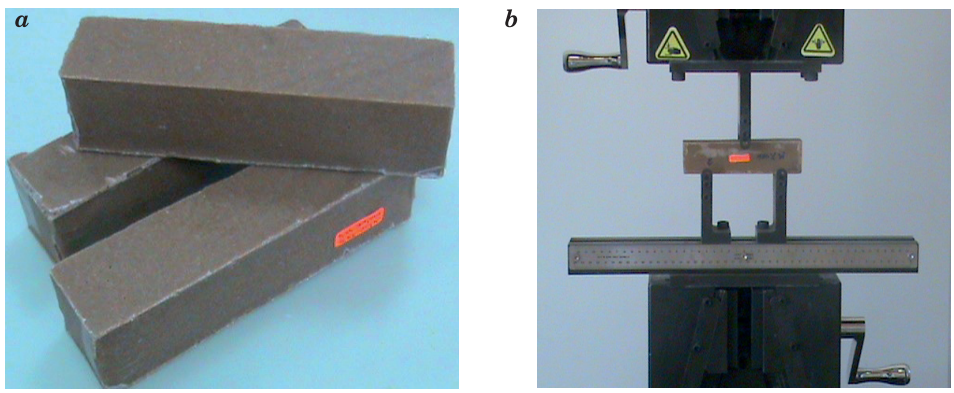

Fig. 3. Specimens and testing: *a* – 40×40×160 mm specimens, *b* – Flexural test set-up

The compression test consists of studying the ability of a material to withstand a force that attempts to crush it. In our case, the compression test is performed on cubic specimens for each concrete mixture and were tested for the determination of compression strengths using STRASSEN TEST loading machine. This latter has a crushing capacity of 2000 kN. The compression load was applied at a rate of 2.4 kN/s.

Results and discussion

Effect of WMP replacement

In this paragraph, the effect of substitution of fine sand by different WMP contents on the mechanical performances of PC was studied in order to optimize the amount of WMP added as replacement of Quartz in PC. The WMP is used in various industrial applications as a filler material and it could be assumed as ultrafine aggregates filling voids in PC (ERGÜN 2011).

Table 6 presents the flexural and compressive test results of PC when the fine sand was replaced by different WMP contents. When small amounts of WMP were used, cases of PC97-03 and PC95-05 materials, the flexural strengths

Table 6

Flexural and compressive test results of PC

PC	PC100-00	PC97-03	PC95-05	PC90-10	PC80-20	PC70-30
Maximum load [kN]	12.15 ±0.83	9.67 ±1.33	9.90±1.97	11.89±0.43	14.63±0.37	14.72±0.20
Flexural strength [MPa]	27.9 ±0.85	21.20±1.23	21,60±1.05	27.10±1.23	31.80±0.42	31.10±0.62
Flexural strain [%]	2.41±0.15	1.45±0.30	1.47±0.22	1.53±0.14	1.88±0.28	1.70±0.31

Source: ROKBI et al. (2017).

of materials were decreased of about 24% compared to the materials PC100-00 (see Table 6). The remarkable reduction in flexural strength seems related to the use of a small amount of WMP which had somehow created microscopic defects, and the materials have a greater possibility of early failure. From the same table, the flexural strength of the material PC90-10 has not undergone a remarkable change. In other hand, and compared to the materials PC100-00, the flexural strength of both materials PC80-20 and PC70-30 has increased of about 12% and 10%, respectively, This may suggest that the substitution of WMP by 20% of Quartz allows registration oft he best flexural and compressive strength. The use of 20% of WMP could be considered as the optimum amount to enhance the properties of PC (ROKBI et al. 2017).

Flexural test

For all flexural specimens reinforced with treated and untreated DPF and glass fiber, 20% of WMP amount were used. Figure 4 shows the load-deflection curves for each PC mixture tested in three-point bending. The load-deflection curves were similar to those of fibers reinforced thermoset matrix materials.

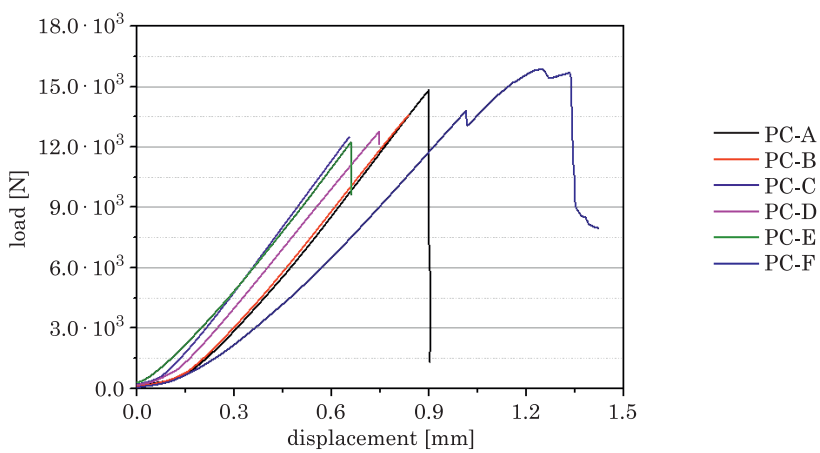

Fig. 4. Load-deflection curves of various test groups

All the tested specimens showed a brittle behavior with a linear elastic deformation up to the catastrophic failure.

From the tests, it was showed that the PC reinforced with untreated PDF fibers materials have maximum load than those reinforced with treated fibers (Fig. 4). This can be explained by the effect that the alkaline treatment can be harmful and leads to fragile fibers (ROKBI et al. 2011, CHIKOUCHE et al. 2015). NaOH concentration would certainly damage the fiber and consequently reduced the flexural strength of the PC reinforced with treated fibers.

Figure 5 shows representative histograms for flexural strength for all specimens tested under statical loading. As indicated in Figure 5, the incorporation of DPF fibers in PC had a significant effect on the flexural strength values. The use of very short untreated DPF (Mat-A) appeared more suitable for use as reinforcement in PC. In this case, an improvement in flexural strength of about 23% and 5% have been observed comprared to the matérials Mat-E and Mat-C, respectively. In one hand, compared to the material Mat-E, the increase in the strength of Mat-A appears to be related to the addition of fibers which play an active role as bridging mechanism by controlling resulting microcracking and reducing the crack propagation rate. In other words, the fiber reinforced concrete can transformt the brittle behavior to a pseudoductile one by maintaining considerable load carrying capacity after cracking of the matrix (PEREIRA et al. 2015).

On the other hand, the remarkable improvement in the strength of Mat-A (about 23%) compared to the material Mat-C was mainly due to the fragile nature of the treated DPF fibers.

The flexural strength values in group 1 was different compared with that of group 2. The best flexural strength in group 1 was obtained when the PC was reinforced by very short fibers (case of Mat-A), while this parameter

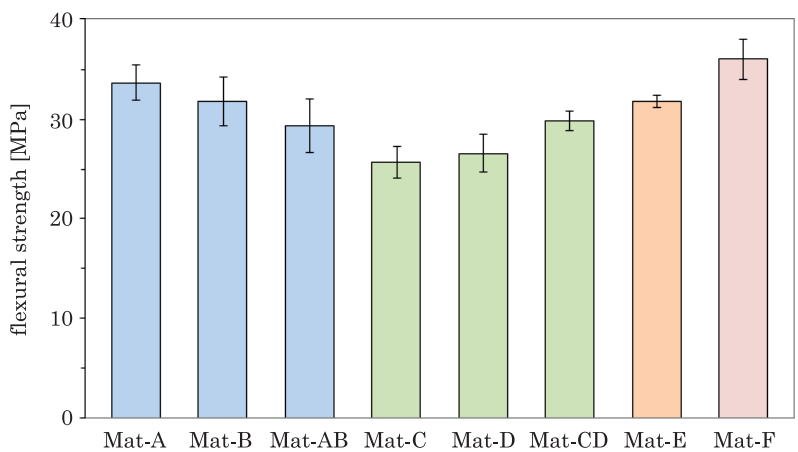

Fig. 5. The flexural strength of different PC samples

is gradually reduced once the short fibers or the mixture of fiber are used. The same observation is reported by (LI et al. 2006) when studying coir fibers reinforced cementitious composites (CFRCCs). These authors compared the flexural strength in cementitious composites reinforced by untreated short coir fiber (2 cm) to that reinforced by untreated long coir fiber (4 cm). From their results, it can be seen that some short fiber CFRCCs show better flexural strength than the long fibre (4 cm) CFRCCs. This may suggest that the long fiber is neither well dispersed nor straightened (LI et al. 2006).

Considering the flexural strength values in group 2, it is to be noted that neither the material Mat-C nor the material Mat-D have proved good results. The best strength was obtained when mixed fibers are used as reinforcement in PC (case of Mat-CD). The fragile nature of the treated fibers has favorised the degradation of properties of the PC when these fibers have almost the same size. However the use of different sizes of treated fibers seemed improve the fiber bridging effect. ALSAEED et al. (2013) investigated the effect of alkali treatment of date palm fiber on its interfacial adhesion with epoxy matrix. They found that higher concentration of chemical treatment might decrease the strength of natural fiber. In other work, ROKBI et al. (2011) studied the influence of alkaline treatment on the flexural properties of polyester matrix composite reinforced with Alfa fibers. The alkali treatment, NaOH, at 1%, 5%, and 10% concentrations for various socking periods of 0, 24 and 48 h has been conducted. The flexural strength and flexural modulus improved by 60% and 62% respectively at 10% NaOH consideration for a period of 24 h. Also, they showed that the longer treatment time of Alfa fiber (48 h with 5% NaOH) decreased the flexural strength and flexural modulus due excess delignification natural fiber that led to weakening of the fiber strength and the damage occurred on the fiber. Due to these damages, interface adhesion and wettability become poor, which decreases the composite properties.

Micrographs of Figure 6 showed the surface of the DPF fiber before and after treatment. The surface of untreated the DPF fiber was found to be considerably covered with waxy substances and impurities (Fig. 6*a*). Certainly, dirt and layers

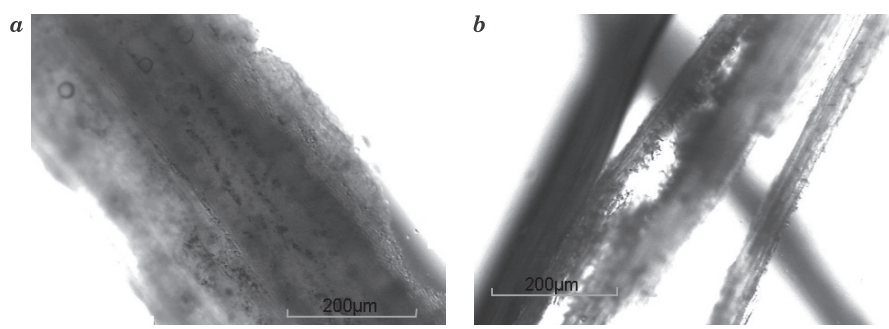

Fig. 6. Optical micrographs of surface morphology of DPF fiber: *a* – Untreated, *b* – Treated

waxy cuticle on the surface of the fibers were completely removed after NaOH treatment, but it seemed that treatment with 5% NaOH for 24 h had significantly deteriorated the PDF fibrils (Fig. 6*b*). At higher alkali concentration, excess delignification of natural fiber occurs resulting in a weaker or damaged fiber, and the treatment of fibers over a prolonged period makes the fibers stiffer and more brittle (ROKBI et al. 2011).

It was found that the optimum properties of DPF fibers were achieved at relatively short treatment times of 2 h and 4 h and alkali concentrations of 2% and 5% NaOH, respectively (TAHA et al. 2007).

In another work, (ALAWAR et al. 2009) investigated on the effect of alkali treatment on DPF behaviors. Their Result shows that the treatment of conditions of 1% NaOH for 1 h at 100°C is the optimum treatment that gives the maximum tensile strength and the better surface morphology of the single DPF.

Figure 7 presents the flexure fracture surfaces micrographs of the Mat-B, Mat-D, and Mat-F. The untreated fibers appear non-covered by the matrix; it was not subjected to any abrasion. The fiber pull-out with a considerable length is clearly visible (Fig. 7*a*). It seemed that PDF fibers needed surface treatment to ensure better adhesion. The contrary, treated DPF with 5% NaOH showed a good adhesion with aggregates. It seemed strangely that the color of these fibers became brick-red (Fig. 7*b*).

It appears that the treated DPF were destroyed before their introduction as reinforcement in PC. The fractured surface of the material Mat-F showed that the fiber surface of chopped glass fiber were coated with aggregate wrapping that have been partially destroyed or abraded (Fig. 7*c*). This may help to explain the remarkably high pull out load (BENZERZOUR et al. 2012). Compared to the Mat-A, the material Mat-F showed slightly larger maximum strength. This result suggests that local DPF are comparable to chopped glass fibers used as reinforcement in PC.

Fig. 7. Optical micrographs of fracture surfaces of: *a* – Mat-B, *b* – Mat-D, *c* – Mat-F

Conclusion

In this study, in the first step, the influence of various amount of waste marble powder on both flexural and compressive properties of the PC samples based on Quartz, waste marble powder and orthophthalic polyester were studied, and the optimum of the amount of WMP addition by weight (20%) was identified and reported.

In the second step, and based on the optimum of WMP content, eight mixtures of flexural specimens were prepared using different reinforcement for the purpose of reflecting the effect of nature of fibers (treated or untreated), and/or the fibers sizing (short, very short or mixed) on the flexural performances of PC.

The analysis of flexural results for all specimens tested under statical loading allow the following interpretations:

– the use of very short untreated date palm fruit bunches fibers appeared more suitable for use as reinforcement in PC. In this case, an increasing in flexural strength from 31.78 MPa to 33.67 MPa was attributed to the fiber bridging mechanism;

– the longer treatment time and/or higher concentration of chemical treatment reduced the performance of the natural fiber, However, the use of different sizes of treated fibers would seem to participate effectively to to increase the fiber bridging effect;

– the PC reinforced with glass fibers showed slightly larger maximum strength (36.01 MPa) compared to the PC reinforced by untreated DPF (36.01 MPa). This result suggests that local DPF are comparable to chopped glass fibers, and can be used successfully as a reinforcing agent in civil engineering construction;

– finally, it is important to mention that low concentration of NaOH can give good results. Studies are in progress in this direction.

References

ACHOUR A., GHOMARI F., BELAYACHI N. 2017. *Properties of cementitious mortars reinforced with natural fibers*. Journal of Adhesion Science and Technology, 31(17): 1938–1962.

ALAWAR A., HAMED A.M., AL-KAABI K. 2009. *Characterization of treated date palm tree fiber as composite reinforcement*. Composites. Part B: Engineering, 40(7): 601–606.

ALSAEED T., YOUSIF B., KU H. 2013. *The potential of using date palm fibres as reinforcement for polymeric composites*. Materials & Design, 43: 177–184.

ANISKEVICH K., HRISTOVA J. 2000. *Creep of polyester resin filled with minerals*. Journal of Applied Polymer Science, 77(1): 45-52.

AWAL A.A., MOHAMMADHOSSEINI H. 2016. *Green concrete production incorporating waste carpet fiber and palm oil fuel ash*. Journal of Cleaner Production, 137: 157-166.

BENZERZOUR M., SEBAIBI N., ABRIAK N.E., BINETRUY C. 2012. *Waste fibre-cement matrix bond characteristics improved by using silane-treated fibres*. Construction and Building Materials, 37: 1-6.

Bouguessir H., Harkati E., Rokbi M., Priniotakis G., Vassilliadis S., Boughanem H., Fellah L. 2018. *Physico-chemical and mechanical characterization of Jute fabrics for civil engineering applications*. Journal of Computational Methods in Sciences and Engineering, 18: 129–147.

Chikouche M.D.L., Merrouche A., Azizi A., Rokbi M., Walter S. 2015. *Influence of alkali treatment on the mechanical properties of new cane fibre/polyester composites*. Journal of Reinforced Plastics and Composites, 34(16): 1329-1339.

Choudhary M., Singh T., Dwivedi M., Patnaik A. 2019. *Waste marble dust filled glass fiber-reinforced polymer composite*. Part I. *Physical, thermomechanical, and erosive wear properties*. Polymer Composites. In press.

Ergün A. 2011. *Effects of the usage of diatomite and waste marble powder as partial replacement of cement on the mechanical properties of concrete*. Construction and Building Materials, 25(2): 806-812.

Güneyisi E., Gesoğlu M., Özbay E. 2009. *Effects of marble powder and slag on the properties of self compacting mortars*. Materials and Structures, 42(6): 813-826.

Hristova J., Minster J. 2003. *Filler fraction effect on creep response of crosslinked polyester matrix with mineral filler*. Journal of Applied Polymer Science, 89(12): 3329-3335.

Li Z., Wang L., Wang X. 2006. *Flexural characteristics of coir fiber reinforced cementitious composites*. Fibers and Polymers, 7(3): 286-294.

Magniont C., Escadeillas G., Coutand M., Oms-Multon C. 2012. *Use of plant aggregates in building ecomaterials*. European Journal of Environmental and Civil Engineering, 16: 17-33.

Mohammadhosseini H., Tahir M.M., Sam A.R.M. 2018. *The feasibility of improving impact resistance and strength properties of sustainable concrete composites by adding waste metalized plastic fibres*. Construction and Building Materials, 169: 223-236.

Mohammadhosseini H., Yatim J.M., Sam A.R.M., Awal A.A. 2017. *Durability performance of green concrete composites containing waste carpet fibers and palm oil fuel ash*. Journal of Cleaner Production, 144: 448-458.

Pereira M.V., Fujiyama R., Darwish F., Alves G.T. 2015. *On the strengthening of cement mortar by natural fibers*. Materials Research, 18(1): 177-183.

Reis J. 2006. *Fracture and flexural characterization of natural fiber-reinforced polymer concrete*. Construction and Building Materials, 20(9): 673-678.

Reis J. 2012. *Sisal fiber polymer mortar composites: Introductory fracture mechanics approach*. Construction and Building Materials, 37: 177-180.

Rilem P. 1995. *Technical Comittee TC-113. Method of making polymer concrete and mortar specimens*. In Symposium on properties and test methods for concrete-polymer composites, Oostende, p. 129-132.

Rokbi M., Imad A., Herbelot C., Belouadah Z. 2018. *Fracture Toughness of Random Short Natural Fibers Polyester Composites*. Diffusion Foundations, 18: 94-105

Rokbi M., Osmani H., Imad A., Benseddiq N. 2011. *Effect of chemical treatment on flexure properties of natural fiber-reinforced polyester composite*. Procedia Engineering, 10: 2092-2097.

Rokbi M, Rahmouni Z., Baali B. 2017. *Performance of polymer concrete incorporating waste marble and alfa fibers*. Advances in Concrete Construction, 5(4): 331-343.

Taha I., Steuernagel L.,Ziegmann G. 2007. *Optimization of the alkali treatment process of date palm fibres for polymeric composites*. Composite Interfaces, 14(7-9): 669-684.

Tahri I., Ziegler-Devin I., Ruelle J., Segovia C., Brosse N. 2016. *Extraction and characterization of fibers from palm tree*. BioResources, 11(3): 7016-7025.

Vytlacilova V. 2011. *Effect of recycled aggregate on mechanical–physical properties of fly ash-based composites with fibres*. International Journal of Chemical and Environmental Engineering, 59.

Technical Sciences, 2019, 22(2), 183–194

UNIWERSYTET WARMIŃSKO-MAZURSKI W OLSZTYNIE

Quarterly peer-reviewed scientific journal
ISSN 1505-4675
e-ISSN 2083-4527
TECHNICAL SCIENCES
Homepage: www.uwm.edu.pl/techsci/

APPLICATION OF 3D PRINTING TECHNOLOGY FOR MECHANICAL PROPERTIES STUDY OF THE PHOTOPOLYMER RESIN USED TO PRINT POROUS STRUCTURES

Ewelina Małek, Danuta Miedzińska, Arkadiusz Popławski, Wiesław Szymczyk

Faculty of Mechanical Engineering
Military University of Technology

Received 10 June 2018, accepted 11 June 2019, available online 14 June 2019.

K e y w o r d s: Mechanical Properties, Rapid Prototyping, SLA (stereolitography), Fractal Models.

A b s t r a c t

In the field of numerical research there are various approaches and methods for structures of porous materials modeling. The solution is the use of fractal models to develop the porous structure.

In the case of modeling the geometry of natural (random) materials, there is a problem of compatibility of the FE model geometry and real one. This is a source of differences between the results of calculations and experimental ones. Application of 3D printing technology will allow to receive a real structure in a controlled manner, which exactly reflects the designed structure and is consistent with the geometry of the numerical model. An experimental research on the standard samples made of photopolymer resin using 3D printing technique was presented in the paper. The aim of the research was to determine the base material properties and, consequently, to select the constitutive model, which is necessary to carry out numerical analyses.

Correspondence: Ewelina Małek, Katedra Mechaniki i Informatyki Stosowanej, Wydział Mechaniczny, Wojskowa Akademia Techniczna, ul. Kaliskiego 2, 00-908 Warszawa, phone: 261 83 7867, e-mail: ewelina.malek@wat.edu.pl.

Introduction

The "3D printing" was originally referred to a process that deposits a binder material onto a powder bed with inkjet printer heads layer by layer. More recently, the term is being used to encompass a wider variety of additive manufacturing techniques. United States and global technical standards use the official term *additive manufacturing* for this broader sense.

3D printing technology is any of various processes in which material is joined or solidified under computer control to create a three-dimensional object, with material being added together (such as liquid molecules or powder grains being fused together). The process consists of printing successive layers of materials that are formed on top of each other. This technology has been developed by Charles Hull in 1986 in a process known as stereolithography (SLA), which was followed by subsequent developments such as powder bed fusion, fused deposition modeling (FDM), inkjet printing and contour crafting (CC). 3D printing, which involves various methods, materials and equipment, has evolved over the years and has the ability to transform manufacturing and Logistics processes. Additive manufacturing has been widely applied in different industries, including construction, prototyping and biomechanical. The uptake of 3D printing in the construction industry, in particular, was very slow and limited despite the advantages e.g. less waste, freedom of design and automation (NGO et al. 2018).

The growing consensus of adapting the 3D manufacturing system over traditional techniques is attributed to several advantages including fabrication of complex geometry with high precision, maximum material savings, flexibility in design, and personal customization. A wide range of materials that are currently used in 3D printing include metals, polymers, ceramics and concrete. Polylactic acid (PLA) and acrylonitrile butadiene styrene (ABS) are the main polymers used in the 3D printing of composites. Advanced metals and alloys are typically utilized in the aerospace sector because traditional processes are more time consuming, difficult and costly. Ceramics are mainly used in 3D printed scaffolds and concrete is the main material employed in the additive manufacturing of buildings.

However, the inferior mechanical properties and anisotropic behavior of 3D printed parts still limit the potential of large-scale printing. Therefore, an optimized pattern of 3D priming is important to control flaw sensitivity and anisotropic behavior. Also, changes in the printing environment have an influence on the quality of finished products (IVANOVA et al. 2013).

Methods of additive manufacturing (AM) have been developed to meet the demand of printing complex structures at fine resolutions.

Rapid prototyping, the ability to print large structures, reducing printing defects and enhancing mechanical properties are some of the key factors that have driven the development of AM technologies (Fig. 1). The most common

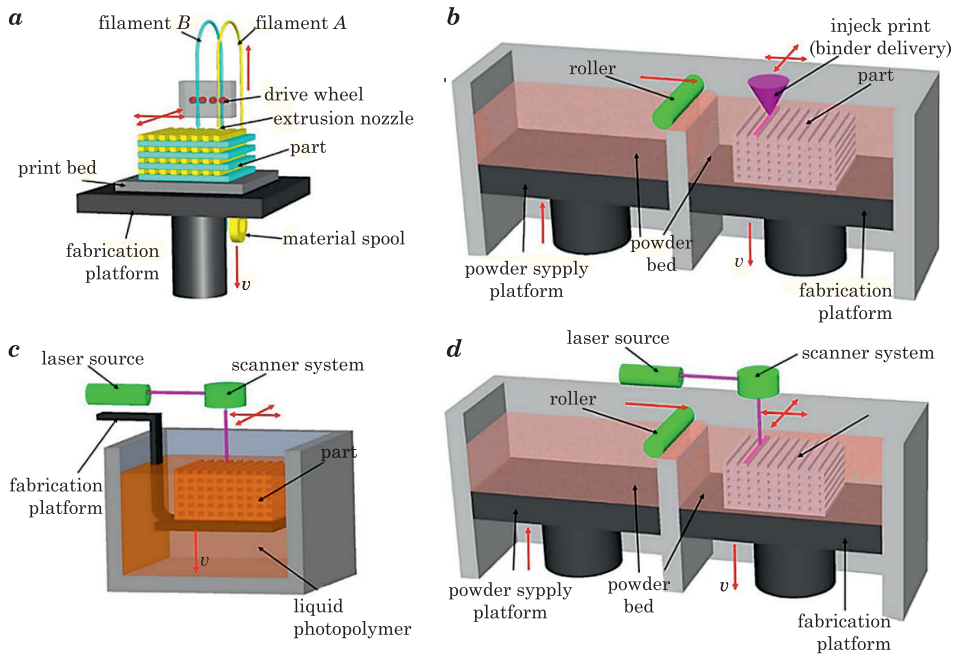

Fig. 1. Scheme of main methods of additive manufacturing: *a* – fused deposition modelling; *b* – inkjet printing, *c* – stereolithography, *d* – powder bed fusion
Source: based on WANG et al. (2017).

method of 3D printing that mainly uses polymer filaments is known as fused deposition modelling (FDM). In addition, additive manufacturing of powders by selective laser sintering (SLS), selective laser melting (SLM) or liquid binding in three-dimensional printing (3DP), as well as inkjet printing, contour crafting, stereolithography, direct energy deposition (DED) and laminated object manufacturing (LOM) are the main methods of AM (BHUSHAN, CASPERS 2017).

SLA (Stereolitography)

Stereolithography (SLA) is an additive manufacturing — commonly referred to as 3D printing — technology that converts liquid materials into solid parts, layer by layer, by selectively curing them using a light source in a process called photopolymerization. SLA is widely used to create models, prototypes, patterns, and production parts for a range of industries from engineering and product design to manufacturing, dentistry, jewelry, model making, and education.

The polymerization process

Plastics are made out of long carbon chains. The shorter the chain, the less solid or viscous the plastic. Resin is a plastic composed of short(er) carbon chains —from 1 carbon to a few thousand carbons. It has all of the components of the final plastic, but hasn't been fully polymerized yet. When the resin is exposed to UV light, the chains join together to create much longer and therefore stiffer chains (Fig. 2). When enough chains have reacted, the result is a solid part (*The ultimate guide…* 2017).

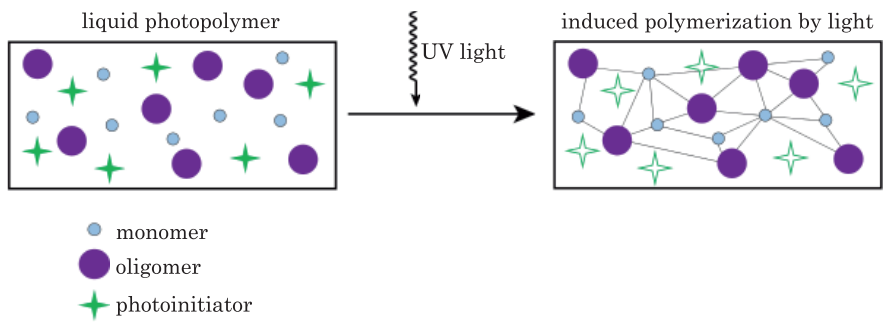

Fig. 2. Steps of the polymerization process
Source: based on FOUASSIER et al. (2003).

The monomer and oligomer chains in the resin have active groups at their ends. When the resin is exposed to UV light, the photo initiator molecule breaks down into two parts, and the bond holding it together becomes two very reactive radicals. These molecules transfer the reactive radicals to the active groups on the monomers and oligomer chains, which in turn react with other active groups, forming longer chains. As the chains get longer and create cross-links, the resin begins to solidify. The entire process, from liquid to highly polymerized solid state, takes place in a matter of milliseconds (*The ultimate guide…* 2017).

Polymers

Polymers are considered as the most common materials in the 3D printing industry due to their diversity and ease of adoption to different 3D printing processes. Polymers for additive manufacturing are found in the form of thermoplastic filaments, reactive monomers, resin or powder. The capability of employing 3D printing of polymers and composites has been explored for several years in many industrial applications, such as the aerospace, architectural, toy fabrication and medical fields.

Photopolymer resins can polymerize when activated by UV light in stereolithography 3D printing. According to the annual industry survey conducted by Wohlers Associates, nearly 50% of the 3D printing market in the industrial sectors is attributed to generated prototypes using photopolymers (LIGON et al. 2017). However, the thermomechanical properties of photopolymers should still be improved. For instance, molecular structure and alignment of 3D printed polymers depend on the thickness of the layers because of the gradient in UV exposure and intensity (GUNDRATI et al. 2018a, b) On the other hand, plastic for selective laser sintering (SLS) is reported to be the second most important class for 3D printing. Among SLS polymers are polystyrene, polyamides and thermoplastic elastomers (LIGON et al. 2017).

Printing of test samples

In presented work, photoreactive resin with trade name Clear Resin, belonging to the group of plastics is analyzed.

This resin is a mixture of methacrylic acid esters and photoinitiator and is used in Formlabs printer Form 1, Form 2.

Standard samples for experimental tensile test were developed using rapid prototyping technology. SLA 3D printing method was implemented using Formlabs Form 2 printer. The steps of preparing objects by SLA method are as follows:

– preparation of the geometric model of the object for printing in dedicated PreForm software (Fig. 3);

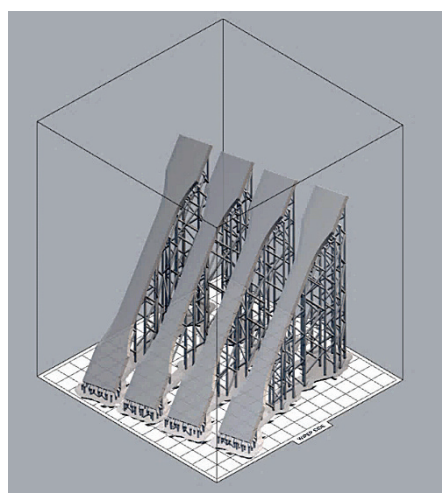

Fig. 3. Model for printing design

– the printing process of the object in the SLA printer (Fig. 4);

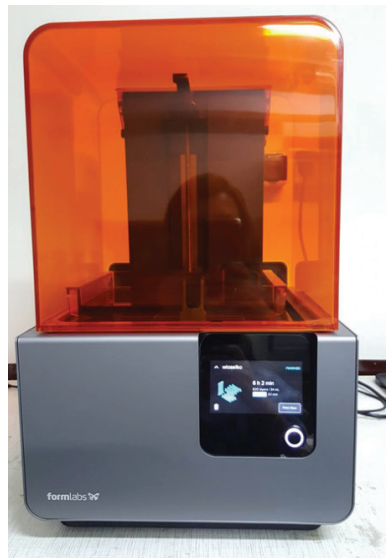

Fig. 4. Form 2 desktop 3D printer

– finishing sections:
  • washing to excess a liquid resin from the parts' surfaces and cavities,
  • post-curing with light and heat (Fig. 5). Post-cured parameters to assure the best strength properties of developed samples were presented in Table 1.

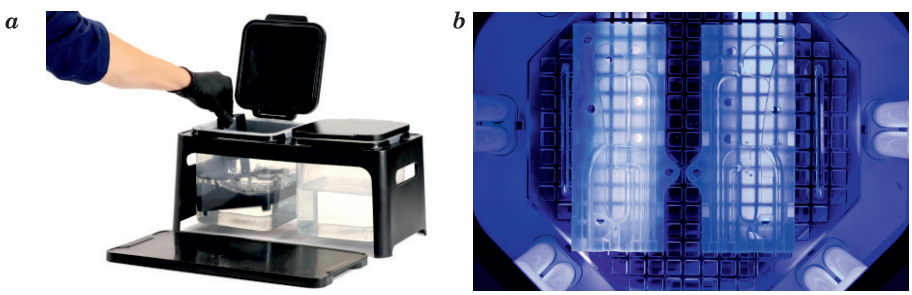

Fig. 5. Washing equipment (*a*), UV lamp (*b*)

Table 1

Post-cured properties for Clear Resin

Material	Temperature of curing [°C]	Time of curing [min]	Wavelength of UV lamp light [nm]
Clear Resin	60	60	405

Tensile testing

Tensile testing is a fundamental materials science and engineering experimental method in which a sample is subjected to a controlled uniaxial tension until failure. Properties that are directly measured via this test are: ultimate tensile strength, breaking strength, maximum elongation and reduction in gauge length cross-sectional area.

The conditions and the method of performing the tensile testing of plastics are described in the PN-EN ISO 527 standard. The sample for testing is flat and "paddle" shaped (Fig. 6). The dimensions of the sample were as follows: thickness $h = 4.0 \pm 0.2$ mm, width of narrow portion $B1 = 10 \pm 0.2$ mm and overall length $L3 > 150$ mm. The cross-section dimension $B1$, h were presented in Table 2.

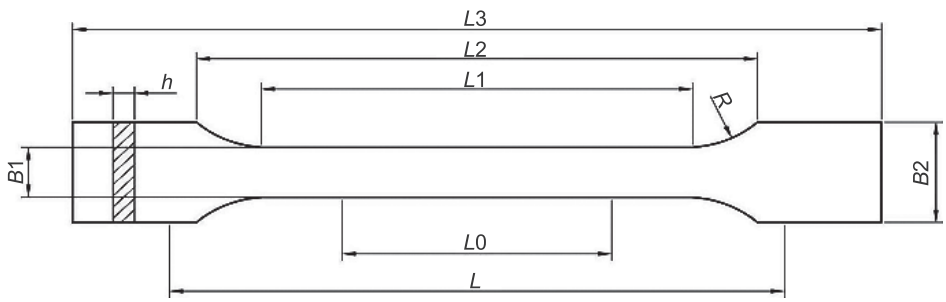

Fig. 6. Test specimen scheme according to PN-EN ISO 527 standard

Table 2

The cross-section dimensions of the samples in the gauge length for the Clear Resin

Number of samples	Dimension $B1$ [mm]	Dimension h [mm]	Cross-section area [mm^2]
Sample 1	10.03	4.04	40.47
Sample 2	10.02	4.05	40.56
Sample 3	10.04	4.03	40.45
Sample 4	10.07	4.07	40.97
Sample 5	10.00	4.04	40.38
Average value	10.04	4.05	40.61

Tensile test was carried out using Zwick Roell Kappa 500 testing machine (Fig. 7), at a room temperature of 20°C. The stand was equipped with a videoextensometer, which allows non-contact measurement of deformation of the sample in various axes. Thanks to special modules, it allows measuring the narrowest or the widest place of the sample, the angle of deflection, the distribution of deformations in a given axis.

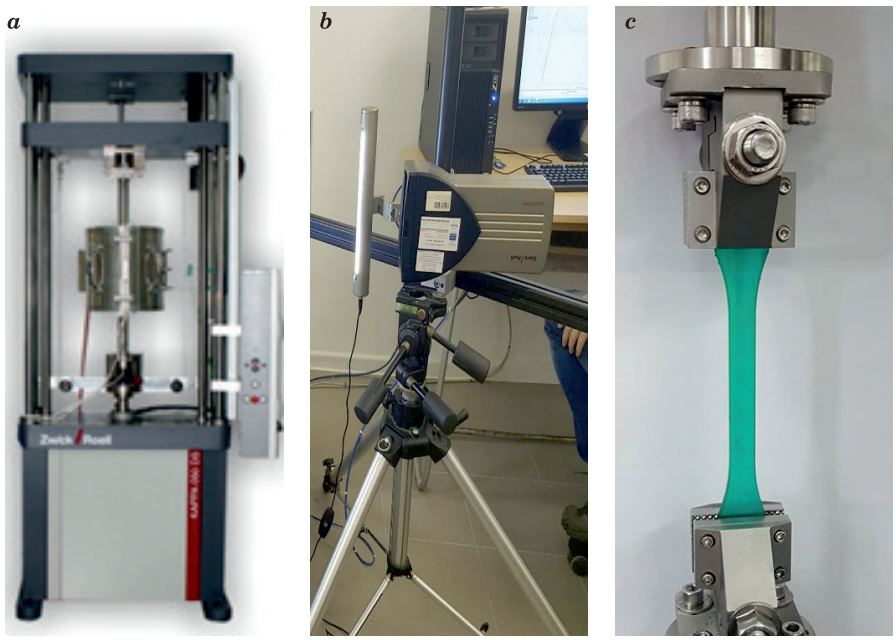

Fig. 7. Zwick Roell Kappa 500 testing machine (*a*), videoextensometer (*b*), sample in the machine's clamps (*c*)

The experiment conditions were as follows:
– 5 standard samples were researched in tensile test;
– The samples were loaded with displacement of 5 mm/min;
– The reaction force was measured on the strength machine head;
– Tensile tests were carried out to sample damage.

Results and discussion

On the base characteristic of force – displacement of the traverse were obtained (Fig. 8). Stress-strain curves were determined (Fig. 9).

The forces and displacements obtained from the experiment were converted into engineering stresses and engineering deformations according to the following relations:

– engineering stress

$$\sigma_{\text{eng}} = \frac{P}{A}[\text{MPa}] \tag{1}$$

– engineering strain

$$\varepsilon_{\text{eng}} = \frac{\Delta l}{l_0}[-] \tag{2}$$

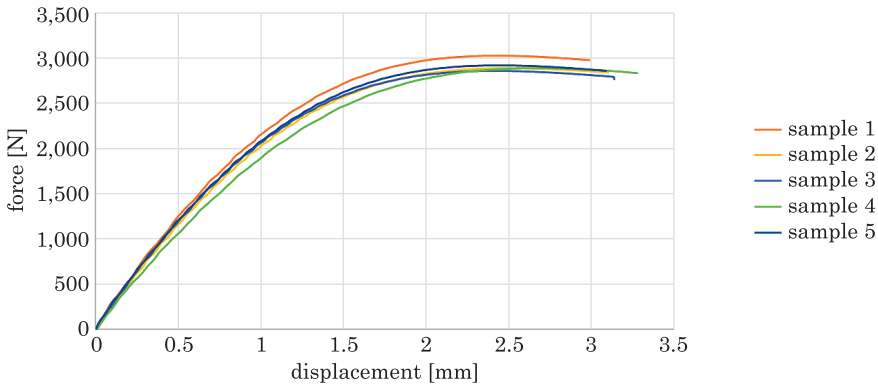

Fig. 8. Force –displacement curves for Clear Resin tensile test

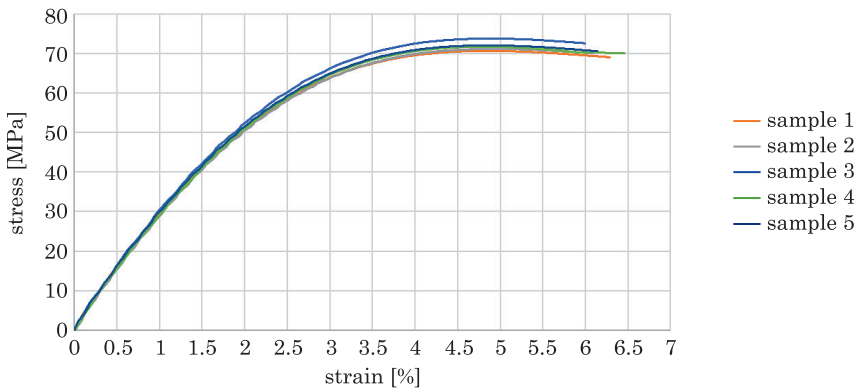

Fig. 9. Stress – strain curves for Clear Resin tensile test

On the base of obtained curves Young's modulus, elongation at break and tensile strength were determined. These data are summarized in Table 3.

Table 3

Material properties of Clear Resin determined from the experiment

Samples	Young's Modulus [MPa]	Elongation at failure [%]	Tensile Strength [MPa]
Sample 1	2,893.91	6.35	71.71
Sample 2	2,892.94	6.29	70.64
Sample 3	2,980.49	5.99	73.78
Sample 4	2,881.01	6.64	71.16
Sample 5	2,921.86	6.13	72.04
Average value	2,914.04	6.28	71.86

The method of determining material data from the experiment according to the standard (Tab. 3) was as follows:

– Modulus of Elasticity was calculated by extending the initial linear portion of stress-strain curve and dividing the difference in stress corresponding to any segment of section on this straight line by the corresponding difference in strain. All elastic modulus values were computed using the average initial cross-sectional area of the test specimens in the calculations;

– Tensile Strength was calculated by dividing the maximum load in newtons by the original minimum cross-sectional area of the specimen in square meters;

– Percent Elongation was calculated by reading the extension (change in gauge length) at the moment the applicable load is reached. The extension was divided by the original gauge length and multiply by 100.

Material data for Clear Resin given by the producer were presented in Table 4.

Table 4

Material data for Clear Photopolymer Resin given by the producer

Mechanical properties	Young's Modulus [MPa]	Elongation at failure [%]	Ultimate Tensile Strength [MPa]
Post-cured	2,800	6.2	65
Standard	ASTM D 638-10	ASTM D 638-10	ASTM D 638-10

Comparing the values obtained in the experiment (Tab. 3) to the values given by the producer (Tab. 4) it can be seen that the values of both Young's modulus and elongation at failure are consistent, while the ultimate tensile strength is larger in the case of experimental tests.

Summary

As it was mentioned the results of the tensile test for Clear Resin will be adopted in numerical modeling of fractal porous structure.

Comparing the values obtained in the experiment to the values given by the producer it can be seen that they are similar, which proves that the process of producing samples was carried out correctly. The tensile strength is larger for the experimental samples. Values of the tensile strength are depending of the variable condition parameters. Printing samples and post-cured processes could change the finally structure of the samples, in the small range. It caused the minor differences in obtained values.

Future implementation of presented research

It should be noted that the main idea of the work is to develop a numerical research methodology whose behavior can be fully controlled. The next step will be numerical research of the natural structures whose construction creates problems in their modeling.

The proposed numerical models of the selected porous structure will be based on the geometry of the Menger cube (Fig. 10). This geometry is commonly used for fractal media simulations.

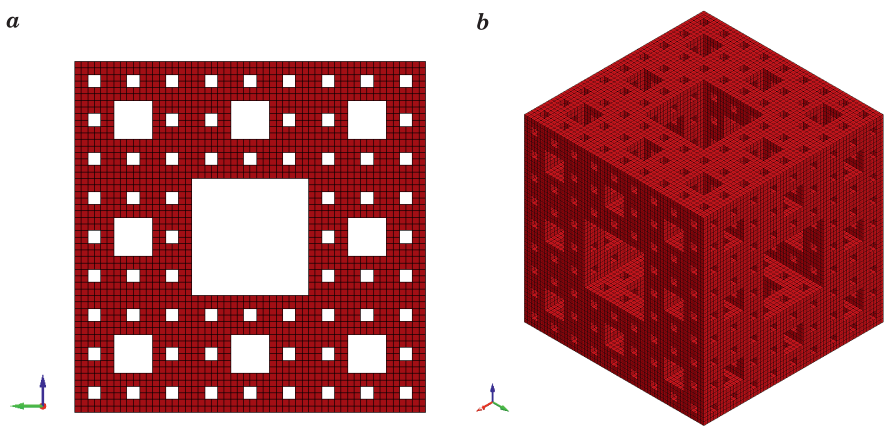

Fig. 10. Numerical model: *a* – 2D, *b* – 3D Menger's structure, as the basic fractal model

The idealistic structure (Fig. 10) will be modified to break the symmetry of the sample. The example of such modification (Fig. 11) was developed by introducing the directivity of structure by multiplying the geometry in one direction.

In addition the presented research will be used to constitutive material model selection in the chosen FE computer code.

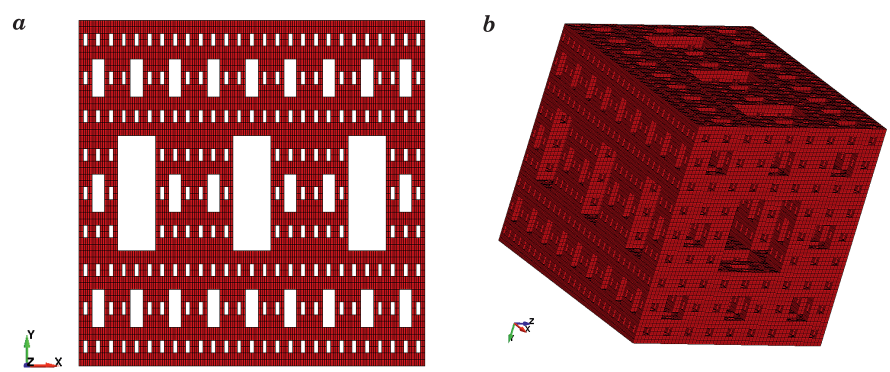

Fig. 11. Proposed numerical model: *a* – 2D, *b* – 3D of Menger's structure after modification

Acknowledgements

The paper supported by a grant No BG2/DIOX4SHELL/14 financed in the years 2014-2018 by The National Centre for Research and Development, Poland.

References

BHUSHAN B., CASPERS M. 2017. *An overview of additive manufacturing (3D printing) for microfabrication*. Microsystem Technologies, 23(4): 1117–1124.

The ultimate guide to stereolitography (SLA) 3D printing. 2017. Formlabs, https://formlabs.com.

FOUASSIER J.P., ALLONAS X., BURGET D. 2003. *Photopolimerization reactions under visible lights: principle, mechanisms and examples of applications*. Progress in Organic Coatings, 47(1): 16–36.

GUNDRATI N.B., CHAKRABORTY P., ZHOU C., CHUNG D.D.L. 2018. *First observation of the effect of the layer printing sequence on the molecular structure of three-dimensionally printed polymer, as shown by in-plane capacitance measurement*. Composites, Part B, Engineering, 140: 78–82.

GUNDRATI N.B., CHAKRABORTY P., ZHOU C., CHUNG D.D.L. 2018. *Effects of printing conditions on the molecular alignment of three-dimensionally printed polymer*. Composites, Part B, Engineering, 134: 164–168.

IVANOVA O., WILLIAMS C., CAMPBELL T. 2013. *Additive manufacturing (AM) and nanotechnology promises and challenges*. Rapid Prototyping Journal, 19(5): 353–364.

LIGON S.C., LISKA R., STAMPFL J., GURR M., MÜLHAUPT R. 2017. *Polymers for 3D printing and customized additive manufacturing*. Chemistry Reviev, 117(15): 10212–10290.

NGO T.D., KASHANI A., IMBALZANO G., NGUYEN K.T.Q., HUI D. 2018. *Additive manufacturing (3D printing): A review of materials, methods, application and challenges*. Composites, Part B, Engineering, 143: 173–196.

WANG X., JIANG M., ZHOU Z., GOU J., HUI D. 2017. *3D printing of polymer matrix composites: a review and prospective*. Composites, Part B, Engineering, 110: 442–458.

Guide for Autors

Introduction

Technical Sciences is a peer-reviewed research Journal published in English by thePublishing House of the University of Warmia and Mazury in Olsztyn (Poland). Journal is published continually since 1998. Until 2010 Journal was published as a yearbook, in 2011 and 2012 it was published semiyearly. From 2013, the Journal is published quarterly in the spring, summer, fall, and winter.

The Journal covers basic and applied researches in the field of engineering and the physical sciences that represent advances in understanding or modeling of the performance of technical and/or biological systems. The Journal covers most branches of engineering science including biosystems engineering, civil engineering, environmental engineering, food engineering, geodesy and cartography, information technology, mechanical engineering, materials science, production engineering etc.

Papers may report the results of experiments, theoretical analyses, design of machines and mechanization systems, processes or processing methods, new materials, new measurements methods or new ideas in information technology.

The submitted manuscripts should have clear science content in methodology, results and discussion. Appropriate scientific and statistically sound experimental designs must be included in methodology and statistics must be employed in analyzing data to discuss the impact of test variables. Moreover there should be clear evidence provided on how the given results advance the area of engineering science. Mere confirmation of existing published data is not acceptable. Manuscripts should present results of completed works.

There are three types of papers: a) research papers (full length articles); b) short communications; c) review papers.

The Journal is published in the printed and electronic version. The electronic version is published on the website ahead of printed version of Technical Sciences.

Technical Sciences does not charge submission or page fees.

Types of paper

The following articles are accepted for publication:

Reviews

Reviews should present a focused aspect on a topic of current interest in the area of biosystems engineering, civil engineering, environmental engineering, food engineering, geodesy and cartography, information technology, mechanical engineering, materials science, production engineering etc. They should include all major findings and bring together reports from a number of sources. These critical reviews should draw out comparisons and conflicts between work, and provide an overview of the 'state of the art'. They should give objective assessments of the topic by citing relevant published work, and not merely present the opinions of individual authors or summarize only work carried out by the authors or by those with whom the authors agree. Undue speculations should also be avoided. Reviews generally should not exceed 6,000 words.

Research Papers

Research Papers are reports of complete, scientifically sound, original research which contributes new knowledge to its field. Papers should not exceed 5,000 words, including figures and tables.

Short Communications

Short Communications are research papers constituting a concise description of a limited investigation. They should be completely documented, both by reference list, and description of the experimental procedures. Short Communications should not occupy more than 2,000 words, including figures and tables.

Letters to the Editor

Letters to the Editor should concern with issues raised by articles recently published in scientific journals or by recent developments in the engineering area.

Contact details for submission

The paper should be sent to the Editorial Office, as a Microsoft Word file, by e-mail: techsci@uwm.edu.pl

Referees

Author/authors should suggest, the names, addresses and e-mail addresses of at least three potential referees. The editor retains the sole right to decide whether or not the suggested reviewers are used.

Submission declaration

After final acceptance of the manuscript, the corresponding author should send to the Editorial Office the author's declaration. Submission of an article implies that the work has not been published previously (except in the form of an abstract or as part of a published lecture or academic thesis or as an electronic preprint), that it is not under consideration for publication elsewhere, that publication is approved by all authors and tacitly or explicitly by the responsible authorities where the work was carried out, and that, if accepted, it will not be published elsewhere in the same form, in English or in any other language.

To prevent cases of ghostwriting and guest authorship, the author/authors of manuscripts is/are obliged to: (i) disclose the input of each author to the text (specifying their affiliations and contributions, i.e. who is the author of the concept, assumptions, methods, protocol, etc. used during the preparation of the text); (ii) disclose information about the funding sources for the article, the contribution of research institutions, associations and other entities.

Language

Authors should prepare the full manuscript i.e. title, abstract and the main text in English (American or British usage is accepted). Polish version of the manuscript is not required.

The file type

Text should be prepared in a word processor and saved in doc or docx file (MS Office).

Article structure

Suggested structure of the manuscript is as follows:

Title
Authors and affiliations
Corresponding author
Abstract
Keywords
Introduction
Material and Methods
Results and Discussion
Conclusions

Acknowledgements (optional)
References
Tables
Figures

Subdivision – numbered sections

Text should be organized into clearly defined and numbered sections and subsections (optionally). Sections and subsections should be numbered as 1. 2. 3. then 1.1 1.2 1.3 (then 1.1.1, 1.1.2, …). The abstract should not be included in numbering section. A brief heading may be given to any subsection. Each heading should appear on its own separate line. A single line should separate paragraphs. Indentation should be used in each paragraph.

Font guidelines are as follows:

– Title: 14 pt. Times New Roman, bold, centered, with caps
– Author names and affiliations:12 pt. Times New Roman, bold, centered, italic, two blank line above
– Abstract: 10 pt. Times New Roman, full justified, one and a half space. Abstract should begin with the word Abstract immediately following the title block with one blank line in between. The word Abstract: 10 pt. Times New Roman, centered, indentation should be used
– Section Headings: Not numbered, 12 pt. Times New Roman, bold, centered; one blank line above
– Section Sub-headings: Numbered, 12 pt. Times New Roman, bold, italic, centered; one blank line above
– Regular text: 12 pt. Times New Roman, one and a half space,full justified, indentation should be used in each paragraph

Title page information

The following information should be placed at the first page:

Title

Concise and informative. If possible, authors should not use abbreviations and formulae.

Authors and affiliations

Author/authors' names should be presented below the title. The authors' affiliation addresses (department or college; university or company; city, state and zip code, country) should be placed below the names. Authors with the same affiliation must be grouped together on the same line with affiliation information following in a single block. Authors should indicate all affiliations with a lower-case superscript letter immediately after the author's name and in front of the appropriate address.

Corresponding author

It should be clearly indicated who will handle correspondence at all stages of refereeing and publication, also post-publication process. The e-mail address should be provided (footer, first page). Contact details must be kept up to date by the corresponding author.

Abstract

The abstract should have up to 100-150 words in length. A concise abstract is required. The abstract should state briefly the aim of the research, the principal results and major conclusions. Abstract must be able to stand alone. Only abbreviations firmly established in the field may be eligible. Non-standard or uncommon abbreviations should be avoided, but if essential they must be defined at their first mention in the abstract itself.

Keywords

Immediately after the abstract, author/authors should provide a maximum of 6 keywords avoiding general, plural terms and multiple concepts (avoid, for example, 'and', 'of'). Author/authors should be sparing with abbreviations: only abbreviations firmly established in the field may be eligible.

Abbreviations

Author/authors should define abbreviations that are not standard in this field. Abbreviations must be defined at their first mention there. Author/authors should ensure consistency of abbreviations throughout the article.

Units

All units used in the paper should be consistent with the SI system of measurement. If other units are mentioned, author/authors should give their equivalent in SI.

Introduction

Literature sources should be appropriately selected and cited. A literature review should discuss published information in a particular subject area. Introduction should identify, describe and analyze related research that has already been done and summarize the state of art in the topic area. Author/authors should state clearly the objectives of the work and provide an adequate background.

Material and Methods

Author/authors should provide sufficient details to allow the work to be reproduced by other researchers. Methods already published should be indicated by a reference. A theory should extend, not repeat, the background to the article already dealt within the Introduction and lay the foundation for further work. Calculations should represent a practical development from a theoretical basis.

Results and Discussion

Results should be clear and concise. Discussion should explore the significance of the results of the work, not repeat them. A combined Results and Discussion section is often appropriate.

Conclusions

The main conclusions of the study may be presented in a Conclusions section, which may stand alone or form a subsection of a Results and Discussion section.

Acknowledgements

Author/authors should include acknowledgements in a separate section at the end of the manuscript before the references. Author/authors should not include them on the title page, as a footnote to the title or otherwise. Individuals who provided help during the research study should be listed in this section.

Artwork

General points

– Make sure you use uniform lettering and sizing of your original artwork
– Embed the used fonts if the application provides that option
– Aim to use the following fonts in your illustrations: Arial, Courier, Times New Roman, Symbol
– Number equations, tables and figures according to their sequence in the text
– Size the illustrations close to the desired dimensions of the printed version

Formats

If your electronic artwork is created in a Microsoft Office application (Word, PowerPoint, Excel) then please supply 'as is' in the native document format

Regardless of the application used other than Microsoft Office, when your electronic artwork is finalized, please 'Save as' or convert the images to one of the following formats (note the resolution requirements given below):

EPS (or PDF): Vector drawings, embed all used fonts

JPEG: Color or grayscale photographs (halftones), keep to a minimum of 300 dpi

JPEG: Bitmapped (pure black & white pixels) line drawings, keep to a minimum of 1000 dpi or combinations bitmapped line/half-tone (color or grayscale), keep to a minimum of 500 dpi

Please do not:

– Supply files that are optimized for screen use (e.g., GIF, BMP, PICT, WPG); these typically have a low number of pixels and limited set of colors
– Supply files that are too low in resolution
– Submit graphics that are disproportionately large for the content

Color artwork

Author/authors should make sure that artwork files are in an acceptable format (JPEG, EPS PDF, or MS Office files) and with the correct resolution. If, together with manuscript, author/authors submit color figures then Technical Sciences will ensure that these figures will appear in color on the web as well as in the printed version at no additional charge.

Tables, figures, and equations

Tables, figures, and equations/formulae should be identified and numbered consecutively in accordance with their appearance in the text.

Equations/mathematical and physical formulae should be presented in the main text, while tables and figures should be presented at the end of file (after References section). Mathematical and physical formulae should be presented in the MS Word formula editor.

All types of figures can be black/white or color. Author/authors should ensure that each figure is numbered and has a caption. A caption should be placed below the figure. Figure must be able to stand alone (explanation of all symbols and abbreviations used in figure is required). Units must be always included. It is noted that figure and table numbering should be independent.

Tables should be numbered consecutively in accordance with their appearance in the text. Table caption should be placed above the table. Footnotes to tables should be placed below the table body and indicated with superscript lowercase letters. Vertical rules should be avoided. Author/authors should ensure that the data presented in tables do not duplicate results described in figures, diagrams, schemes, etc. Table must be able to stand alone (explanation of all symbols and abbreviations used in table is required). Units must be always included. As above, figure and table numbering should be independent.

References

References: All publications cited in the text should be presented in a list of references following the text of the manuscript. The manuscript should be carefully checked to ensure that the spelling of authors' names and dates of publications are exactly the same in the text as in the reference list. Authors should ensure that each reference cited in the text is also present in the reference list (and vice versa).

Citations may be made directly (or parenthetically). All citations in the text should refer to:

1. Single author

The author's name (without initials, with caps, unless there is ambiguity) and the year of publication should appear in the text

2. Two authors

Both authors' names (without initials, with caps) and the year of publication should appear in the text

3. Three or more authors

First author's name followed by et al. and the year of publication should appear in the text

Groups of references should be listed first alphabetically, then chronologically.

Examples:

"... have been reported recently (ALLAN, 1996a, 1996b, 1999; ALLAN and JONES, 1995). KRAMER et al. (2000) have recently shown..."

The list of references should be arranged alphabetically by authors' names, then further sorted chronologically if necessary. More than once reference from the same author(s) in the same year must be identified by the letters "a", "b", "c" etc., placed after the year of publication.

References should be given in the following form:

KUMBHAR B.K., AGARVAL R.S., DAS K. 1981. Thermal properties of fresh and frozen fish. International Journal of Refrigeration, 4(3), 143–146.

MACHADO M.F., OLIVEIRA F.A.R., GEKAS V. 1997. Modelling water uptake and soluble solids losses by puffed breakfast cereal immersed in water or milk. In Proceedings of the Seventh International Congress on Engineering and Food, Brighton, UK.

NETER J., KUTNER M.H., NACHTSCHEIM C.J., WASSERMAN W. 1966. Applied linear statistical models (4th ed., pp. 1289–1293). Irwin, Chicago.

THOMSON F.M. 1984. Storage of particulate solids. In M. E. Fayed, L. Otten (Eds.), Handbook of Powder Science and Technology (pp. 365–463). Van Nostrand Reinhold, New York.

Citation of a reference as 'in press' implies that the item has been accepted for publication.

Note that the full names of Journals should appear in reference list.

Submission checklist

The following list will be useful during the final checking of an article prior to the submission. Before sending the manuscript to the Journal for review, author/authors should ensure that the following items are present:

– Text is prepared with a word processor and saved in DOC or DOCX file (MS Office). One author has been designated as the corresponding author with contact details: e-mail address
– Manuscript has been 'spell-checked' and 'grammar-checked'
– References are in the correct format for this Journal
– All references mentioned in the Reference list are cited in the text, and vice versa
– Author/authors does/do not supply files that are too low in resolution
– Author/authors does/do not submit graphics that are disproportionately large for the content